LEVEL A ①

$79-98D$

ADA070466

SIXTH ORDER ANALYSES OF CLOSURE

IN A CRACKED, ELASTO-PLASTIC PLATE

FRANCIS S. HEMING, JR.
Captain, USAF

Report SM-78-25   November 1978

Submitted in partial fulfillment of the
requirements for the degree of
Doctor of Philosophy at Carnegie-Mellon University

Department of Mechanical Engineering
Carnegie Institute of Technology
Carnegie-Mellon University
Pittsburgh, Pennsylvania

79 06 25 074

REPORT DOCUMENTATION PAGE		READ INSTRUCTIONS BEFORE COMPLETING FORM
1. REPORT NUMBER CI 79-98D	2. GOVT ACCESSION NO.	3. RECIPIENT'S CATALOG NUMBER
4. TITLE *(and Subtitle)* Sixth Order Analyses of Closure in a Cracked- Elasto-Plastic Plate.		5. TYPE OF REPORT & PERIOD COVERED Dissertation
		6. PERFORMING ORG. REPORT NUMBER
7. AUTHOR(s) Captain Francis S. Heming		8. CONTRACT OR GRANT NUMBER(s)
9. PERFORMING ORGANIZATION NAME AND ADDRESS AFIT Student, Carnegie-Mellon University, Pittsburgh PA		10. PROGRAM ELEMENT, PROJECT, TASK AREA & WORK UNIT NUMBERS 155p.
11. CONTROLLING OFFICE NAME AND ADDRESS AFIT/CI WPAFB OH 45433		12. REPORT DATE Nov 1978
		13. NUMBER OF PAGES 115 +
14. MONITORING AGENCY NAME & ADDRESS(*if different from Controlling Office*) AFIT-CI-79-98D		15. SECURITY CLASS. *(of this report)* Unclassified
		15a. DECLASSIFICATION/DOWNGRADING SCHEDULE

16. DISTRIBUTION STATEMENT *(of this Report)*

Approved for Public Release, Distribution Unlimited

Doctoral thesis

17. DISTRIBUTION STATEMENT *(of the abstract entered in Block 20, if different from Report)*

18. SUPPLEMENTARY NOTES

JOSEPH P. HIPPS, Major, USAF
Director of Information, AFIT

19. KEY WORDS *(Continue on reverse side if necessary and identify by block number)*

20. ABSTRACT *(Continue on reverse side if necessary and identify by block number)*

012 200

REPORT DOCUMENTATION PAGE

	READ INSTRUCTIONS BEFORE COMPLETING FORM
1. REPORT NUMBER CI 79-95D	2. GOVT ACCESSION NO. 3. RECIPIENT'S CATALOG NUMBER

4. TITLE (and Subtitle)

Sixth Order Analyses of Closure in a Cracked-Elasto-Plastic Plate

5. TYPE OF REPORT & PERIOD COVERED

Dissertation

6. PERFORMING ORG. REPORT NUMBER

7. AUTHOR(s)

Captain Francis S. Fleming

8. CONTRACT OR GRANT NUMBER(s)

9. PERFORMING ORGANIZATION NAME AND ADDRESS

AFIT/Student, Carnegie-Mellon University, WPAFB OH PA

10. PROGRAM ELEMENT, PROJECT, TASK AREA & WORK UNIT NUMBERS

11. CONTROLLING OFFICE NAME AND ADDRESS

AFIT/CI
WPAFB OH 45433

12. REPORT DATE

May 1979

13. NUMBER OF PAGES

115 +

14. MONITORING AGENCY NAME & ADDRESS(if different from Controlling Office)

15. SECURITY CLASS. (of this report)

Unclassified

15a. DECLASSIFICATION/DOWNGRADING SCHEDULE

16. DISTRIBUTION STATEMENT (of this Report)

Approved for Public Release, Distribution Unlimited

17. DISTRIBUTION STATEMENT (of the abstract entered in Block 20, if different from Report)

18. SUPPLEMENTARY NOTES

JOSEPH P. HIPPS, Major, USAF
Director of Information, AFIT

19. KEY WORDS (Continue on reverse side if necessary and identify by block number)

20. ABSTRACT (Continue on reverse side if necessary and identify by block number)

Carnegie-Mellon University

CARNEGIE INSTITUTE OF TECHNOLOGY

THESIS

SUBMITTED IN PARTIAL FULFILLMENT OF THE REQUIREMENTS
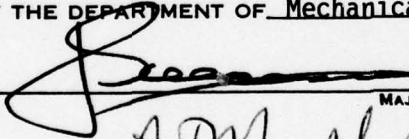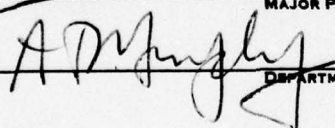
FOR THE DEGREE OF ___Doctor of Philosophy___

TITLE ___SIXTH ORDER ANALYSES OF CLOSURE___

___IN A CRACKED, ELASTO-PLASTIC PLATE___

PRESENTED BY ___Francis S. Heming, Jr.___

ACCEPTED BY THE DEPARTMENT OF ___Mechanical Engineering___

_____ ___8 Dec 78___
MAJOR PROFESSOR   DATE

_____ ___Dec 18, 1978___
DEPARTMENT HEAD   DATE

APPROVED BY THE COLLEGE COUNCIL

_____ ___12/18/78___
DEAN   DATE

ACKNOWLEDGMENTS

TABLE OF CONTENTS

LIST OF TABLES

LIST OF FIGURES

LIST OF SYMBOLS

Most symbols are defined explicitly where they occur in the text. Those that are not defined in the text are listed here for convenience.

$F(\theta,\lambda)$	Angular function in Williams' [2] solution
I	Moment of Inertia
L	Length of beam described in Section 7.1
M_x, M_y, M_{xy}	Moment Resultants
N_x, N_y, N_{xy}	In-plane force resultants
Q_x, Q_y	Transverse shear force resultants
r	Distance from the crack tip
v_x, v_y	Transverse shear forces

The superscript (p) refers to the plastic portion of the quantity. The dot over a symbol refers to time derivatives. Subscript B refers to the bending component of stress only, i.e., the membrane component has been taken out.

ABSTRACT

The bending of a plate containing a centrally located, through crack is analyzed. Results are obtained numerically via a finite element analysis based on the assumptions of Mindlin sixth order plate theory, which admits three boundary conditions at any point and includes the effects of transverse shear. Special features of the analysis are the modelling of crack face interference, or closure, and of elasto-plastic behavior for a work hardening material. The closure constraint is imposed using Lagrange multiplier concepts, and the elasto-plastic behavior is based on the incremental theory of plasticity.

Elastic and elasto-plastic results are presented for two cases, one that includes the effects of closure and one that does not. The influence of closure on the local displacements, stress distributions, bending stress intensity factors, crack tip blunting, and the growth of the plastic enclave is demonstrated. The effect of thickness and the significance of transverse shear is also discussed. The results show that boundary conditions are critical to the modelling process, that the effects of closure are significant and must be included when demanded by the actual physical situation, and that the important issues regarding the plate bending problem have been identified and analyzed, so that issues regarding more detailed behavior may be addressed.

x

CHAPTER I

INTRODUCTION

The analysis and design of structures and the effect of
flaws on the performance of these structures involves the
examination of many different types of problems. The problem
of particular interest here is the bending of a plate containing
a centrally located, through crack. Although the plate bending
problem is one of some import, the complexity of the solution
has inhibited the amount of analysis reported relative to the
extensional problem. Nevertheless, the results that have been
reported have provided valuable insights into the mechanics of
the bending problem. With this background, the present analyses
have completed the identification and discussion of the signi-
ficance of the important issues involved.

Chapter II traces the development of the bending problem
as reported in the literature. The results reported progress
from relatively simple elastic analyses based on classical
plate theory (thus implying the use of approximate boundary
conditions) to more extensive analyses involving higher order
plate theories, elasto-plastic behavior, and the effects of
crack closure. While these analyses have considered the main
features of the bending problem one or two at a time, an
analysis involving all of these features remained as the final
objective. Thus, the development of the plate bending problem
has provided the impetus for the sixth-order, elasto-plastic
analysis of closure effects that is reported here.

The sixth order theory chosen for the analyses is Mindlin plate theory, which is a displacement based theory and which admits the specification of three independent boundary conditions at any point. The importance of the boundary conditions becomes very evident in later discussions. The elastic and elasto-plastic formulation of Mindlin theory is contained in Chapter III. Also contained in Chapter III is a discussion of the modelling of the crack face interference (or closure) that is inherent to the bending problem.

The complexity of the sixth order analyses precludes a closed form solution to the problem and necessitates a numerical approach. Accordingly, a finite element representation based on the assumptions of Mindlin theory is used for the analyses. The finite element model uses the eight-node isoparametric plane quadratic element, which allows the required inclusion of transverse shear, and permits closure to occur at the compression surface where the crack flanks come together as a bending load is applied. The model incorporates the closure constraint through the use of Lagrange multiplier techniques and provides the required capability for isolating the effects of closure. In addition, elasto-plastic behavior for a work hardening material is included in the analyses. The elasto-plastic capability is based on the familiar incremental theory of plasticity. A discussion of the elastic and elasto-plastic finite element representations and of the modelling of the closure constraint is presented in Chapter IV.

Although the closure problem is in reality a three-dimensional contact problem (i.e., the crack flanks come together to form a contact surface, not just a contact line as modelled here), the results obtained are highly credible and clearly indicate the effects of closure on the plate bending problem. Good accuracy of the data is inferred by comparison to earlier analyses for special cases of the problem.

The elastic and elasto-plastic results are presented in Chapter V and Chapter VI, respectively. In both chapters the results are presented in a form that clearly shows the changes in material behavior that occur when the effects of closure are considered.

In Chapter VII the important aspects of closure are identified and discussed, and the significance of the closure phenomenon emerges. Where appropriate, the results obtained here are compared with expected behavior and with previously published results. The discussions contained in Chapter VII provide a strong foundation for the conclusions presented in Chapter VIII.

CHAPTER II

PROBLEM SCOPE

Although numerous results have been reported for the problem
of the extensional loading of a plate containing a stationary,
through crack, discussions of the analogous bending problem have
appeared only infrequently. In addition, although elasto-plastic
results for the extensional problem are being reported with
increasing frequency, the results that have been reported for the
bending problem have dealt primarily with elastic behavior only.
The discussion which follows traces the development of the
bending problem as reported in the literature and places the
formulation and results of the present study in perspective.

The bending of an elastic plate containing a stationary,
centrally located, through crack has been a problem of interest
for some time. Williams [1] used Kirchhoff fourth order plate
theory to obtain a solution to the generic problem in 1951.
In that work he solved the biharmonic equation, $\nabla^4 w = 0$, for a
wedge-shaped section by assuming a solution of the form $w(r,\theta) =
r^{\lambda+1} F(\theta,\lambda)$ and obtaining the eigenvalue solutions appropriate to
the applied boundary conditions. Williams [2] later considered
the bending stress distribution around the crack tip. He found,
as expected, that the stresses are characterized by the inverse
square root singularity as in the extensional problem. Of
greater interest though was the result that the normal stress
ratio along the direction of crack propagation is $\frac{\nu - 1}{3 + \nu}$ rather

than the extensional value of unity. This difference between the
bending and extensional solutions is attributed to the difference
in admissible boundary conditions inherent with Kirchhoff plate
theory. In order to correct for the unavoidable Kirchhoff approxi-
mation of using equivalent rather than physically natural boundary
conditions, Knowles and Wang [3] solved the problem in 1960 for a
vanishingly thin plate using Reissner sixth order plate theory [4].
Since the additional complexity of the sixth order theory pre-
cluded an eigenvalue solution to Reissner's equations, Knowles
and Wang couched the problem in terms of a set of integral equations
which they reduced to a single, singular integral equation. They
then obtained an approximate solution for a plate whose thickness
is vanishingly small. Although the higher order theory is
inherently more complex, it does admit to three boundary conditions,
and the results obtained by Knowles and Wang showed that the stress
distribution for the bending problem replicates the extensional
results.

Although the solution obtained by Knowles and Wang corrected
the boundary condition problem, their results were deficient in
that they were not applicable to plates of finite thickness. It
was not until 1968 that the question of finite plate thickness
was addressed. Employing Reissner theory and an integral equation
approach, Hartranft and Sih [5] and Wang [6] independently presented
results that included the effects of plate thickness on the bending
stress distribution. Their results also included the Knowles and
Wang [3] solution as a limiting case. While demonstrating the

influence of plate thickness, the principal deficiency of these
solutions, and of all the solutions discussed so far, is their
inability to account for crack closure. That is, the crack
surfaces open on the tension side, but are allowed to overlap,
or pass through each other, on the compression side as bending
proceeds. In reality, the compression surfaces do not overlap;
the crack physically closes on itself. Obviously, the actual
physical situation requires a model that accounts for the closure
phenomenon and for the induced interaction between bending and
extension.

One method of treating the bending-extension interaction
problem is to apply an extensional load of sufficient magnitude
to preclude closure when the bending load is applied. Folias [7]
and Wynn [8] are noted for their use of superposition of elastic
bending and extensional solutions to treat this problem. However,
in at least some cases this approach circumvents the actual
physical situation and does not provide any information about
induced closure effects.

Indeed, experimental investigations have shown that crack
closure can have a significant influence on the elastic behavior
of the plate. Smith and Smith [9] made a photoelastic evaluation
of the influence of closure (and other effects) on the stress
distribution around the crack. For the tests they conducted,
the effect of closure was non-conservative and indicated an
increase in local stress of up to 40% over the theoretical
results obtained by Hartranft and Sih [5]. Smith and Smith [10]

later reported additional results for cracked plates under
bending where precatastrophic extension on the tensile side
and crack closure on the compression side were present. They
found that significant stress relaxation occurs near the crack
tip in the presence of precatastrophic extension. Smith and
Smith thus concluded that when both crack closure and pre-
catastrophic extension were present, the Hartranft and Sih
theory provided a fairly accurate estimate of the local stress
distribution. Although admittedly a simplified, order of
magnitude type, two dimensional analysis of a three dimensional
contact problem, the work of Smith and Smith provided a strong
impetus for further study of crack closure effects.

In 1972, Jones [11] took the first step in making a
comprehensive analysis of crack closure effects in plate bending.
Jones used a finite element analysis based on Kirchhoff theory
to compare the results of two cases, one that included closure
effects versus one that did not. For the elastic case with
closure effects included, Jones reported a significant increase
in crack opening displacement, a redistribution of stresses
local to the crack, and an increase in the bending stress
intensity factor on the tension surface. Perhaps of greater
significance was his contribution of the first elasto-plastic
results for the bending problem, including the effects of
closure. Jones reported that in the presence of closure,
yielding begins on the tension surface and proceeds part-way
through the thickness before yielding occurs on the compression

surface, that yielding is more constrained when compared with the case that ignores closure, and that crack tip blunting is less pronounced.

Although the results reported by Jones contributed significantly toward understanding the effects of crack closure for both the elastic and elasto-plastic bending problems, they are inherently deficient due to the difficulty in modeling the free surface of the crack with the Kirchhoff approximation of the boundary conditions. For example, as a consequence of Kirchhoff theory, the singular shear stress term along the crack face approaching the crack tip forces the yield zones to generate along the crack face first and then to propagate into the material. If the singular shear stress were not present, as in sixth order plate theory, the shape of the yield zone would presumably be similar to that found in the extensional case (see Swedlow, Williams and Yang, [12]). Thus, at the completion of Jones' work there remained only one major problem to be resolved; that is, the reformulation and solution of the problem using a sixth order plate theory. It is presumed that such a formulation would not only resolve the boundary condition problem inherent to Kirchhoff theory, but would lead to results similar to the elasto-plastic extensional problem. The results of such a study are reported here.

CHAPTER III

PROBLEM FORMULATION

The problem of interest is a sixth order analysis of an isotropic plate containing a centrally located, through crack and subjected to an applied uniform bending moment at the plate boundaries. The cracked plate geometry is depicted in Figure 3-1 with a thickness of h, a total crack length of 2a, and a uniform bending moment of M_o. The displacements of the plate in the x, y, and z directions are represented by u, v, and w, respectively. The plate length and width are of sufficient size to approximate an infinite plate, and the crack length to thickness ratio is large enough to warrant a thin plate, plane stress analysis.

3.1 Mindlin Plate Theory

The sixth order theory chosen for the analysis is due to Mindlin [15] (see Appendix A for a discussion of Kirchhoff, Mindlin, and Reissner plate theories). The assumed displacement field allows for both extensional and bending loads, i.e.,

$$u(x,y,z) = u_s(x,y) + z\phi(x,y) \tag{3-1a}$$

$$v(x,y,z) = v_s(x,y) - z\psi(x,y) \tag{3-1b}$$

$$w(x,y) = w(x,y) \tag{3-1c}$$

where u_s and v_s are the in plane displacements due to extensional loading and ϕ, ψ, and w are the bending terms.

Assumption of a generalized plane stress distribution of σ_z and application of variational techniques to minimize the potential energy produce the applicable differential equations and boundary conditions. The details of this procedure are well documented [14, 15] and will not be presented here. The governing equations that result are:

$$\frac{1 - \nu}{1 + \nu} \nabla^2 u_s + \frac{\partial}{\partial x}\left[\frac{\partial u_s}{\partial x} + \frac{\partial v_s}{\partial y}\right] = 0 \tag{3-2a}$$

$$\frac{1 - \nu}{1 + \nu} \nabla^2 v_s + \frac{\partial}{\partial y}\left[\frac{\partial u_s}{\partial x} + \frac{\partial v_s}{\partial y}\right] = 0 \tag{3-2b}$$

$$D\left[\frac{\partial^2 \phi}{\partial x^2} + \frac{1 - \nu}{2}\frac{\partial^2 \phi}{\partial y^2} + \frac{1 - \nu}{2}\frac{\partial^2 \psi}{\partial x \partial y}\right] + kGh\left[\frac{\partial w}{\partial x} + \phi\right] = 0 \tag{3-2c}$$

$$D\left[\frac{1 - \nu}{2}\frac{\partial^2 \psi}{\partial x^2} + \frac{\partial^2 \psi}{\partial y^2} + \frac{1 - \nu}{2}\frac{\partial^2 \phi}{\partial x \partial y}\right] + kGh\left[\frac{\partial w}{\partial y} - \psi\right] = 0 \tag{3-2d}$$

$$kGh\left[\nabla^2 w + \frac{\partial \phi}{\partial x} - \frac{\partial \psi}{\partial y}\right] = 0 \tag{3-2e}$$

where ν is Poisson's ratio, $D = Eh^3/12(1 - \nu^2)$ is the plate bending rigidity, $G = E/2(1 + \nu)$ is the shear modulus, and k is a shear factor that corrects for the constant shear (no warping) assumption. Note that the extensional and bending problems decouple for the elastic case; the first two of equations 3-2 contain only membrane terms while the remaining three contain only bending terms.

The boundary conditions, as expected, also decouple. Along the boundary $x = x_o$, the natural and kinematic boundary conditions may be written as:

Either $N_x = 0$ or u_s is prescribed (3-3a)

Either $N_{xy} = 0$ or v_s is prescribed (3-3b)

Either $M_x = 0$ or ϕ is prescribed (3-3c)

Either $M_{xy} = 0$ or ψ is prescribed (3-3d)

Either $Q_x = 0$ or w is prescribed (3-3e)

Similarly, along $y = y_o$:

Either $N_{yx} = 0$ or u_s is prescribed (3-4a)

Either $N_y = 0$ or v_s is prescribed (3-4b)

Either $M_{yx} = 0$ or ϕ is prescribed (3-4c)

Either $M_y = 0$ or ψ is prescribed (3-4d)

Either $Q_y = 0$ or w is prescribed (3-4e)

3.2 The Closure and No Closure Cases

With the general fundamentals of Mindlin theory defined, more specific aspects of the problem may be considered. The analysis consists primarily of a comparison of two cases.

The first case, designated here as the no closure case, allows the compression sides of the crack surfaces to overlap, or pass through each other. The crack surface is modelled as stress free

in terms of the Mindlin theory, which means that the bending moment, twisting moment, and shear force resultants are zero on the crack face. Thus, for the no closure problem, the boundary conditions for the crack surface are (with reference to Figure 3-1):

$$M_{yx} = 0 \quad (-a < x < a, 0, z) \tag{3-5a}$$

$$M_y = 0 \quad (-a < x < a, 0, z) \tag{3-5b}$$

$$Q_y = 0 \quad (-a < x < a, 0, z) \tag{3-5c}$$

Since there is no extensional loading and the extensional and bending problems decouple, the boundary conditions for N_{yx} and N_x are automatically satisfied.

The second case, designated here as the closure case, models the actual physical situation that occurs for the bending problem; that is, as bending occurs, the crack surfaces come together at the compression surface and do not overlap. The crack surface is still modelled as stress free with the same boundary conditions as for the no closure case. However, an additional constraint equation must be added to account for the closure phenomenon. This constraint condition takes the form of zero displacement v wherever the crack surfaces come together. For example, for closure at the compression surface the constraint equation is

$$v(x,0,-h/2) = v_s(x,0) + h\psi(x,y)/2, \quad -a < x < a \tag{3-6}$$

Thus, the primary effects of the closure phenomenon are to introduce additional constraint into the bending problem and

increase the complexity of the solution due to the interaction of the extensional and bending terms, v_s and ψ, respectively.

3.3 Elasto-Plastic Formulation

The elasto-plastic analysis of the plate bending problem also involves additional complexity. For the elasto-plastic formulation incremental, rather than accumulated, quantities are used [12, 18]. Therefore, the assumed displacement field is recast in the form of displacement rates, i.e.,

$$\dot{u}(x,y,z) = \dot{u}_s(x,y) + z\dot{\phi}(x,y) \tag{3-7a}$$

$$\dot{v}(x,y,z) = \dot{v}_s(x,y) - z\dot{\psi}(x,y) \tag{3-7b}$$

$$\dot{w}(x,y) = \dot{w}(x,y) \tag{3-7c}$$

and the strain-displacement relations are recast in rate form as

$$\dot{\varepsilon}_{ij} = \frac{1}{2}(\dot{u}_{i,j} + \dot{u}_{j,i}) \tag{3-8}$$

The incremental stresses and strains are related via a flow rule; in this case, the flow rule used is the form developed by Fung [19] from Drucker's hypothesis. The flow rule may be written as

$$2\mu\dot{\varepsilon}_{ij} = \dot{\sigma}_{ij} - \left[\frac{\nu}{1+\nu}\right]\dot{\sigma}_{kk}\delta_{ij} + (\mu/\mu_o^{(p)})\,s_{ij}s_{k\ell}\dot{\sigma}_{k\ell}/3\tau_o^2 \tag{3-9}$$

where μ is the elastic shear modulus, $\mu_o^{(p)}$ is the plastic octahedral shear modulus, δ_{ij} is the Kronecker delta, ν is Poisson's ratio, τ_o is the octahedral shear stress, and s_{ij} is the deviator of the stress tensor.

The governing differential equations and boundary conditions are obtained in a manner analogous to the elastic formulation; that is, an energy-like functional analogous to the potential energy functional is minimized. Although somewhat tedious, this procedure is quite straightforward and leads to governing equations and boundary conditions in which the extensional and bending terms are fully coupled. A more detailed discussion of this procedure is contained in Appendix B.

3.4 Additional Comments

Although the formulation of the bending problem, both with and without the closure constraint, is straightforward, the problem is sufficiently complex to inhibit a closed form solution. Due to this inherent complexity, published solutions to the problem have been the result of numerical analyses. For example, Hartranft and Sih [5] solved the elastic, no closure problem by reducing Reissner's equations to a single integral equation which they solved numerically. Jones [11] later used a finite element analysis based on Kirchhoff theory to solve the elasto-plastic problem, including the effects of closure. Thus, to complete the development of solutions to the bending problem, a finite element approach based on Mindlin theory is used here to analyze closure effects in the bending of an elasto-plastic, cracked plate.

FIGURE 3-1

CRACKED PLATE GEOMETRY
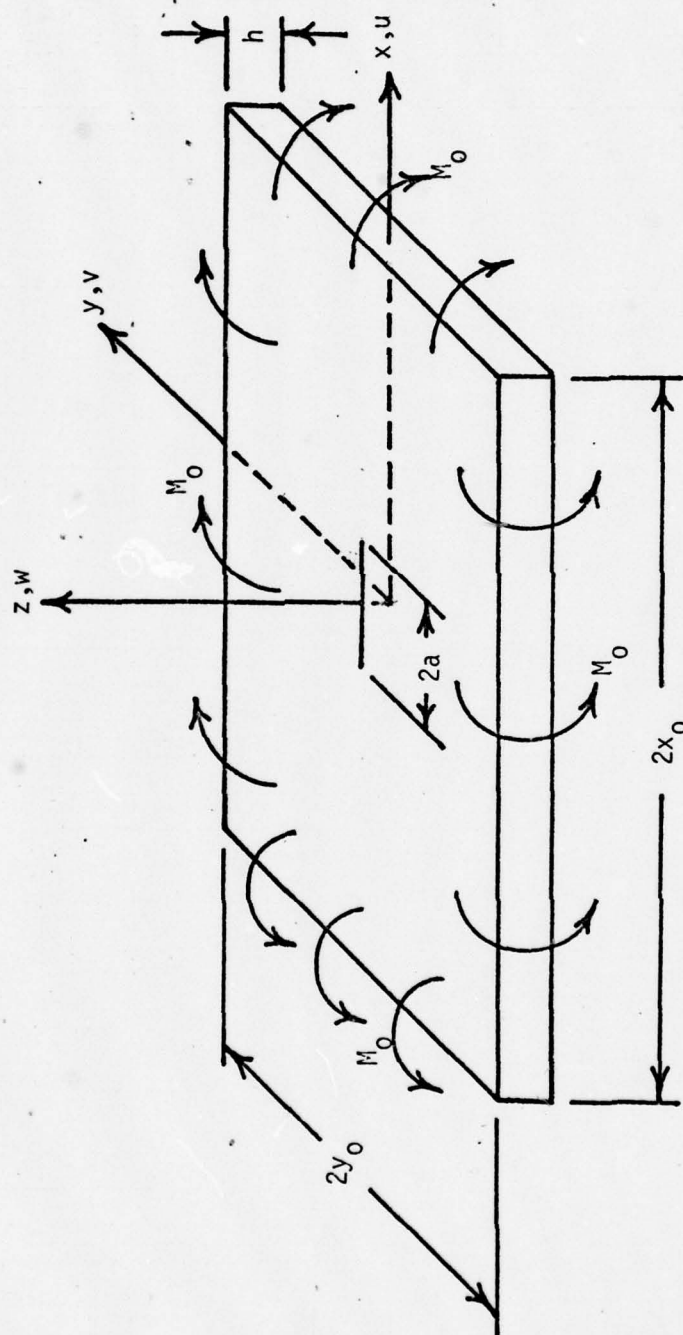
CHAPTER IV

FINITE ELEMENT REPRESENTATION

The finite element method is well recognized as a convenient and accurate means of analyzing complex elastic and elasto-plastic problems where theoretical solutions are not tractable. For the analyses presented here, a finite element approach based on the assumed displacement field of Mindlin's sixth order plate theory was used. The discussion that follows presents the details of this finite element representation.

4.1 The Eight-Node Isoparametric Plate Element

The element chosen for the analysis is the eight-node, isoparametric plate element as shown in Figure 4-1. This element was developed by Ahmad, et al. [21] as a specialized form of the 20-node isoparametric solid element. In their development, the strain energy of stresses normal to the midplane is ignored and straight lines initially normal to the midplane are constrained to remain straight. This results in a reduction of the number of nodes to eight, and, since the straight lines initially normal to the midplane are not constrained to remain normal to the midplane during deformation, the element is capable of modelling transverse shear deformation.

As is the nature of isoparametric elements, the geometry and displacements are defined in terms of the same interpolation functions. The eight-node element is a plane quadratic element,

and the interpolation functions are written in terms of the natural coordinate system (ξ, η):

$$N_i = \frac{1}{4}(1 + \xi\xi_i)(1 + \eta\eta_i)(\xi\xi_i + \eta\eta_i - 1)(\xi_i^2\eta_i^2)$$

$$+ \frac{1}{4}(1 - \xi^2)(1 + \eta\eta_i)(1 - \xi_i^2)$$

$$+ \frac{1}{2}(1 + \xi\xi_i)(1 - \eta^2)(1 - \eta_i^2) \qquad (4-1)$$

where ξ_i and η_i are the nodal values of ξ and η, i.e., -1, 0, and 1. The geometry and displacements are then defined as

$$x = \sum_{i=1}^{8} N_i x_i \qquad y = \sum_{i=1}^{8} N_i y_i$$

$$u = \sum_{i=1}^{8} N_i u_i \qquad v = \sum_{i=1}^{8} N_i v_i \qquad w = \sum_{i=1}^{8} N_i w_i$$

where x_i, y_i, u_i, v_i and w_i refer to nodal quantities.

Based on Mindlin theory, the assumed displacements for the element are

$$u(x,y,z) = u_s(x,y) + z\phi(x,y) \qquad (4-2a)$$

$$v(x,y,z) = v_s(x,y) - z\psi(x,y) \qquad (4-2b)$$

$$w(x,y) = w(x,y) \qquad (4-2c)$$

where $-h/2 \leq z \leq h/2$ is the through-thickness coordinate and where u_s, v_s, ϕ, ψ, and w are the nodal degrees of freedom defined

as follows: u_s and v_s are the inplane translations in the x and y directions, respectively; ϕ and ψ are the rotations about the y and x axes, respectively; and w is the transverse deflection. Thus, there are five degrees of freedom per node and 40 degrees of freedom per element.

With the displacement field defined, the stiffness formulation proceeds in the usual manner. Note that the in plane integration leading to the (elastic) stiffness matrix is performed numerically via Gauss quadrature; the integration through the thickness is explicit. Thus, stresses and strains are typically calculated at Gauss points rather than at the nodes. Cook [22], as well as others, has demonstrated the validity of the isoparametric formulation and has shown that rigid body modes, constant strain behavior, and interelement compatibility are provided for. For a more detailed discussion of this element, or of the isoparametric formulation, see References 21, 22 and 23.

4.2 The Elasto-Plastic Finite Element Program

Having selected the eight-node isoparametric element, a finite element program, PLABEP, was developed that incorporated that element. Although the program was written with as much generality as possible, some portions of the code were specifically tailored to meet the requirements of the bending problem only. That is, only extensional and bending loads and prescribed zero displacements are admissible. However, other boundary conditions could easily be introduced if desired.

An elastic version of the program was developed and verified first. At each point in the development a series of test cases or check problems were run to insure the accuracy of the program. A discussion of the verification procedure and of the results obtained is contained in Appendix C. After the elastic program was completed and verified, a series of elastic problems were run that included and excluded closure effects. The results of this elastic study are contained in Chapter V.

Once the elastic study was complete, the program was modified to accept elasto-plastic material behavior. The approach taken was to solve a series of incremental, quasi-linear sub-problems. The results of the sub-problems were then summed to form accumulated values. Thus, the total solution is presented in terms of these accumulated quantities and is highly nonlinear. For a more detailed discussion of this procedure, see Reference 24.

An important feature of the elasto-plastic analyses is the proper characterization of the yielding process. Since yielding initiates at the plate surfaces and propagates through the thickness, an elastic core is preserved for most of the loading sequence. To correctly model this situation, the stiffness formulation through the thickness is performed numerically at Gauss points where yielding has begun. A variation of Gauss quadrature called the Lobatto formula [25] was used (with eleven points through the thickness) in order to obtain information on yielding at the surfaces of the plate as well as the interior. As outlined in Appendix C, checks were also made on the validity

of the elasto-plastic program before the elasto-plastic plate
bending analyses were made.

4.3 <u>Plate</u> <u>Geometry</u> <u>and</u> <u>Material</u> <u>Properties</u>

The capability developed in PLABEP is now applied to a
rectangular plate containing a centrally located, through crack
subjected to a uniform bending load at the plate boundaries (see
Figure 3-1). The plate dimensions are set so that the finite
plate models an infinite plate with sufficient accuracy that
finite plate corrections may be neglected. In addition, the
plate width and length to crack length ratios are large enough
that the plate boundaries do not interfere with the crack
behavior. The specific plate ratios and dimensions were chosen
to replicate the problem solved by Jones [11] and thus facilitate
comparisons of the two solutions. Figure 4-2 shows the finite
element model and pertinent dimensionless ratios for the plate
bending problem. Note that due to the symmetry of the problem,
only a quarter of the plate need be modelled. The finite element
model consists of 66 elements, 233 nodes and 1165 degrees of
freedom with the elements around the crack tip being (a/16) square.
This model is used for both the closure and the no closures cases.

The material properties for the problem are shown in Figure
4-3. The material chosen is a work hardening material that follows
the Ramsberg-Osgood power law

$$\tau_{oct} = \tau_L [(\frac{\gamma^{(p)}_{oct}}{\varepsilon_y})^n + 1] \qquad (4-3)$$

where τ_{oct} is the octahedral shear stress, $\gamma^{(p)}_{oct}$ is the plastic octahedral shear strain, τ_L is the proportional limit, and ε_y and n are constants. The PLABEP program uses discrete points on the curve defined by equation (4-3); the spacing between the points is chosen to be roughly proportional to the curve's radius of curvature. The particular material used here is similar to the 2000 series of soft aluminums and was chosen primarily to facilitate comparisons with the results reported by Jones [11] and Swedlow, et al. [12]. To complete the material description, it is necessary to define two elastic constants. For this problem, the elastic constants are the elastic modulus E and Poisson's ratio ν with the values shown in Figure 4-3.

4.4 The No Closure and Closure Cases

There are two cases to be analyzed with the finite element model: the no closure case, which neglects the effects of crack closure, and the closure case, which includes these effects. For each case it remains to specify the boundary conditions and loading parameters.

For both cases, the boundary conditions consist of an applied uniform bending moment at the exterior plate boundaries, symmetry conditions along the interior edges formed by the quarter

plate model, and a stress free surface (in the Mindlin sense) along the crack face. With reference to Figure 4-2, the complete boundary conditions are as follows:

Along the line $x = x_0$,

$$x = x_0, \quad 0 \leq y \leq y_0 \qquad N_x = 0 \qquad N_{xy} = 0$$
$$M_{xy} = 0 \qquad Q_x = 0$$
$$M_x = M_0$$

Along the line $y = y_0$,

$$0 \leq x \leq x_0, \quad y = y_0 \qquad N_y = 0 \qquad N_{yx} = 0$$
$$M_{yx} = 0 \qquad Q_y = 0$$
$$M_y = M_0$$

Along the y axis,

$$x = 0, \quad 0 \leq y \leq y_0 \qquad u_s = 0 \qquad \phi = 0$$
$$N_{xy} = 0 \qquad M_{xy} = 0$$
$$Q_x = 0$$

Along the x axis,

$$a \leq x \leq x_0, \quad y = 0 \qquad v_s = 0 \qquad \psi = 0$$
$$N_{yx} = 0 \qquad M_{yx} = 0$$
$$Q_y = 0$$

$$0 \leq x < a, \quad y = 0 \qquad N_{yx} = 0 \qquad N_y = 0$$
$$M_{yx} = 0 \qquad M_y = 0$$
$$Q_y = 0$$

At $x = 0$, $y = 0$ $\qquad w = 0$

Consideration of the closure case shows that the boundary conditions remain the same, but that an additional constraint equation must be added to account for the crack face interference at the compression surface. As discussed in Chapter III, the closure constraint equation is obtained from the Mindlin displacement relations of equations (3-7) (or equations (4-2)). Referring to Figure 4-2, the closure constraint requires that the displacement v in the y-direction be zero at the compression surface, $z = -h/2$, of the crack face. Along the crack face,

$$v(x,0,z) = v_s(x,0) - z\psi(x,0) \tag{4-4}$$

Therefore the constraint equation is

$$v_s(x,0,-h/2) + \frac{h}{2} \psi(x,0) = 0, \quad 0 \le x < a \tag{4-5}$$

The constraint equations are introduced into PLABEP through the use of Lagrange multiplier concepts. One discussion of the use of Lagrange multipliers may be found in Reference 26; a detailed discussion of the implementation of the constraints into PLABEP is given in Reference 27. The resulting Lagrange multipliers are given a physical interpretation as the compressive force at the contact line along the crack translated into discrete values. The Lagrange multiplier can also be interpreted as a statically equivalent force and moment at each node to represent the inplane loads and bending moment that are present due to the closure induced extensional-bending interaction.

The loading for both cases is applied incrementally through the applied uniform moment, M_o, at the plate's exterior boundaries. Following the procedure outlined by Swedlow [24], the first load step is elastic with the load scaled so that the most highly stressed point in the domain just exceeds the proportional limit, e.g., $\tau_o/\tau_L = 1.00010$. The remaining load steps are applied at 4% of the accumulated load for the previous load step. Table 4-1 lists the load increments and accumulated load levels for the two cases. Note that the initial load step for the closure case corresponds to the ninth load step of the no closure case. The elastic and elasto-plastic results due to these loadings are discussed in the next chapter.

4.5 Computational Benchmarks

The elastic and elasto-plastic problems were obtained on a Digital Equipment Corporation 2050 computer. Geometrically, the bending problem comprised 233 nodes and 1165 degrees of freedom. For the closure problem there were ten additional degrees of freedom due to the presence of the Lagrange multipliers. Approximate core requirements were 135K words for the elastic problem and 210K words for the elasto-plastic problem. The approximate execution times for each problem are shown in Table 4-2.

FIGURE 4-1

THE EIGHT-NODE ISOPARAMETRIC ELEMENT
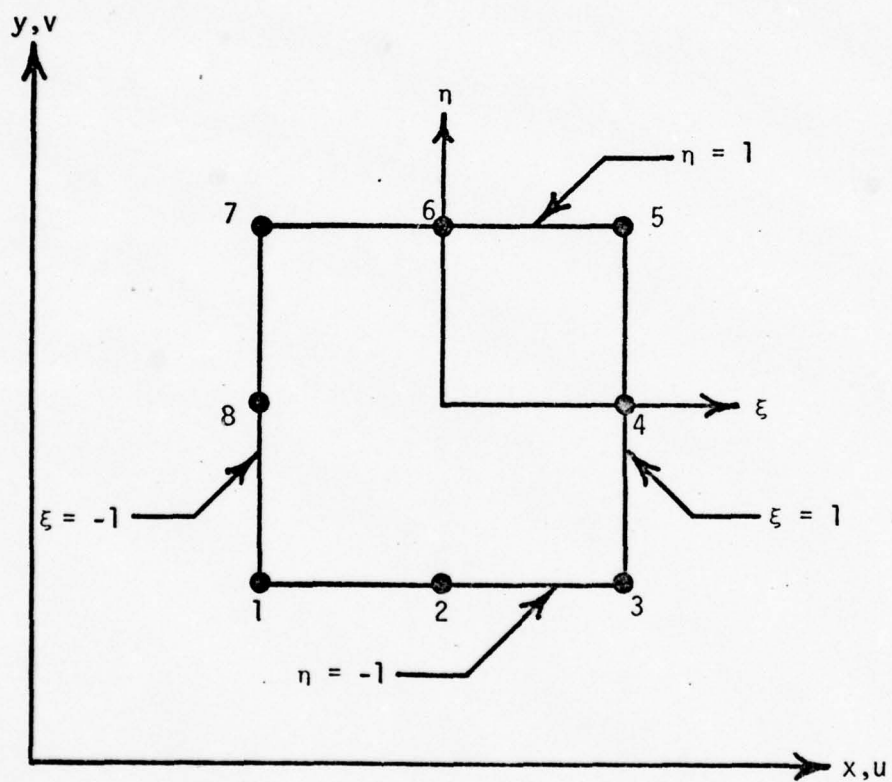
FIGURE 4-2

FINITE ELEMENT MODEL
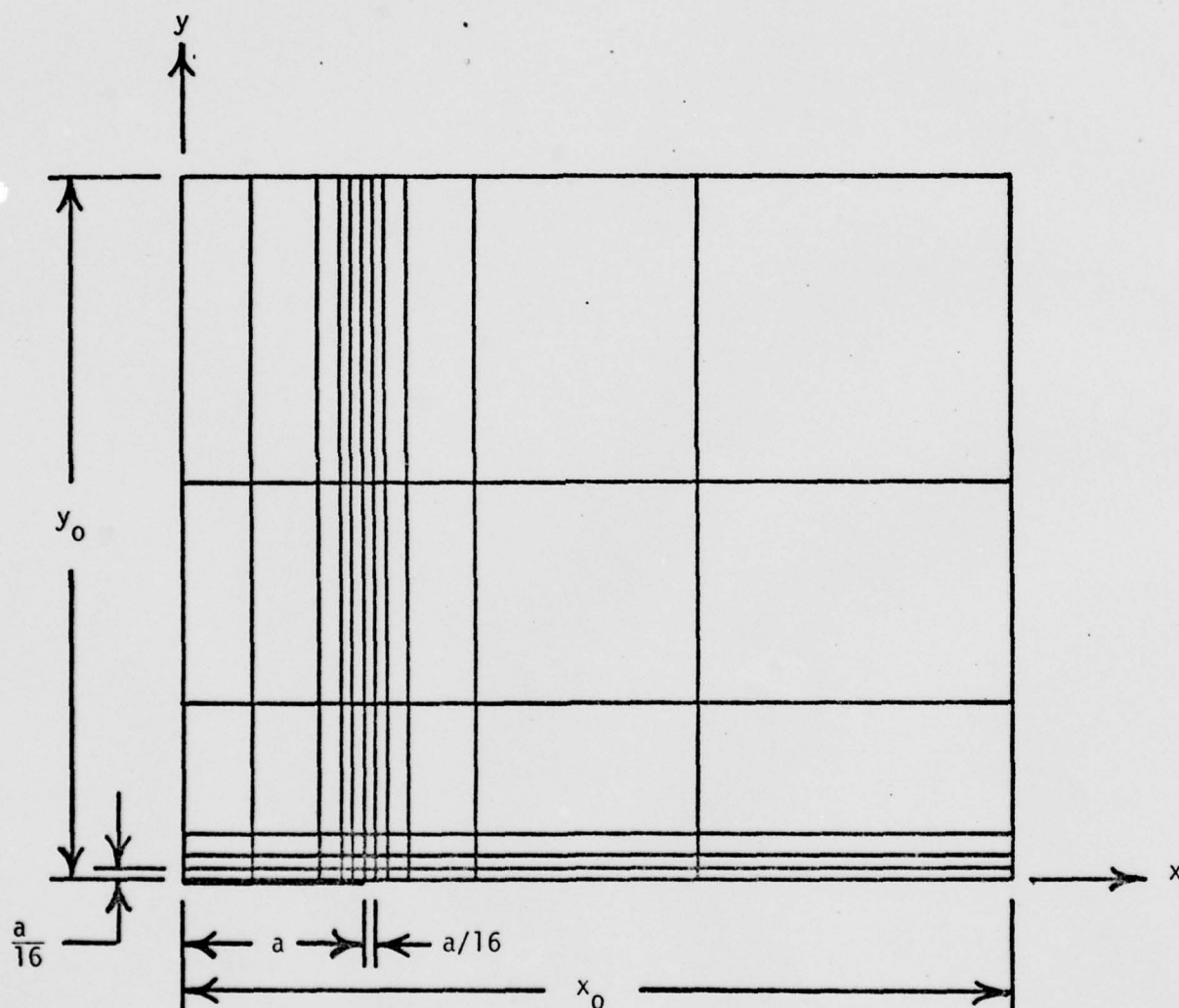
$$\frac{x_o}{a} = 4.625 \qquad \frac{y_o}{a} = 4.000 \qquad \frac{2a}{h} = 4.000 \qquad h = 1.000$$

FIGURE 4-3

MATERIAL PROPERTIES

Material Representation

(Note that the parameters below replicate those used by Jones [11], and, except for minor variations in E and ν, the same as those used by Swedlow, et al. [12].)

$E = 10 \times 10^6$

$\nu = 0.3$

$\varepsilon_y = .009716$

$n = .3964$

$\tau_L = \sqrt{2}\ \sigma_L/3$

$\sigma_L = 11,500$ psi

$$\tau_{oct} = \tau_L \left[\left(\frac{\gamma_{oct}^{(p)}}{\varepsilon_y} \right)^n + 1 \right]$$

$\gamma_{oct}^{(p)}$, 10^3 in./in.

τ_{oct}, ksi
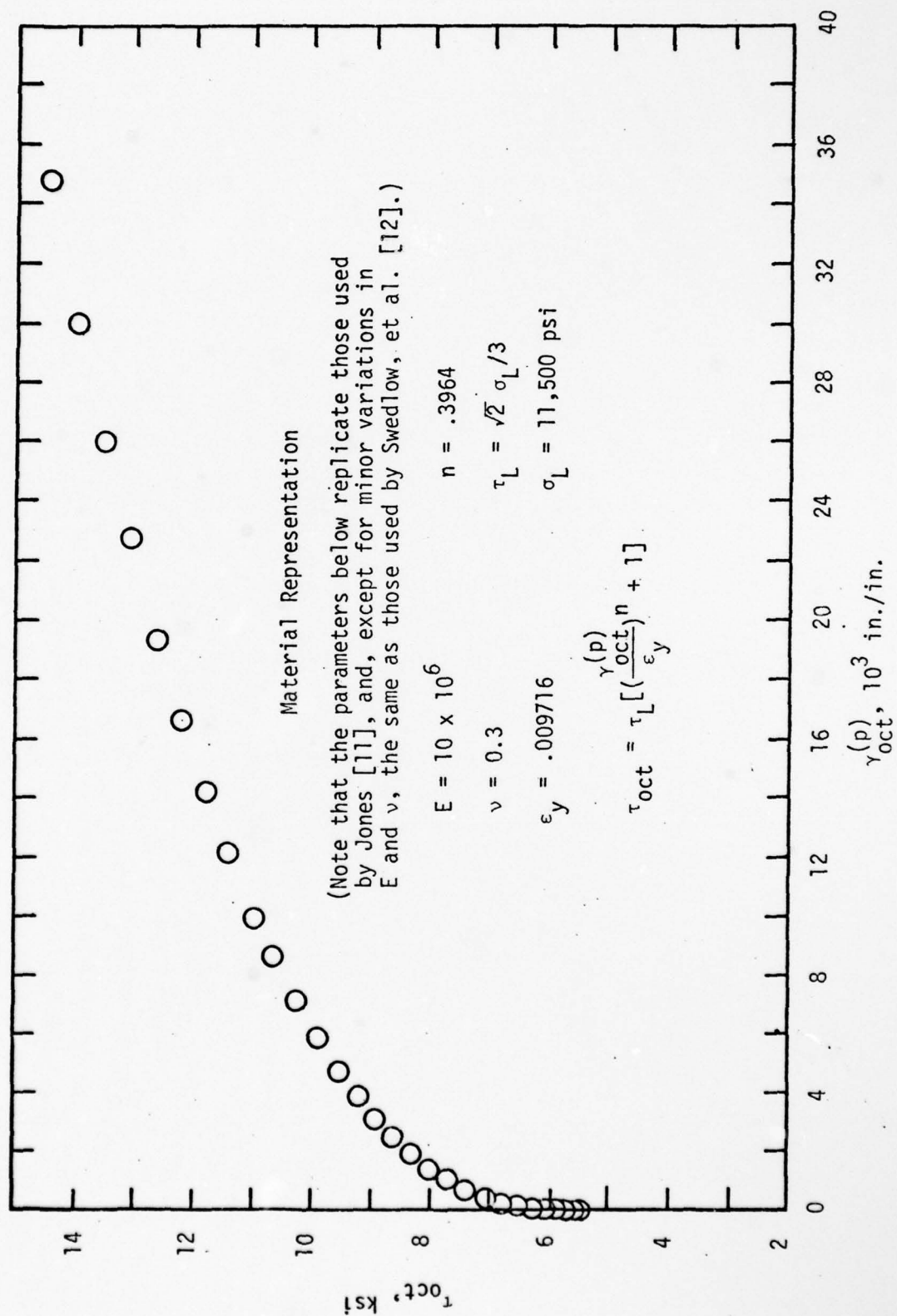
TABLE 4-1

INCREMENTAL LOAD STEPS AND ACCUMULATED

LOAD VALUES FOR THE NO CLOSURE AND CLOSURE CASES

Load Step		Applied Moment Increment $[\frac{\text{in-lbs}}{\text{in}}]$	Accumulated Value $[\frac{\text{in-lbs}}{\text{in}}]$
No Closure	Closure		
1	-	479.8	479.8
2	-	19.2	499.0
3	-	20.0	519.0
4	-	20.7	539.7
5	-	21.6	561.3
6	-	22.5	583.8
7	-	23.3	607.1
8	-	24.2	631.4
9	1	25.3*	656.7
10	2	26.2	682.9
11	3	27.4	710.3
12	4	28.4	738.7
13	5	29.5	768.2
14	6	30.7	798.9
15	7	32.0	830.9
16	8	33.2	864.1
17	9	34.6	898.7
18	10	35.9	934.6
19	11	37.4	972.0
20	12	38.9	1010.9
21	13	40.4	1051.3
22	14	42.1	1093.4
23	15	43.7	1137.1
24	16	45.5	1182.6
25	17	47.3	1229.9
26	18	49.2	1279.1
27	19	51.1	1330.2
28	20	53.2	1383.4
29	21	55.4	1438.8
30	22	57.5	1496.3
31	23	59.9	1556.2
32	24	62.2	1618.4
33	25	64.8	1683.2
34	26	67.3	1750.5
35	27	70.0	1820.5
36	28	72.8	1893.3

*The applied moment increment for load step 1 of the closure case is $M_0 = 656.7$.

TABLE 4-2

PROBLEM EXECUTION TIMES

Case	Elastic	Elasto-Plastic
No Closure	2:17 Minutes	1:58 Hours (48 Load Steps)
Closure	2:21 Minutes	1:45 Hours (40 Load Steps)

Relative to the above execution times, the pertinent parameters are:

- Number of elements: 66

- Number of nodes: 233

- Total degrees of freedom: 1165

- Number of constraint equations (for the closure case only): 10

- Bandwidth: 115

- Core requirements (approx.), elastic: 135K

- Core requirements (approx.), elasto-plastic: 220K

- Solution technique: Gauss elimination (band form)

CHAPTER V
ELASTIC RESULTS

The elastic results obtained from the analyses of the closure
and no closure cases are presented here. In order to make a direct
comparison of the two cases, the analyses were made for the same
value of uniform applied moment M_0. Presentation of the results
is made in graphical form to clarify the comparisons.

5.1 Displacement Results

Figure 5-1 shows the transverse deflection w along the crack
flank. The data is presented in nondimensional form where the
normalizing factor $a^2 M_0/2D(1 + \nu)$ is the coefficient of the
$(x^2 + y^2)$ solution to the pure bending problem multiplied by the
square of the crack length. The figure shows that the presence
of the crack produces a substantial increase in transverse
deflection over the uncracked solution as expected. The effect
of closure is to reduce the transverse deflection of the crack
27-31% when compared with the no closure values. These results
indicate that closure has a moderate effect on the transverse
deflection, and that the effect is fairly constant over the
crack flank.

Figures 5-2 and 5-3 show the effects of closure on the
transverse slopes, ϕ and ψ, along the crack flank. The normalizing
constant for these quantities is the coefficient of the pure
bending solution for the transverse slopes multiplied by the

crack length. Although the rotation of the crack flank about the y-axis ϕ deviates from the linear behavior of the no crack problem as shown in Figure 5-2, the differences between the closure and no closure results are not pronounced. In this case, the effect of closure is to reduce ϕ by 10-20% from the no closure results. Since ϕ represents the slope parallel to the crack face, this result is not unexpected. In contrast, the effects of closure on the rotation of the crack flank about the x-axis are very pronounced. Figure 5-3 shows that the effect of closure is to reduce ψ from 59 to 67 percent below the no closure values. Thus, ψ is very sensitive to the closure phenomenon.

The elastic crack opening, represented by the displacement v of the crack flank in the y-direction, is shown in Figure 5-4 with the values of v normalized in the same manner as the transverse deflection. The results for the no closure case show that the displacements of the tension and compression surfaces are equal in magnitude, but opposite in direction; the displacements of the compression surface are represented as negative values in the figure. As a result of symmetry and the Mindlin assumption that straight lines normal to the midplane remain straight during bending, the midplane has zero v displacement for the no closure case. In contrast, the closure model produces results that are much different. The crack opening on the tension surface is reduced by one third close to the crack tip and by 20% further away. Due to the extension-bending interaction of the closure model, the midplane is no longer undeformed, but displaces

an amount equal to one half the corresponding values of the tension surface. The displacement of the compression surface is now zero, clearly indicating that the closure constraint is being satisfied. Thus, the effects of closure are to reduce the crack opening displacement and produce a crack profile that is less blunt than that of the no closure case.

5.2 Stress Results

The elastic stress results provide additional insight into the effects of closure. Figures 5-5 and 5-6 show the elastic bending stress distributions for σ_x and σ_y along the x-axis. The stresses are normalized by the applied stress σ_o, and the distance along the x-axis is represented by $(x - a)/a$ (i.e., negative values represent the crack face, positive values represent points ahead of the crack). The stress distributions in both figures exhibit the characteristic $(r)^{-1/2}$ singularity near the crack tip. The distribution of $(\sigma_x/\sigma_o)_B$ in Figure 5-5 indicates minimal closure effects as expected. Figure 5-6, showing the $(\sigma_y/\sigma_o)_B$ distribution, indicates that the crack face is stress free for the no closure case. However, for the closure case the crack face interference along the compression edge produces an in plane compressive load normal to the crack face along that line. The static equivalent of this force at the midplane requires the addition of a couple to satisfy equilibrium. As a result of these pseudo-forces and moments at the midplane, a nonzero bending

stress along the crack face is calculated for the closure case
as shown in Figure 5-6. Note that this is a pseudo-stress,
and the stress free boundary condition along the crack flank is
not being violated. Further discussion of this point is contained
in Section 7.1e.

. The variations of σ_x and σ_y through the thickness are shown
in Figures 5-7 and 5-8 for $(r/a) = 3/16$ and $\theta = 0°$, $90°$, $180°$.
For the no closure case, the stress distributions are symmetric
about the midplane as required by pure bending. The linearity
of the stresses and the zero σ_y condition along the crack face
are also evident. For the closure case, the stresses remain
linear in z but are no longer symmetric about the midplane. The
effect of closure is to produce a neutral surface shift (based
on a zero stress definition) that is evidenced by the shift in
the stresses.

Figures 5-9 and 5-10 show the variation of the in plane
membrane loads along the $\theta = 0°$ and $\theta = 90°$ axes for the closure
case. As discussed previously, these loads arise from the
transfer of the crack face interference loads to the midplane.
The compressive forces along the contact line are represented
by the Lagrange multipliers used in the closure analysis. The
variation of these Lagrange multipliers for the corner and
midside nodes lying along the crack are shown in Figure 5-11.
The significant feature of this figure is that the forces are
all negative, indicating that the closure constraint is satisfied
along the crack.

Figure 5-12 shows the variation of the inplane shear stress τ_{xy} with thickness for $\theta = 90°$. The symmetric distribution for the no closure case and the shift induced by closure that was observed for σ_x and σ_y are also present here. Along the crack flank, τ_{xy} is zero as required by the boundary conditions; and along the $\theta = 0°$ axis, τ_{xy} is zero as required by symmetry.

The importance of the transverse shear stress, τ_{xz}, is shown in Figure 5-13. The contribution of the shear stress to the octahedral shear stress, τ_o, is expressed as a percentage, and these values are shown for the crack face and along the $\theta = 0°$ axis. With and without closure, τ_{xz} has a significant influence on the stress distribution along the crack face, contributing up to 86% and 58% of τ_o near the crack tip for the no closure and closure cases, respectively. Ahead of the crack, the shear effect is less significant with maximum values of 25% without closure and 12% with closure near the crack tip. The contribution of the transverse shear then drops off rapidly and approaches zero within one crack length. The effect of closure is to reduce the shear effect, with the greatest reductions occurring near the crack tip. Note that the contribution of τ_{yz} is negligible both along and ahead of the crack as expected.

5.3 Linear Fracture Mechanics Interpretation

The elastic results may also be interpreted in terms of linear elastic fracture mechanics. The focus here is on the

extraction of elastic bending stress intensity factors from the displacement and stress results with the intent of making a qualitative analysis of closure effects.

Figure 5-14 shows the results of using the displacement extrapolation method [28] to obtain values for an apparent elastic bending stress intensity factor defined as $K_A = Ev/\sqrt{r}$. A dimensionless form of K_A defined by

$$Q = K_A/\sigma_o\sqrt{\pi a}$$

is obtained for each case by extrapolation of the crack opening displacement v to the intercept point $(r/a = 0)$. Although displacement data generally provides for a more accurate determination of stress intensity factors, the results shown can only be used qualitatively since there are no displacement relations for Mindlin theory that correlate the displacements with the stress intensity factor. The results do indicate though that the bending stress intensity factor is reduced by about one third when the closure constraint is present.

As an alternative to using the crack opening displacement v Wilson and Thompson [30] have indicated that for Kirchhoff theory, the transverse deflection w is more sensitive to the determination of the bending stress intensity factor K_B^*. Using values of w at $\theta = 90°$, K_B^* is found by extrapolation of

$$K_B^* = -(9\pi)^{1/2} \frac{3 + \nu}{5 - \nu} \frac{Eh}{2(1 + \nu)} [\frac{w - w_o}{r^{3/2}}]$$

where w_o is the crack tip value of w. The results of this approach

are shown in Figure 5-15 for the dimensionless value of K_B^* given by

$$Y^* = K_B^*/\sigma_0 \sqrt{\pi a}$$

The results can be used in a qualitative sense again to conclude that the reduction in Y^* due to closure is approximately 60%. Thus, the two displacement approaches provide the same conclusion as to the effect of closure, but differ in the magnitude of the effect.

The bending stress intensity factors can also be determined from stress data as shown in Figure 5-16. The stress extrapolation method is used to determine the apparent stress intensity factor K_B^* as

$$K_B^* = \sigma_y \sqrt{2\pi r}$$

In Figure 5-16, K_B^* is shown in dimensionless form

$$S^* = K_B^*/\sigma_0 \sqrt{\pi a}$$

The stress based approach indicates a 28% decrease in S^* due to closure. These results are comparable to those obtained using the crack opening displacements v. The stress based results are also comparable to the results of Hartranft and Sih [5] (see Section 7.1h for further discussion).

5.4 Thickness Effects

As discussed in Chapter II, Hartranft and Sih [5] and Wang [6] used Reissner theory to demonstrate the effects of thickness on the bending stress distribution for the elastic, no closure case. Figures 5-17 and 5-18 show the effects of thickness (obtained from additional analyses) on the bending stress intensity factors for plate thickness to crack length ratios h/2a of .0125, .025, .075, .125, .250, .375, and .500. The values of Q and S^* for each thickness were determined by the same procedure used in Section 5.3. The results show that as thickness increases, the stress intensity factor increases, but less rapidly, for the same applied bending stress. The effect of closure is to flatten out and lower the curve, indicating that the bending stress intensity factor is much lower when closure is present and is fairly constant over a large range of thicknesses. The results of Figure 5-18 can be compared directly with those of Hartranft and Sih [5] for the no closure case. This will be done in Section 7.1i.

5.5 Uniaxial Bending Problem

The companion problem to the uniform bending problem is that of uniaxial bending about the x-axis; that is, there is no applied transverse bending stress. Results of such an analysis differ in some respects from those of the uniform bending problem. The differences include reductions in the transverse deflections w and in the rotations about the x-axis ϕ and changes in the

distribution of the bending stress σ_x. Graphical representations of these changes are not included here since they are inconsequential to the closure discussion.

Of greater interest are the quantities that remain the same. These quantities include all of the following: the rotation about the y-axis ψ, the crack opening displacement v, the bending stress distributions for σ_y, the membrane stress distributions for σ_x and σ_y, the Lagrange multipliers, the inplane shear stress distribution τ_{xy} along $\theta = 90°$, and the transverse shear effects of τ_{xz}. Thus, the effects of closure are the same for the uniaxial problem and also produce the same bending stress intensity factors (Q, S^*, Y^*).

FIGURE 5-1

TRANSVERSE DEFLECTION

OF

CRACK FLANK

$w[2D(1 + \nu)/a^2 M_o]$

○ No Closure

● Closure

—— Pure Bending Theory, No Crack

$w[2D(1 + \nu)/a^2 M_o]$

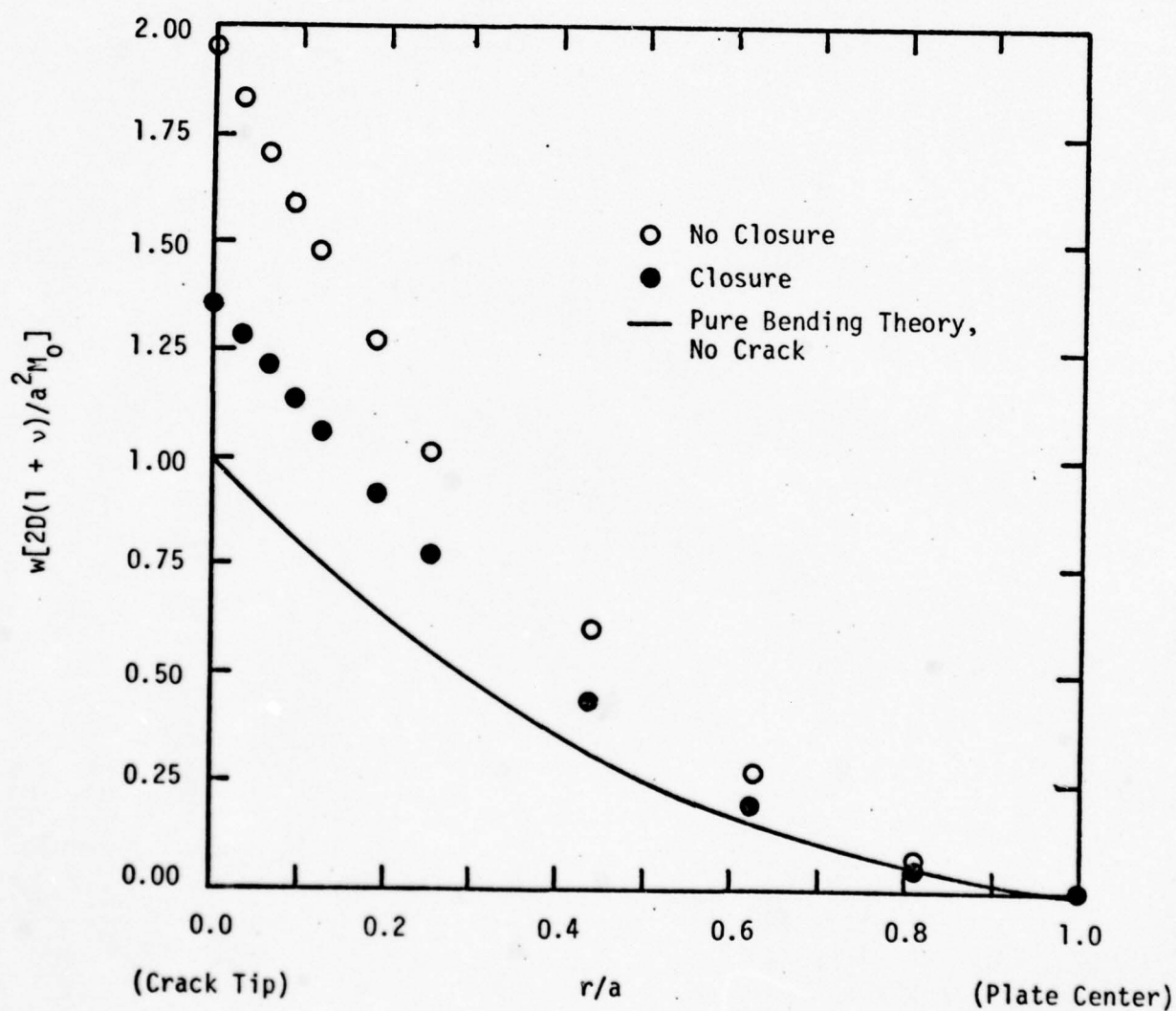(Crack Tip) r/a (Plate Center)

FIGURE 5-2

ROTATION OF CRACK FLANK

ABOUT THE Y-AXIS

$\phi[D(1 + \nu)/aM_0]$
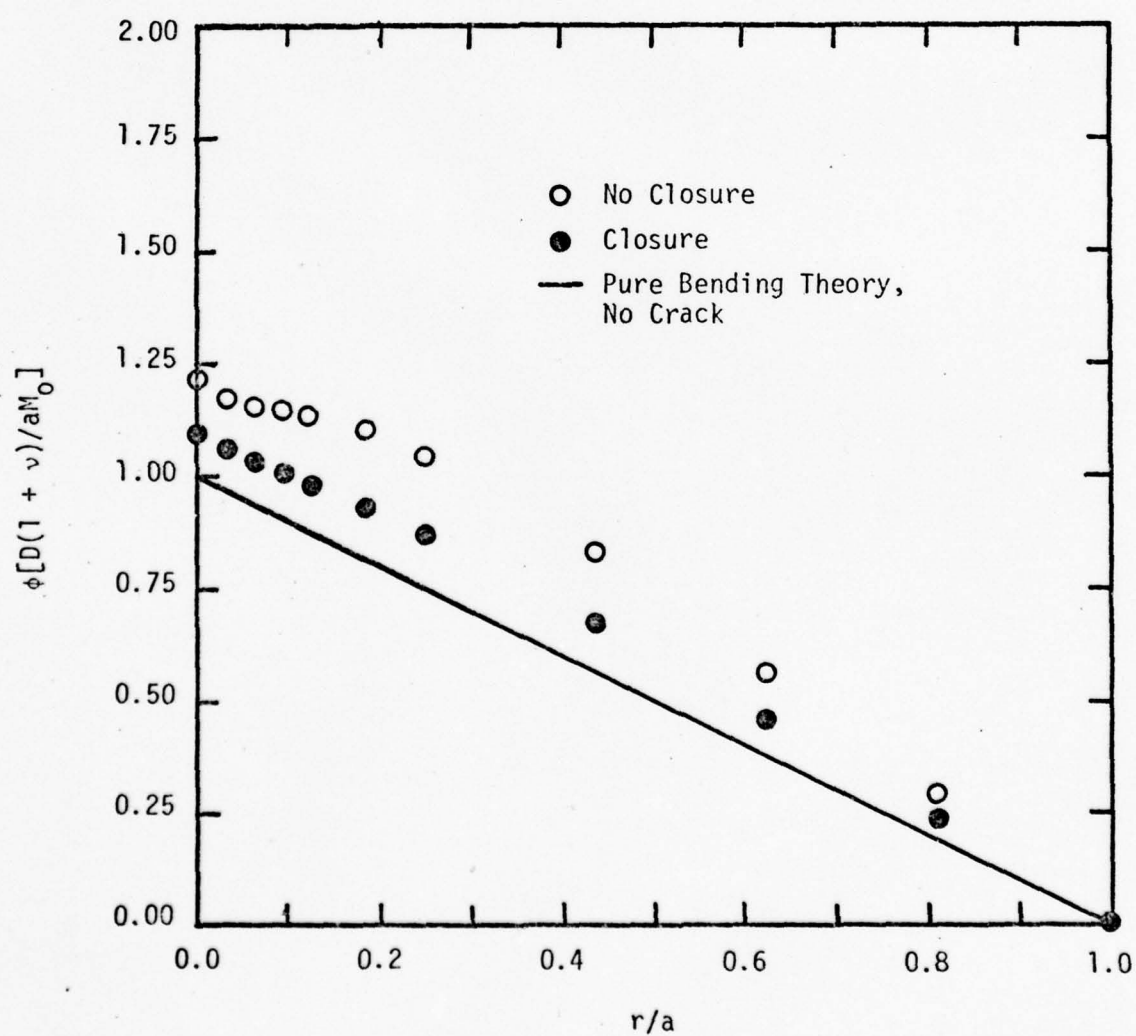
FIGURE 5-3

ROTATION OF CRACK FLANK

ABOUT THE X-AXIS

$\psi[D(1 + \nu)/aM_o]$
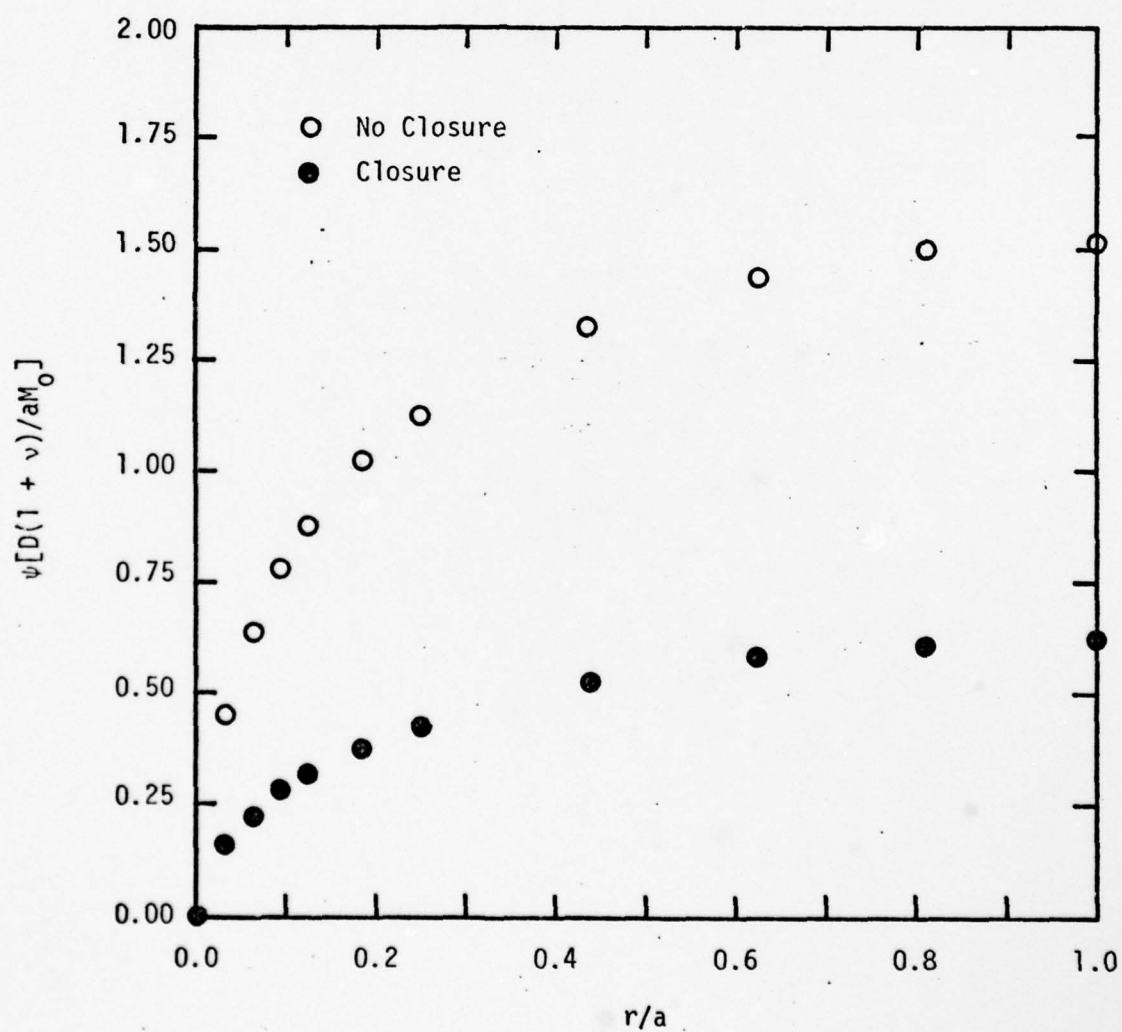
Note: For the pure bending solution, $\psi = 0$ for the r/a values shown.

FIGURE 5-4

ELASTIC CRACK OPENING

$$v[2D(1 + \nu)/a^2 M_o]$$
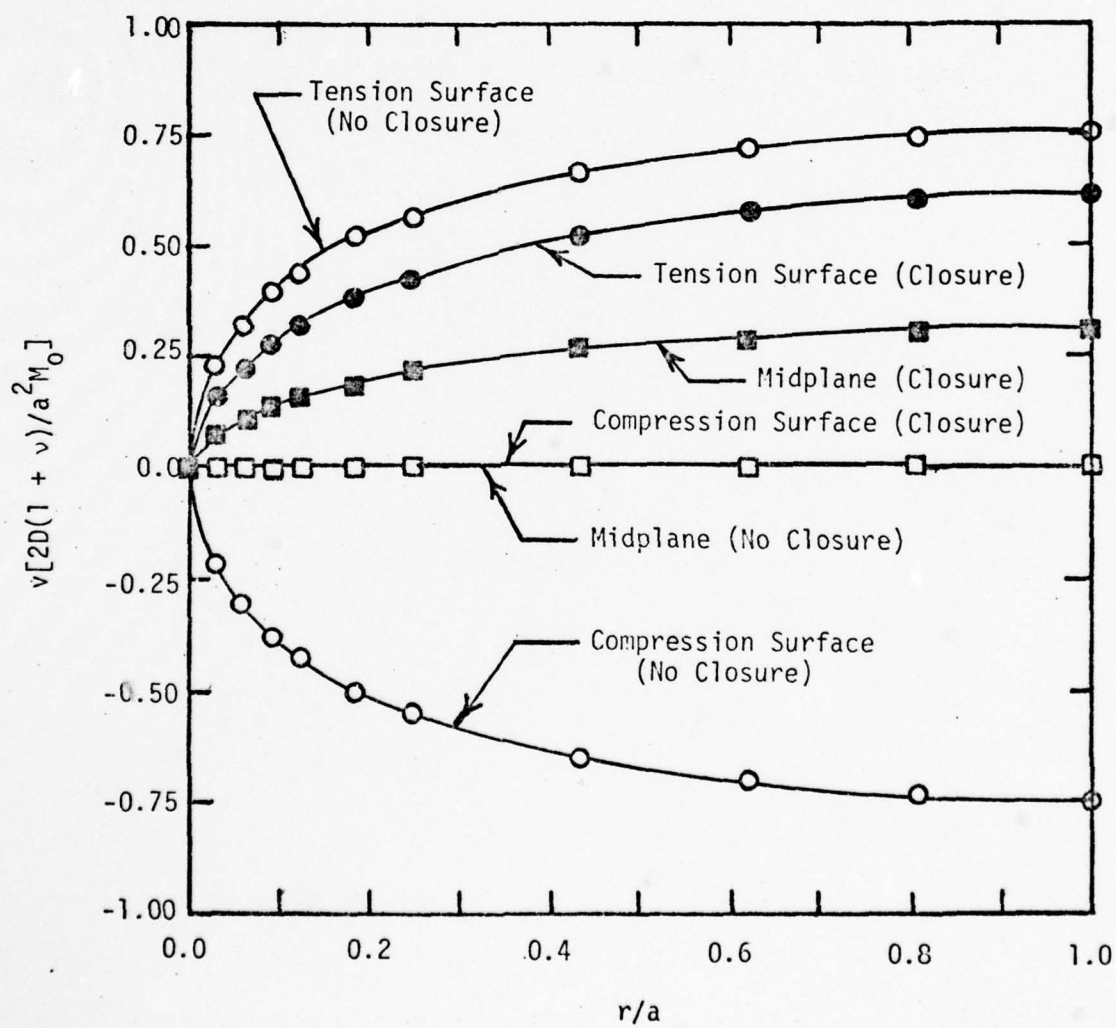
FIGURE 5-5

ELASTIC BENDING STRESS DISTRIBUTION

$(\sigma_x/\sigma_o)B$
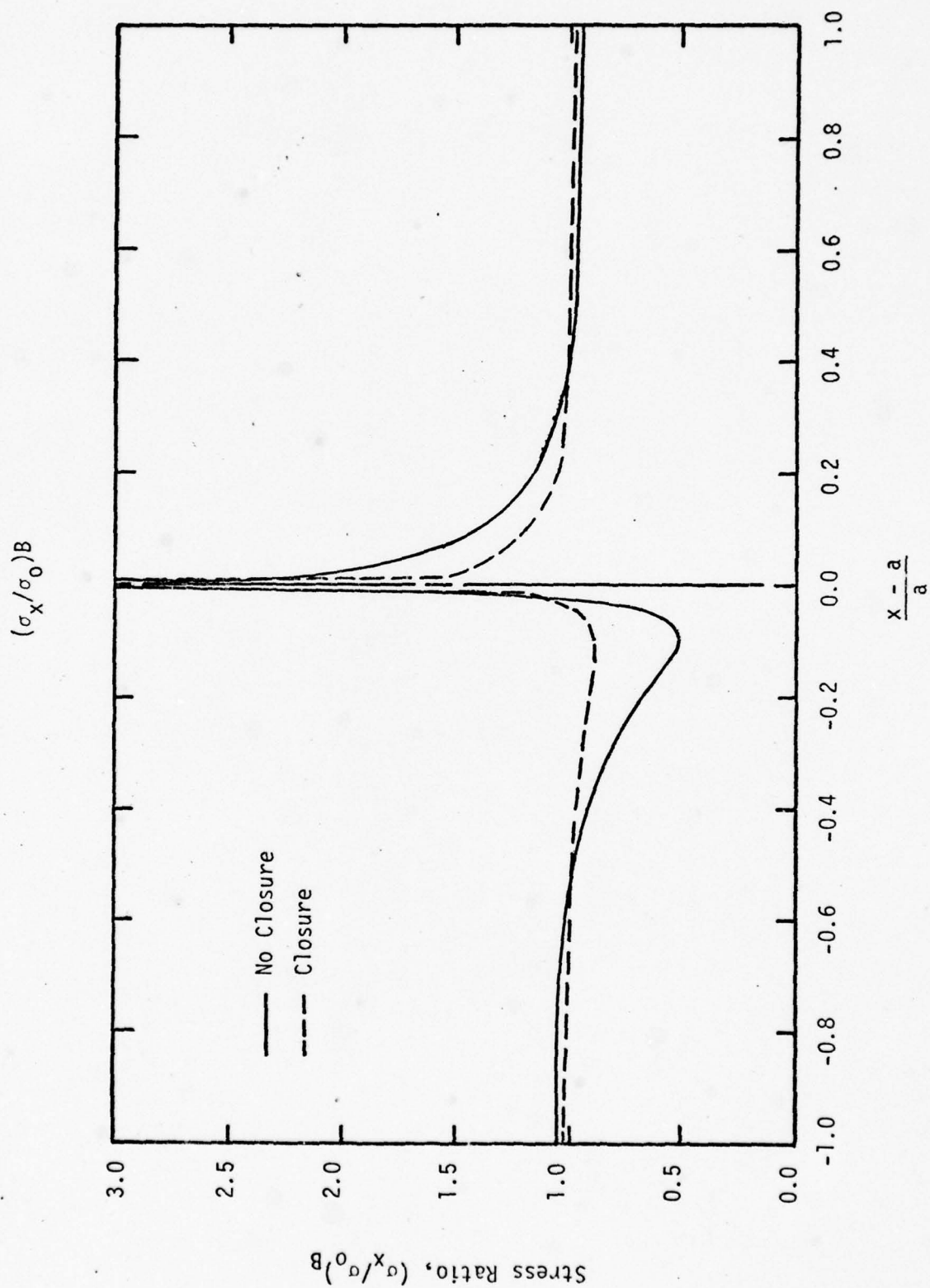
FIGURE 5-6

ELASTIC BENDING STRESS DISTRIBUTION

$(\sigma_y/\sigma_o)_B$

Stress Ratio, $(\sigma_y/\sigma_o)_B$

$\frac{x - a}{a}$
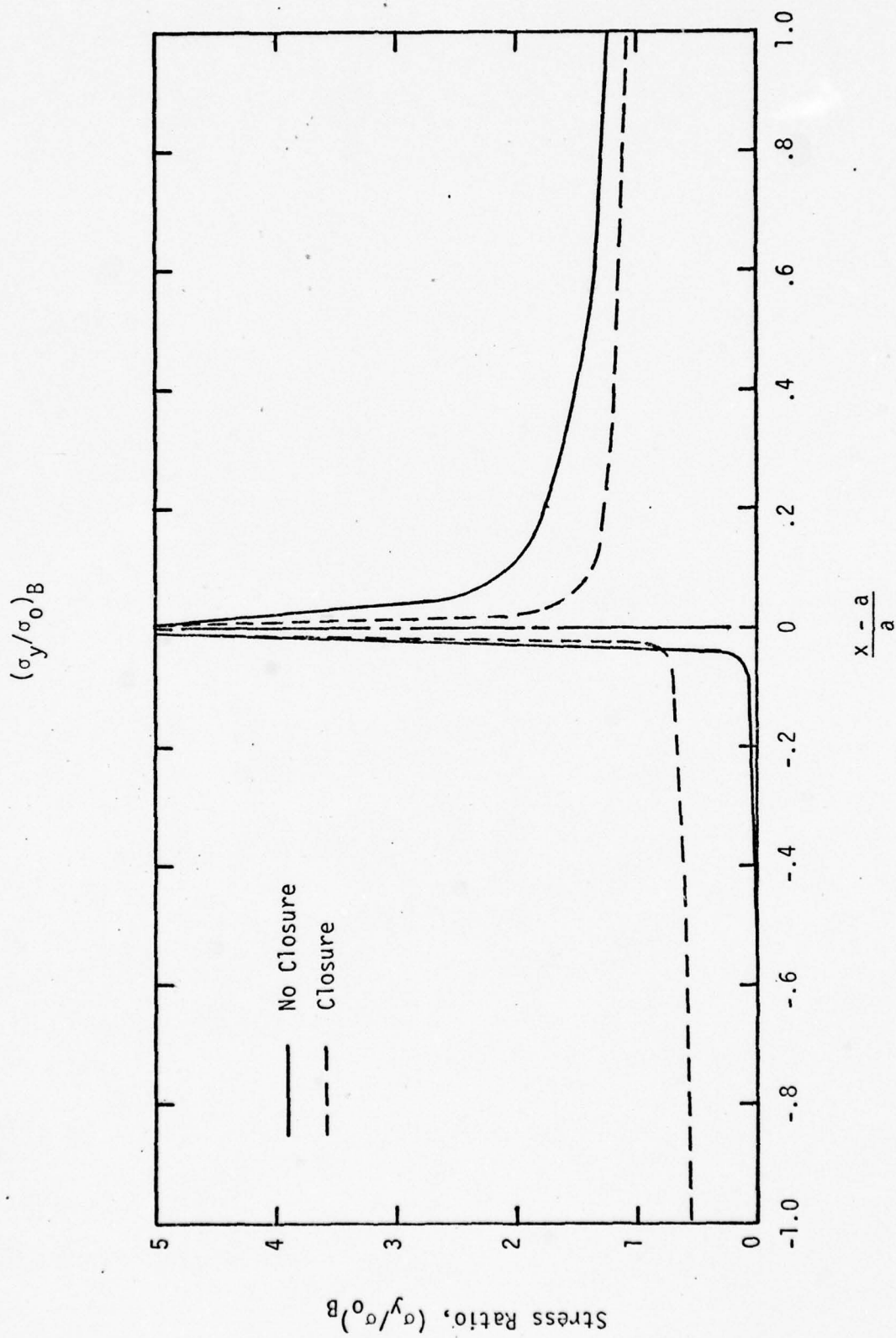
No Closure

Closure

FIGURE 5-7

ELASTIC STRESS DISTRIBUTIONS

(σ_x/σ_0)

σ_x/σ_0 vs z/h at r/a = 3/16
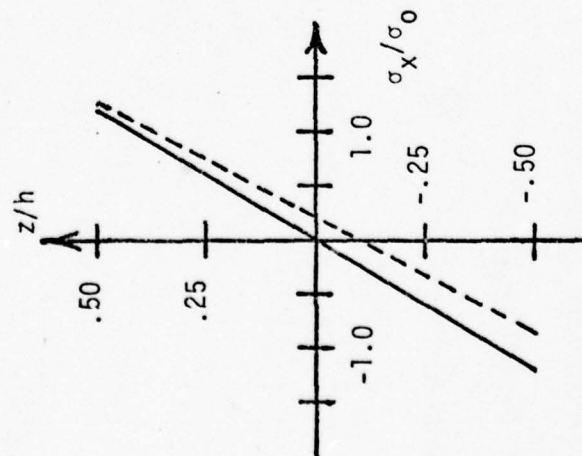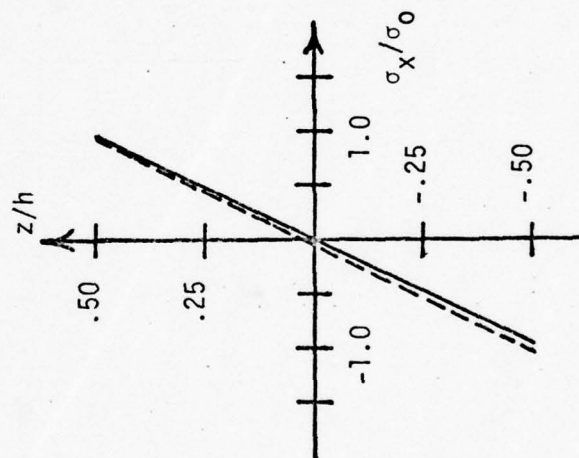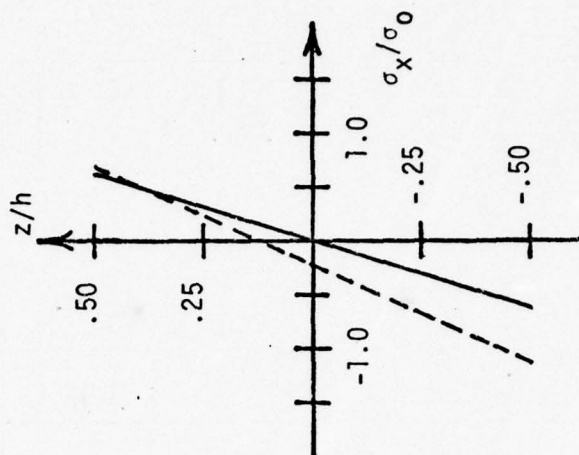
——— No Closure
- - - Closure

FIGURE 5-8

ELASTIC STRESS DISTRIBUTIONS

(σ_y/σ_0)

σ_y/σ_0 vs z/h at r/a = 3/16

—— No Closure
----- Closure

$\theta = 0°$
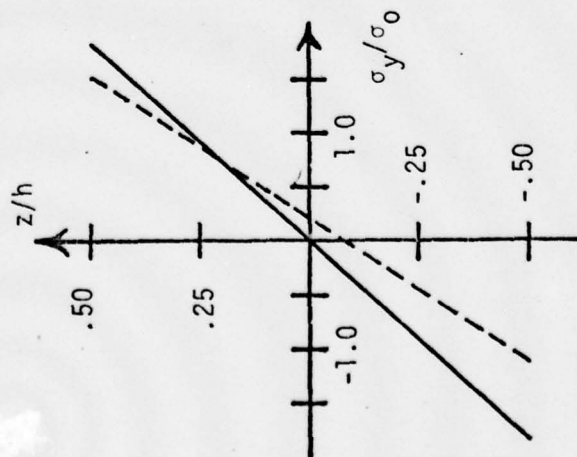
$\theta = 90°$
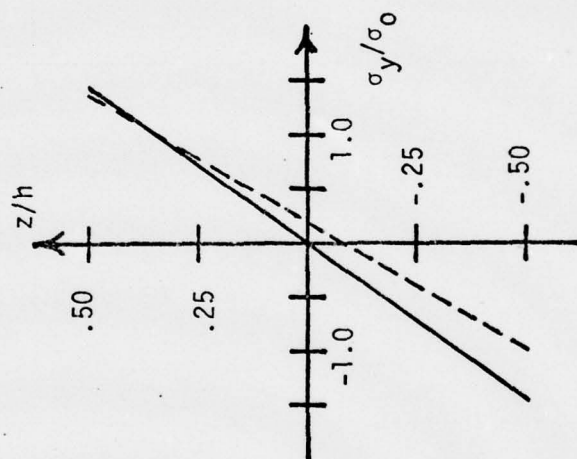
$\theta = 180°$
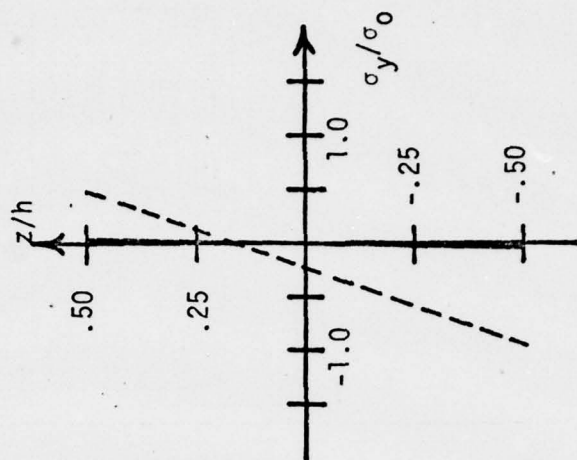
FIGURE 5-9

VARIATION OF IN-PLANE MEMBRANE LOAD N_y FOR THE

ELASTIC CLOSURE PROBLEM (ALONG $y = 0$ AXIS)

$\frac{x-a}{a}$

$\frac{N_y}{\sigma_o h}$

47
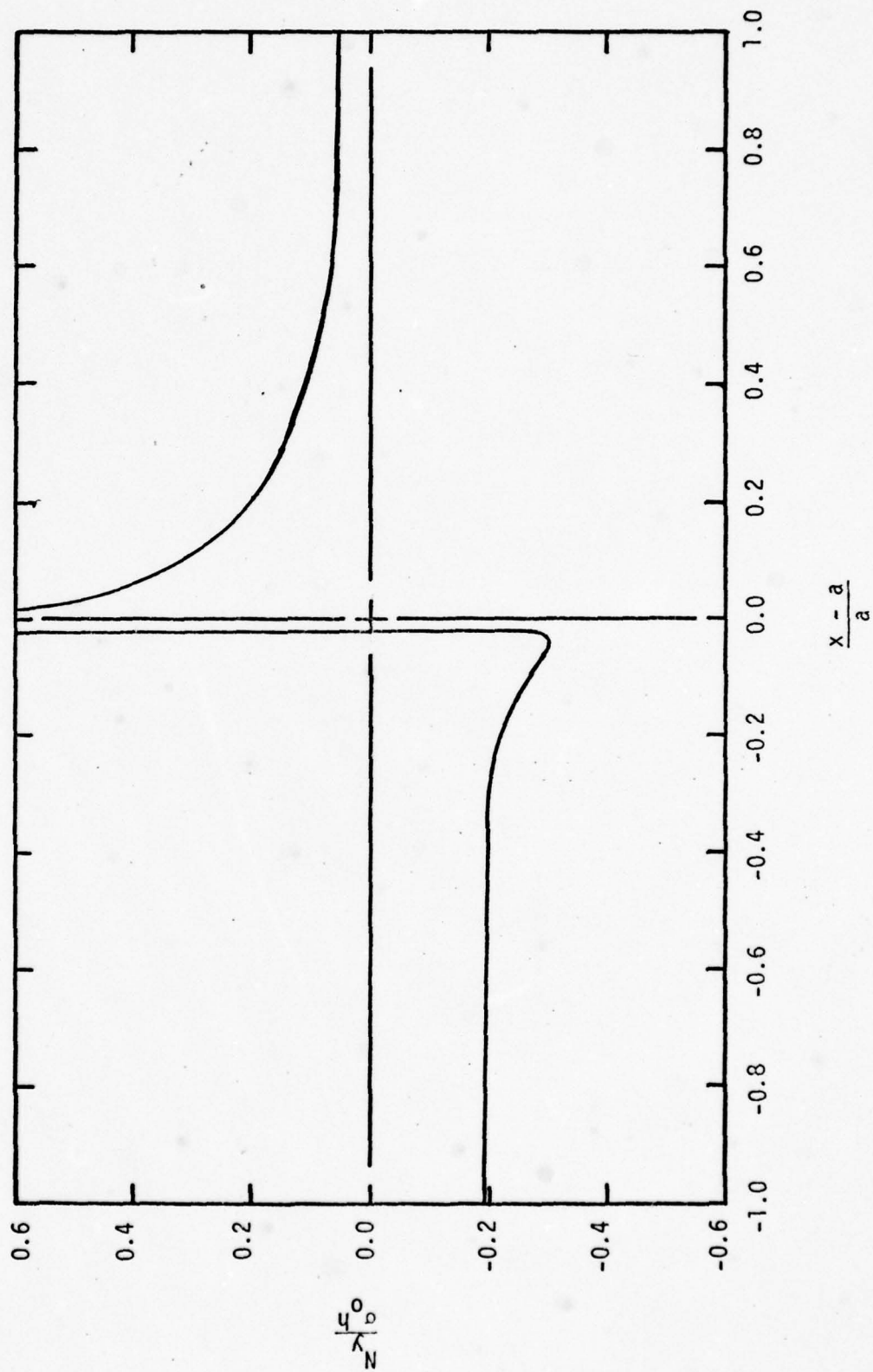
FIGURE 5-10

VARIATION OF IN-PLANE MEMBRANE LOAD N_{xy}

FOR THE ELASTIC CLOSURE PROBLEM

(ALONG $\theta = 90°$ AXIS)
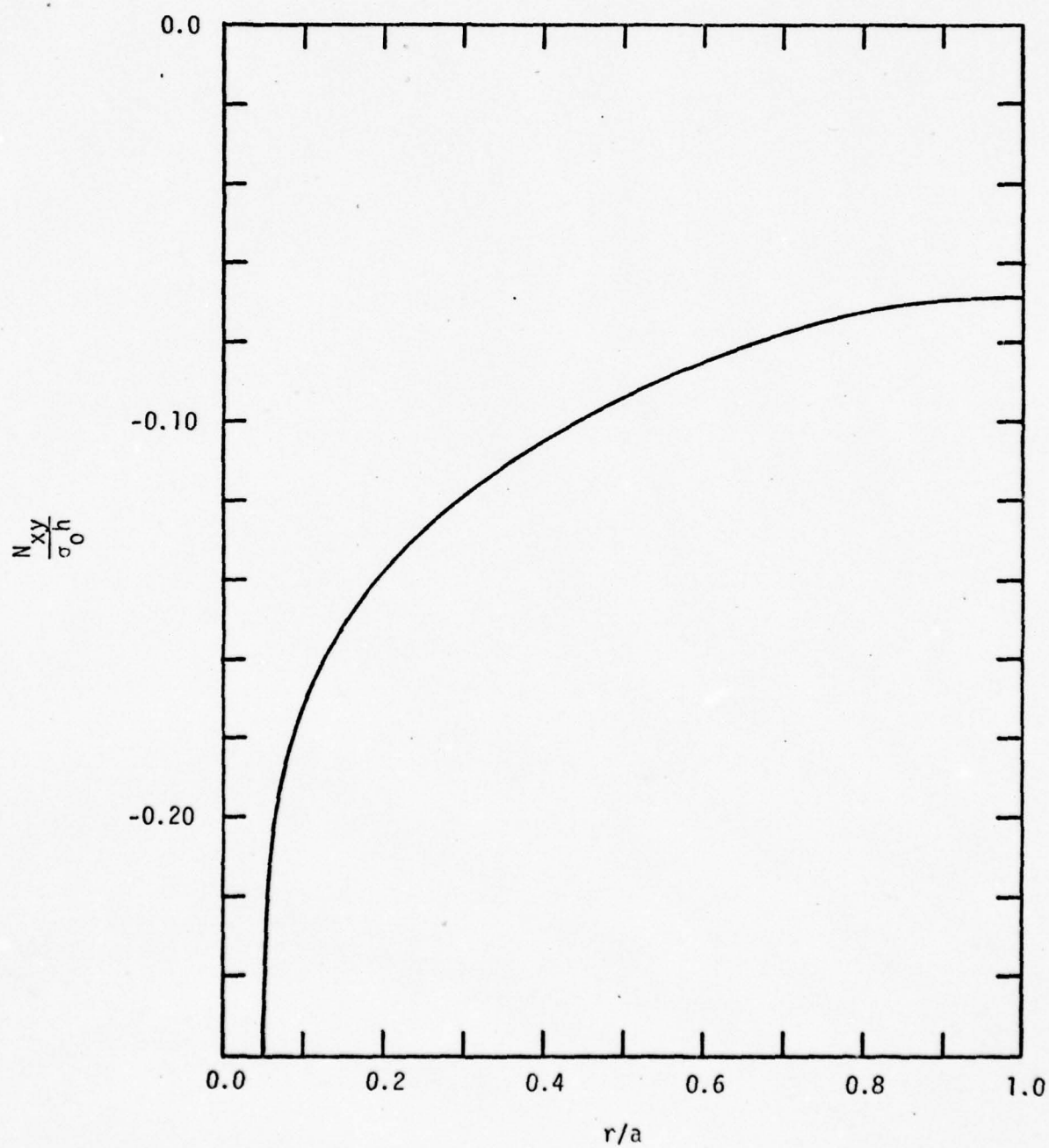
FIGURE 5-11

VARIATION OF LAGRANGE

MULTIPLIERS ALONG CONTACT

LINE OF CRACK FACE
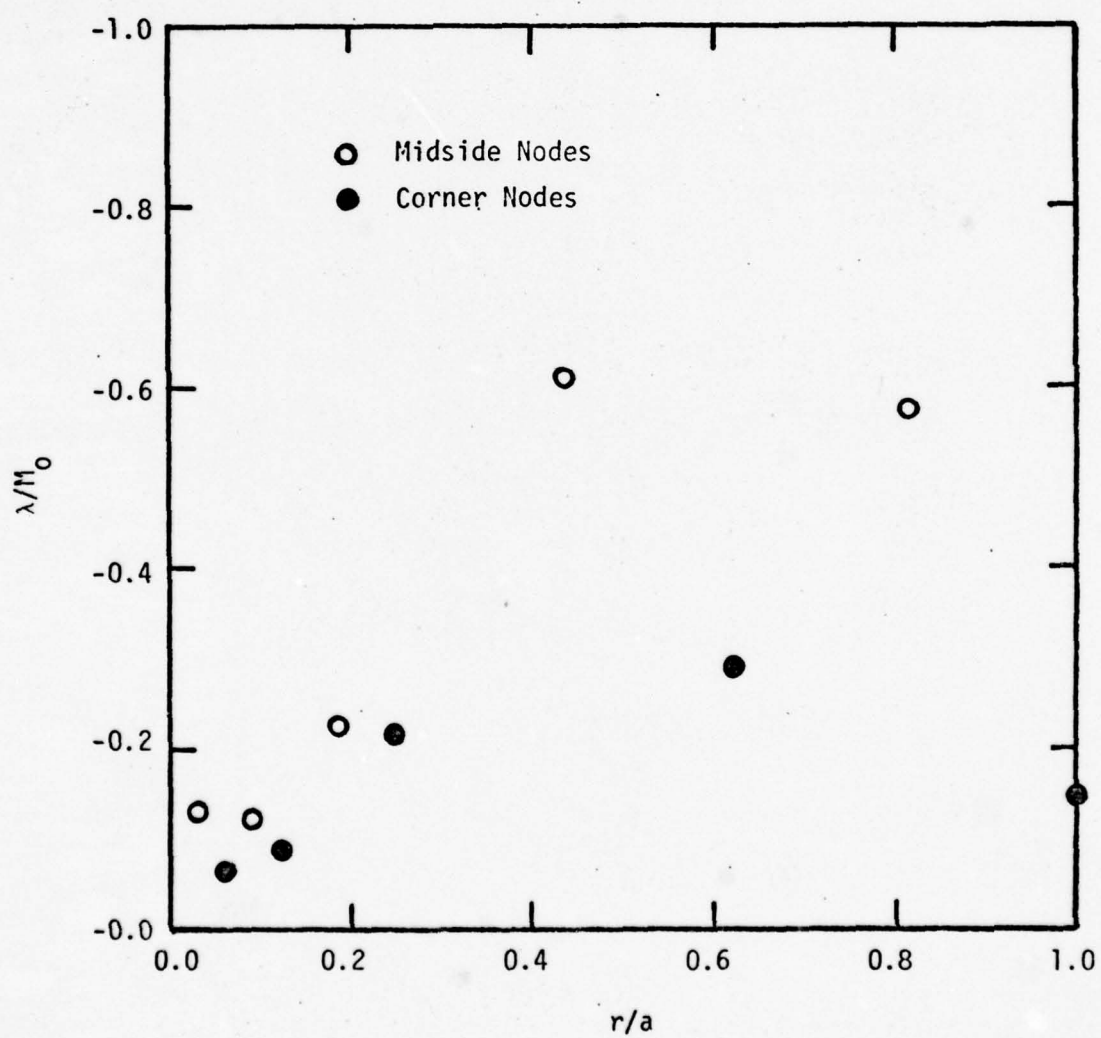
FIGURE 5-12

SHEAR STRESS DISTRIBUTIONS

$$(\tau_{xy}/\sigma_o)$$

$\theta = 90°$
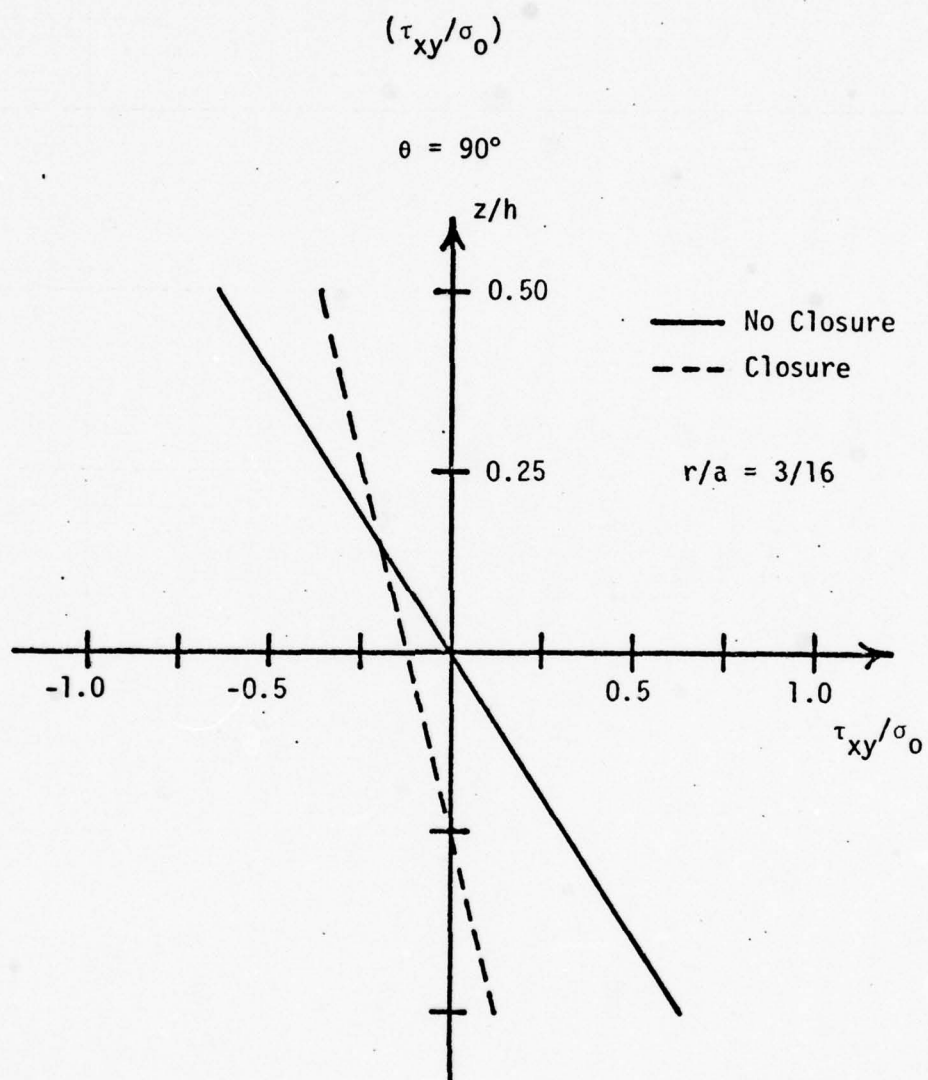
FIGURE 5-13

CONTRIBUTION OF τ_{xz} TO τ_o
(TENSION SURFACE)
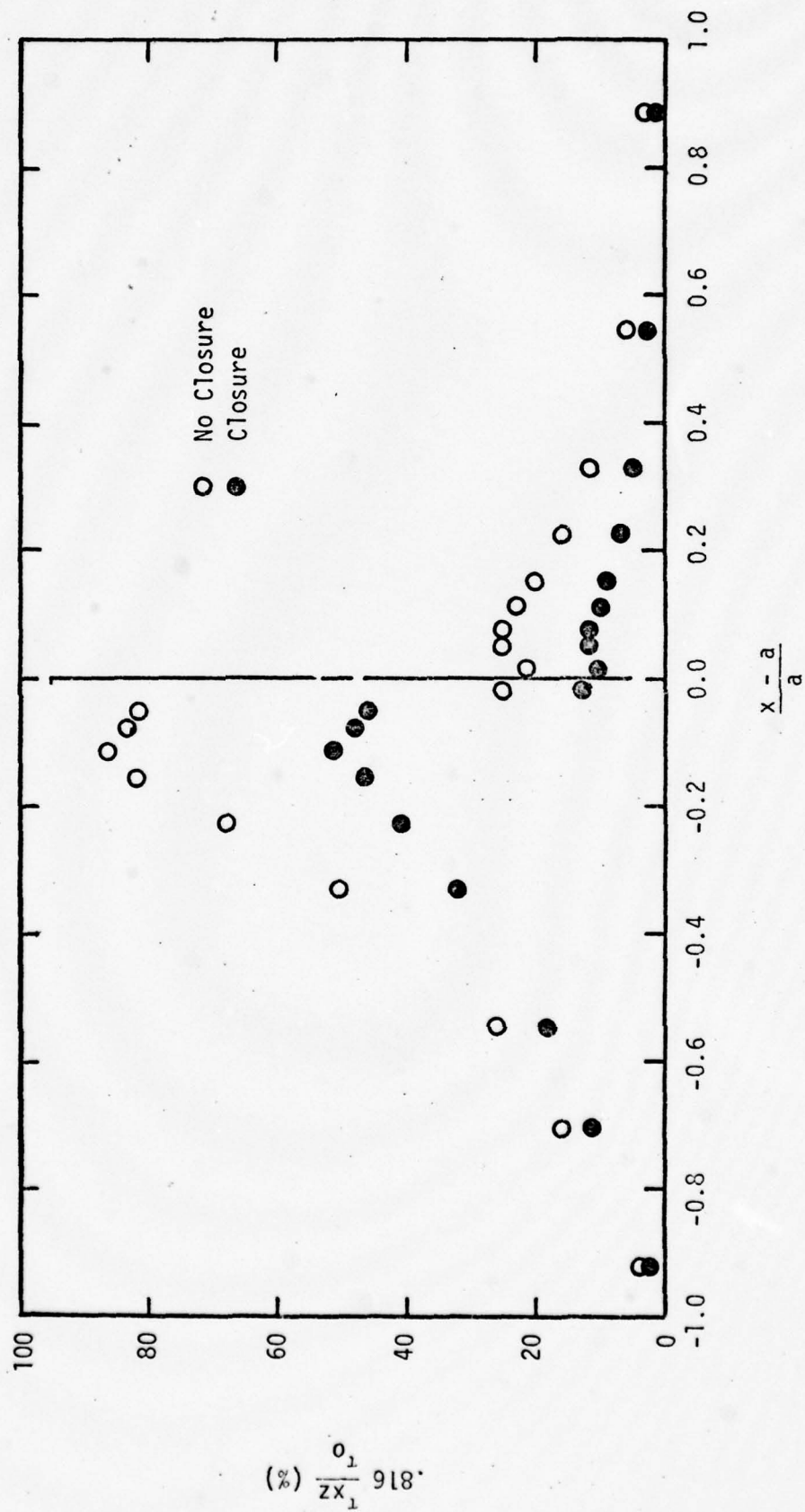
FIGURE 5-14

DETERMINATION OF ELASTIC BENDING

STRESS INTENSITY FACTORS ON THE TENSION

SURFACE (BASED ON CRACK OPENING

DISPLACEMENT v)

$\dfrac{E}{\sigma_0} \dfrac{v}{\sqrt{\pi a}\ \sqrt{r}}$

○ No Closure, Q = 0.988

● Closure, Q = 0.643

$Q = \lim_{r \to 0} \dfrac{E}{\sigma_0 \sqrt{\pi a}} \dfrac{v}{\sqrt{r}}$

r/a
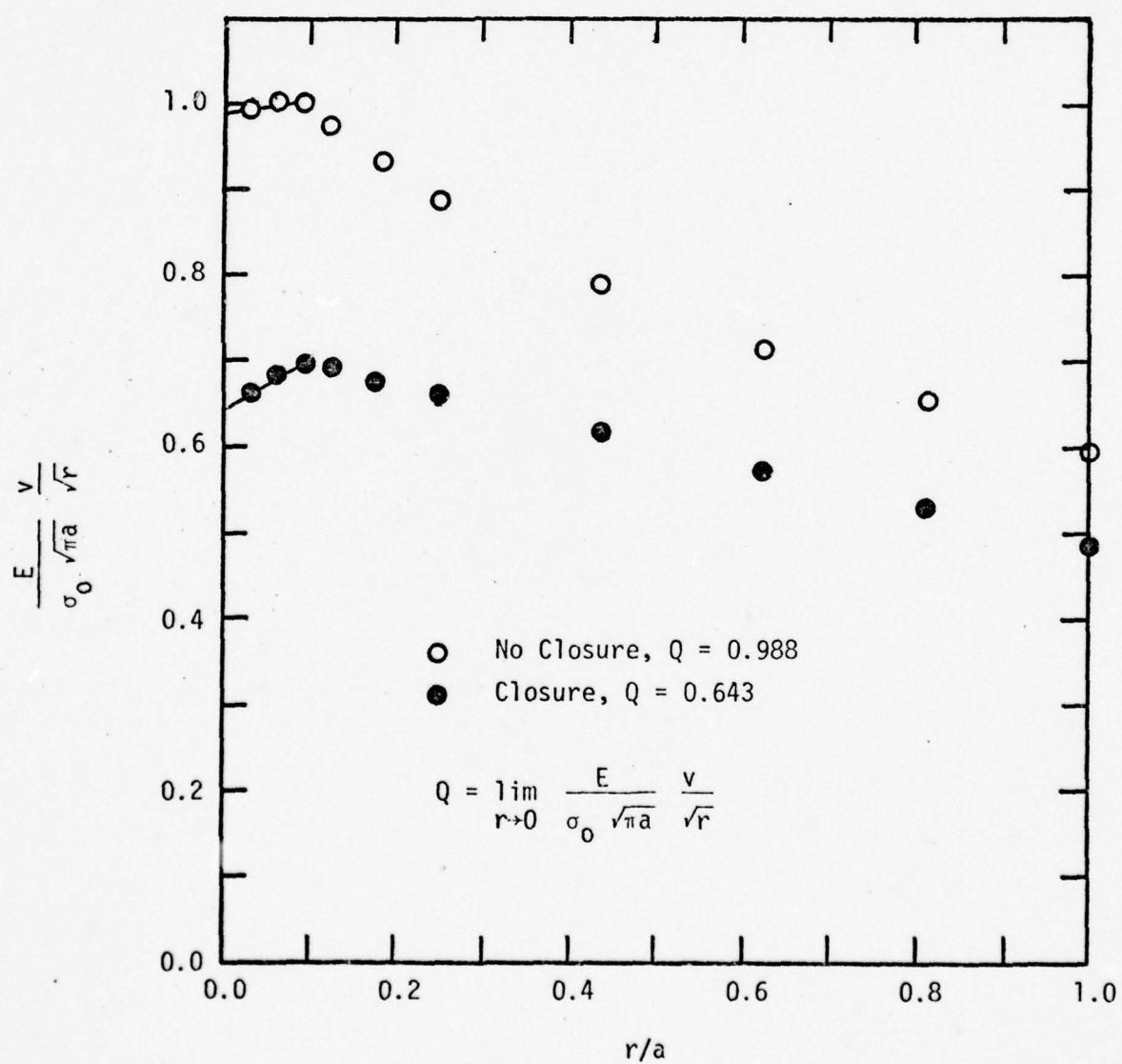
FIGURE 5-15

DETERMINATION OF ELASTIC BENDING STRESS

INTENSITY FACTORS (BASED ON TRANSVERSE

DEFLECTION w)
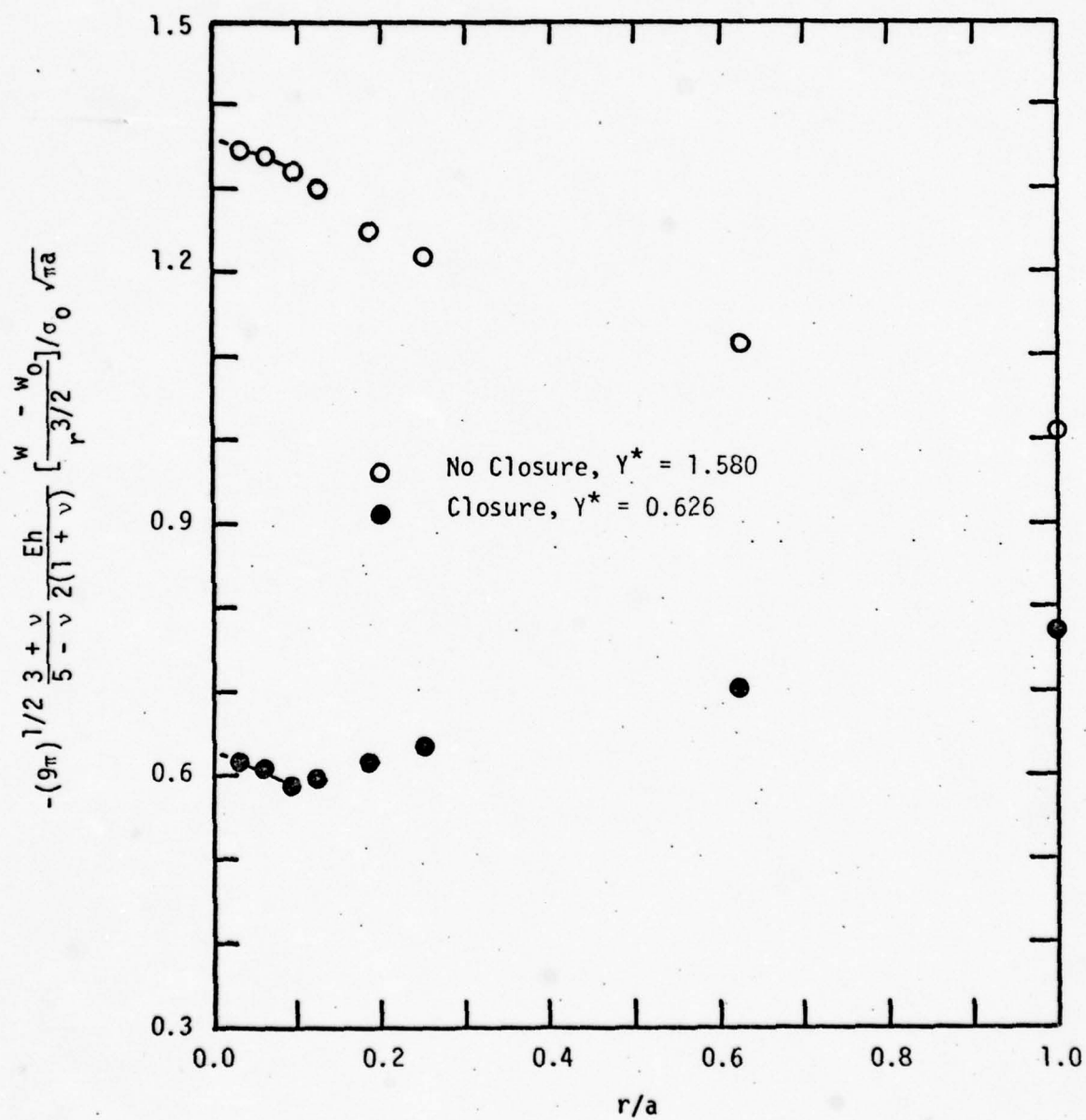
FIGURE 5-16

DETERMINATION OF ELASTIC BENDING STRESS

INTENSITY FACTORS (BASED ON THE BENDING

STRESS σ_y AT THE TENSION SURFACE)
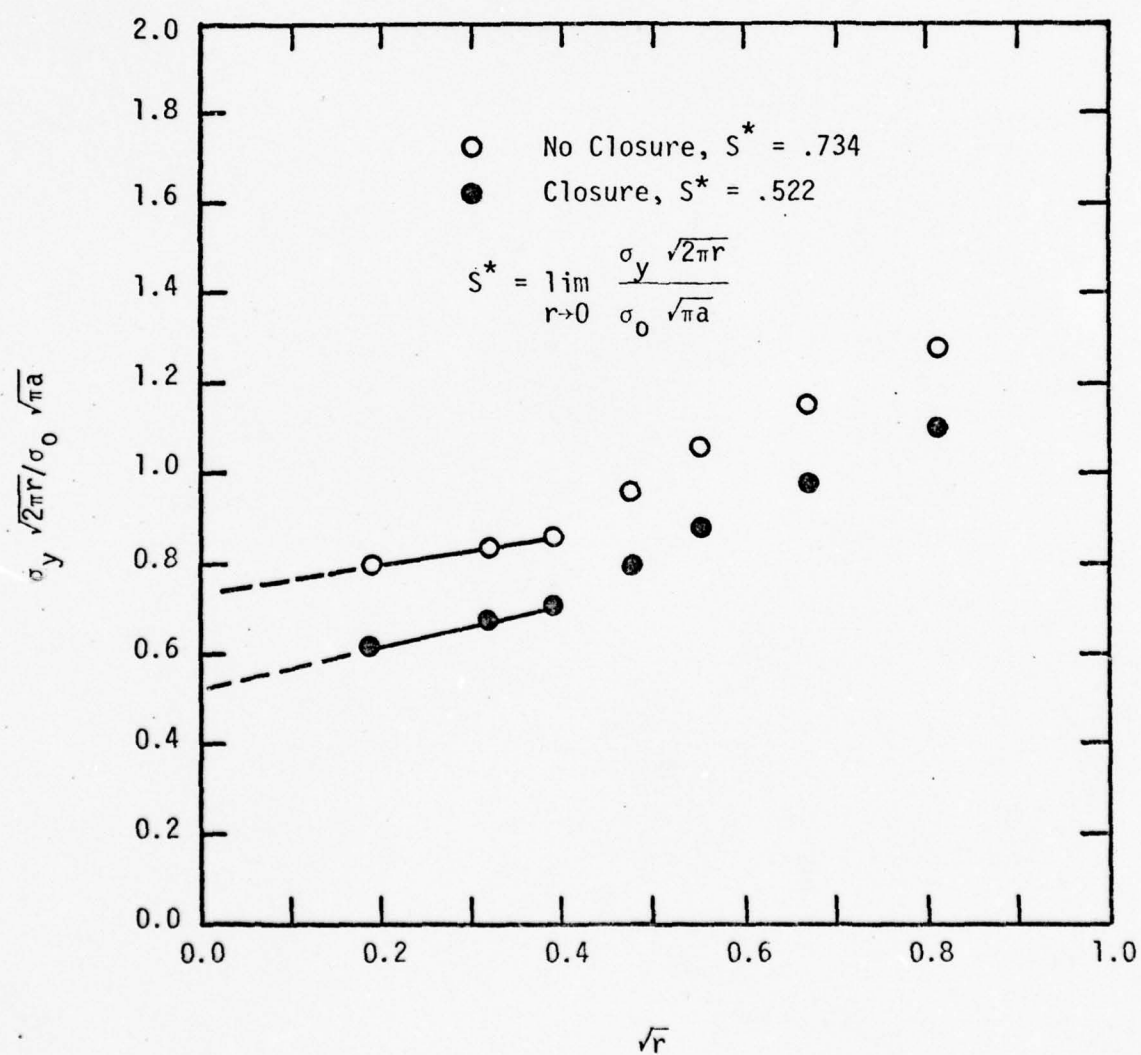
FIGURE 5-17

THICKNESS EFFECTS - BENDING STRESS

INTENSITY FACTORS BASED ON DISPLACEMENTS

$$Q = \lim_{r \to 0} \frac{E}{\sigma_o \sqrt{\pi a}} \frac{v}{\sqrt{r}}$$

○ No Closure

● Closure
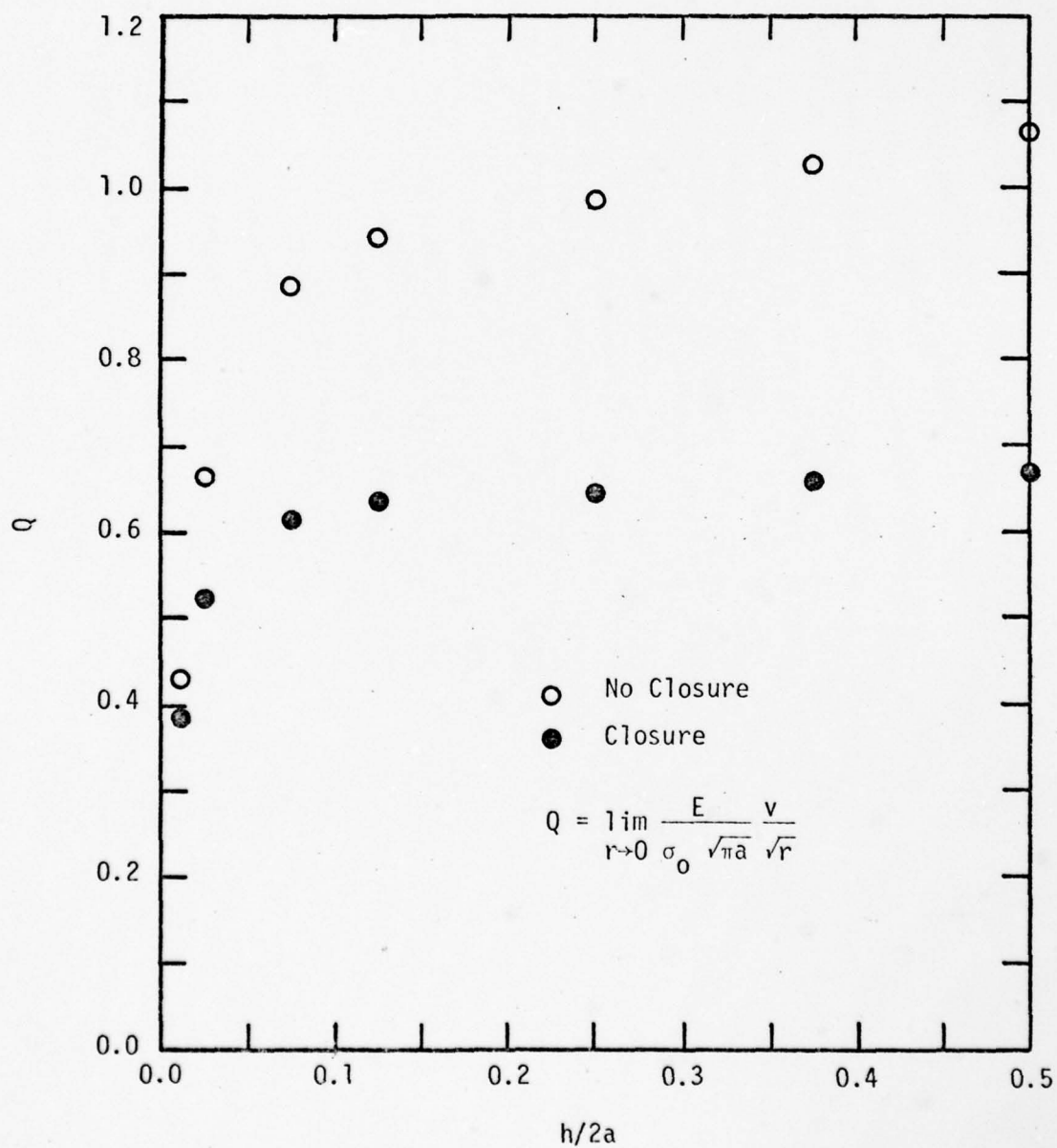
FIGURE 5-18

THICKNESS EFFECTS - BENDING STRESS

INTENSITY FACTORS BASED ON STRESSES
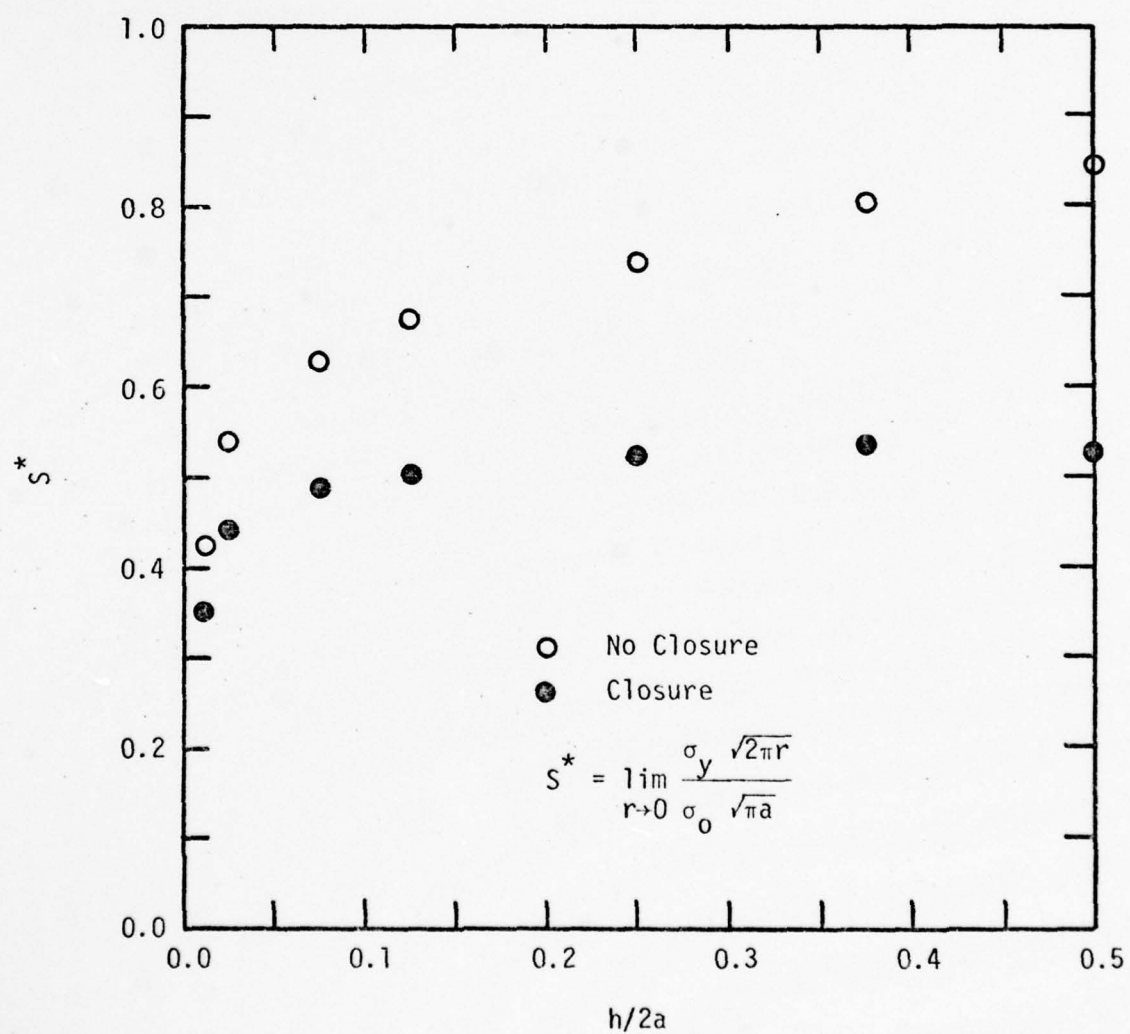
CHAPTER VI

ELASTO-PLASTIC RESULTS

At the onset of yielding the nature of the bending problem
changes gradually from linear to highly nonlinear behavior.
The results are obtained by solving a series of quasi-linear
incremental problems and summing them to obtain the resultant
accumulated values. As noted previously, the no closure and
closure cases were solved for the same incremental loads to
facilitate direct comparison of the two cases. Although 48
load steps were run for the no closure case and 40 load steps
for the closure case, the results presented are for the first
36 and 28 load steps only. The cutoff point for data presenta-
tion corresponds to the last load step before the entire tension
surface of the plate yields, i.e., $\sigma_o/\sigma_L = .988$, where σ_L is
the stress at the proportional limit.

6.1 Load-Deflection Data

In Figures 6-1 through 6-4 the load deflection curves are
shown for the transverse deflection w and displacement parallel
to the y-axis v at representative points. In each figure the
load is presented as the normalized applied moment M_o/M^* where
$M^* = \sigma_L h^2/6$. The displacements are normalized by values
corresponding to the pure bending solution at an applied
stress of σ_L.

Figures 6-1 and 6-2 show the load-deflection curves for far field values of w and v, respectively. The near linearity of the curves implies that for the range of loads analyzed the outer boundaries of the plate are affected very little by the localized yielding around the crack tip. These figures also indicate that the effects of closure are minimal in the far field.

Figures 6-3 and 6-4 indicate the load-deflection behavior local to the crack for the transverse deflection $w(a,0)$ of the crack tip and the crack opening displacement $v(0,0)$ at the center of the plate, respectively. The effect of closure is to reduce $w(a,0)$ by 29% and $v(0,0)$ by 18-22%. Thus, the effect of closure is fairly uniform over the range of loading shown. Although the curves again appear to be linear for most of the loading, it will emerge that the behavior around the crack is indeed nonlinear in nature. This is indicated quite clearly by the growth of the yield zones around the crack tip.

6.2 Growth of the Yield Zones

The growth of the plastic yield zones is shown in Figures 6-5 and 6-6. For the results presented here, yielding is defined at those points that lie on the nonlinear portion of the octahedral stress-strain curve, i.e., where $\tau_0/\tau_L > 1.0$.

For the no closure case, as shown in Figure 6-5, the yield zones are symmetric about the midplane as required by Mindlin plate theory. As yielding proceeds, the yield zone propagates

into the material as expected from the extensional plane stress results (see [12]), and an elastic core is preserved at the crack tip until the latter stages of loading. Yielding does occur along the crack face in the latter stages of loading when yielding of the entire surface of the plate is imminent, but, except as shown, the elastic core remains.

The formation of the yield zones is completely different for the closure case. As shown in Figure 6-6, yielding occurs first on the tension surface and proceeds through the thickness. Yielding does not occur on the compression surface until very late in the loading sequence, at which point the yield zone propagates very rapidly across the compression surface. Note also that a sizeable elastic core is still preserved throughout the material. The yielding occurs at the compression surface of the crack face due to the compressive force (along the contact line) induced by the closure constraint. The effect of closure then is to constrain the crack face in such a way that the induced compressive fields along the crack face inhibit yielding. This is shown by the reduced size of the yield zones on both the tension and compression surfaces and the larger elastic core through the thickness.

A further indication of the greater constraint in the closure case is the reduction of crack tip blunting. The relative crack opening profiles are shown in Figure 6-7 with each profile normalized by the respective crack opening displacement v at the plate center. The profiles show that for the closure case the

crack is less blunt, and that there is relatively less blunting as loading progresses.

6.3 Through Thickness Stress Distributions

The through thickness stress distributions for σ_x, σ_y and τ_{xy} at a distance of r/a = 3/16 from the crack tip are shown in Figures 6-8 through 6-10. The distributions show the nonlinear stress behavior where yielding has occurred and the neutral surface shifts (based on a zero stress definition) induced by closure. Note that at r/a = 3/16 the nonlinearity is less pronounced than at points closer to the crack tip; thus, the nonlinear distributions shown are merely representative and not meant to indicate the most nonlinear behavior that occurs. The σ_y distribution at θ = 180° also serves to illustrate that the stress free boundary condition on the crack face is being satisfied but that pseudo-stresses are induced by the closure constraint. Observation of the Lagrange multipliers as loading proceeds shows that they remain in the same proportion to the applied load as was seen in the elastic results except for a slight amplification of those closest to the crack tip.

6.4 Fracture Mechanics Representations

Applying a fracture mechanics approach to the elasto-plastic results, Figures 6-11 through 6-14 depict various representations

of apparent elasto-plastic bending stress intensity factors. In
each case the stress intensity factors are determined at various
load levels and plotted versus the applied load σ_o/σ_L (or M_o/M^*).
The procedure used to obtain the elasto-plastic values is the
same extrapolation method used to obtain the elastic bending
stress intensity factors.

Figures 6-11 and 6-12 show the trends for the displacement
based bending stress intensity factor Q. In Figure 6-11 the
values of Q are normalized by the elastic value of Q. The values
of $Q/Q_{Elastic}$ increase with increasing load in correspondence
with increasing displacements v. In Figure 6-12 Q is normalized
by a current applied load factor $\sigma_o \sqrt{\pi a}$. The results here show
that the closure values are 35% lower for the elastic values and
48% lower at the maximum load shown. The effect of closure is to
decrease the rate at which Q increases relative to the no closure case.

Figures 6-13 and 6-14 show the trends for the stress based
bending stress intensity factors K^*. In Figure 6-13 K^* is
normalized by the elastic value of K^*. The results show that the
stress intensity increases over the elastic value in the initial
stages of loading with a subsequent redistribution and lowering
of the stress intensity as loading, and yielding, proceeds.
Figure 6-14, where K^* is normalized by the current load factor
$\sigma_o \sqrt{\pi a}$, shows the gradual weakening of the stress intensity as
yielding proceeds. Of added interest is the rapid convergence
of the no closure and closure results with increasing load. The
effect of closure then is to reduce the values of K^*, but not
nearly as much as was indicated by the displacement based results.

6.5 <u>Shear</u> <u>Effects</u>

The effect of the transverse shear stress τ_{xz} at an applied
load of σ_o/σ_L = .988 is compared with the elastic effect in
Figure 6-15. The results show that the contribution of the
transverse shear to the octahedral shear stress local to the
crack is relatively constant over the range of loading. In
addition, the effect of closure is to reduce the transverse
shear and its contribution to the octahedral shear stress through-
out the loading sequence, thereby reducing the effect of shear
on the overall yield.

Figure 6-16 shows the through thickness distribution of τ_{xz}
at σ_o/σ_L = .988 and r/a = 3/16. At θ = 0°, yielding has occurred,
and this is indicated by the nonconstant values of τ_{xz}. At
θ = 180°, no yielding has occurred, and τ_{xz} is a weighted constant
through the thickness, thus indicating an elastic distribution at
that point.

6.6 <u>Uniaxial</u> <u>Bending</u> <u>Results</u>

For the uniaxial bending problem the quantities that change
or remain the same for the elasto-plastic analysis are consistent
with the previous discussion of the elastic results. The results
of interest here are the changes in the plastic yield zones as
shown in Figures 6-17 and 6-18. The yield zones for the uniaxial
no closure case, shown in Figure 6-17, are symmetric about the
midplane. Comparing the results with the uniform (or biaxial)

no closure case shows that the yield zones grow more quickly for the uniaxial case. Figure 6-18 shows that the uniaxial closure results indicate yielding on the tension surface first with yielding at the compression surface appearing much later. Comparison with the uniform closure results again shows that the yield zones grow more quickly for the uniform bending problem. In addition, the yielding on the compression surface begins earlier than in the uniform bending problem, and the yielding propagates rapidly ahead of the crack. These changes in the plastic yield zones, for both the closure and no closure cases, are as anticipated due to the lessened constraint in the uniaxial problem.

Other comparisons of the elasto-plastic biaxial and uniaxial problems show that the same similarities and differences occur as in the elastic problems (see Section 5.5).

FIGURE 6-1

LOAD-DEFLECTION CURVE FOR TRANSVERSE

DEFLECTION $w(x_o, y_o)$

64
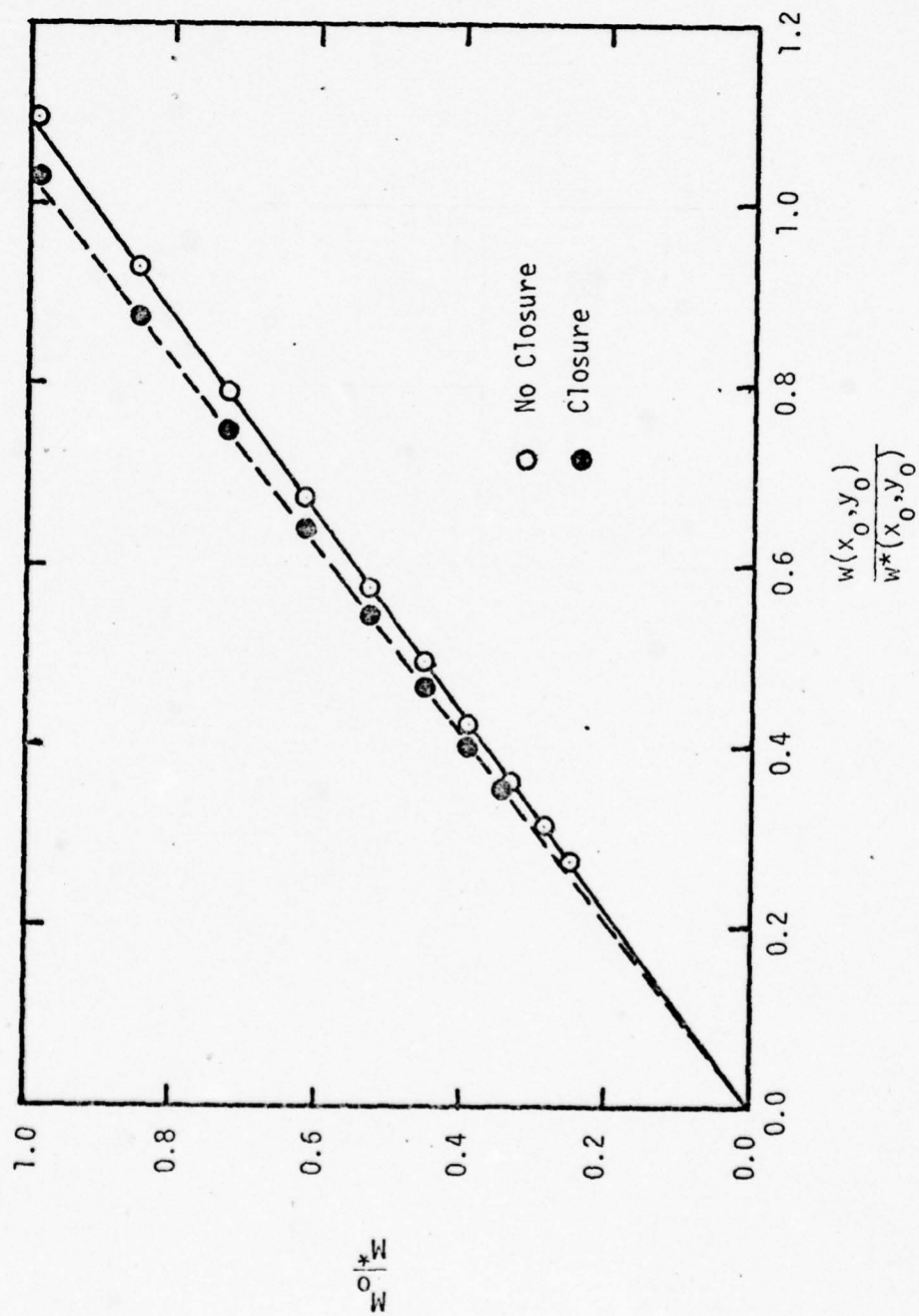
FIGURE 6-2

LOAD-DEFLECTION CURVE FOR $v(0,y_o)$
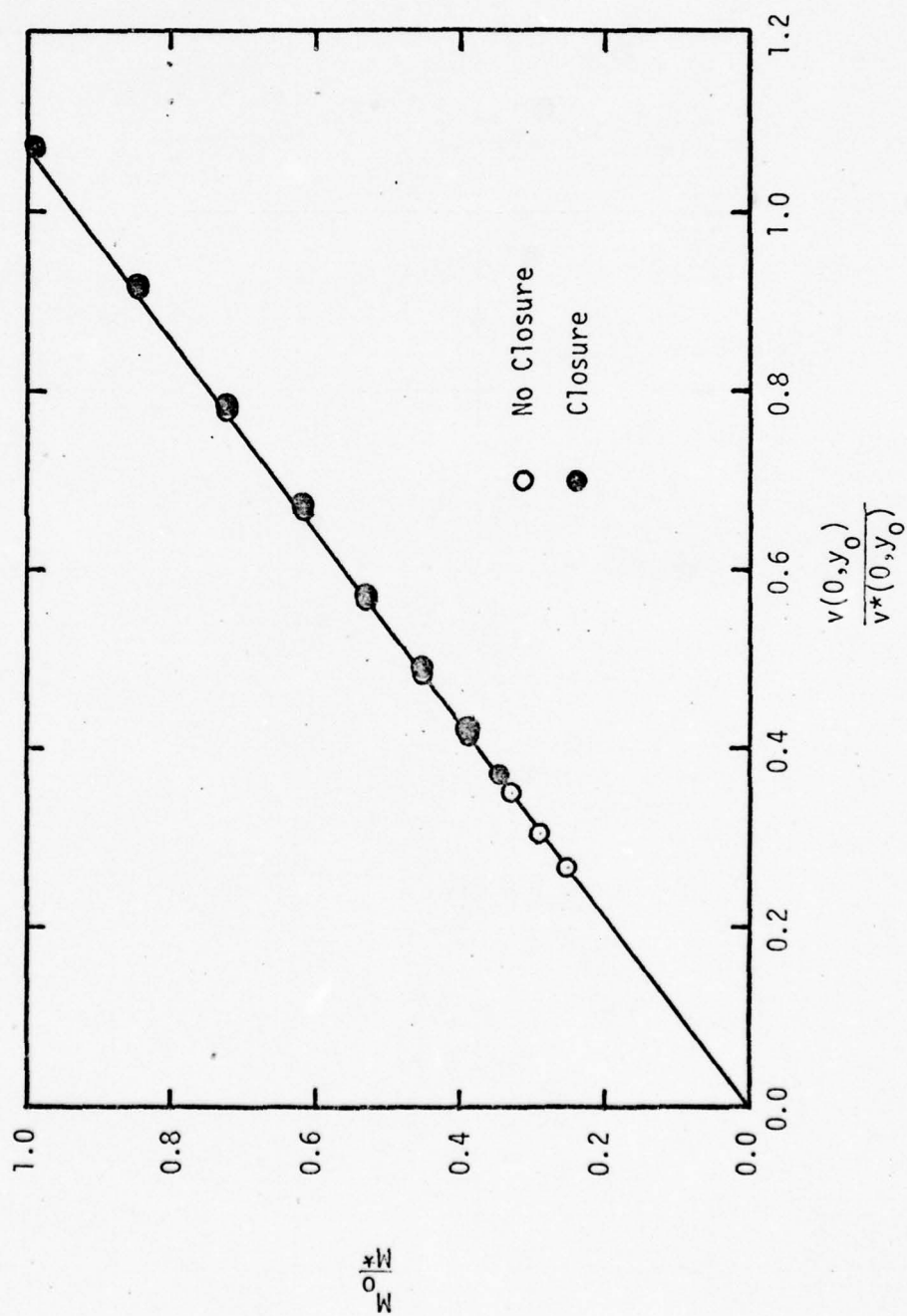
FIGURE 6-3

LOAD-DEFLECTION CURVE FOR TRANSVERSE
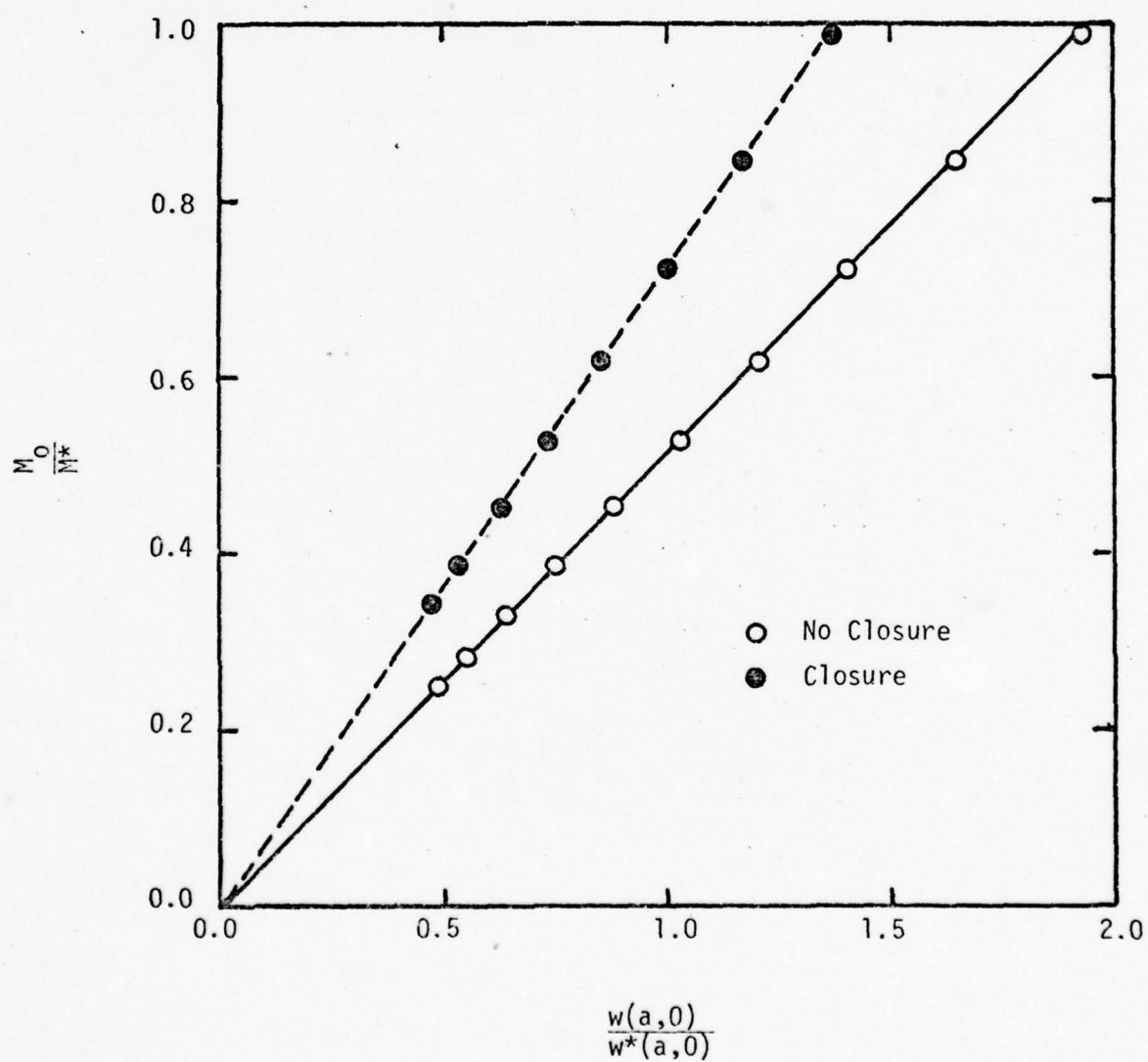
DEFLECTION w(a,0)

FIGURE 6-4

LOAD DEFLECTION CURVE FOR

$v(0,0)$
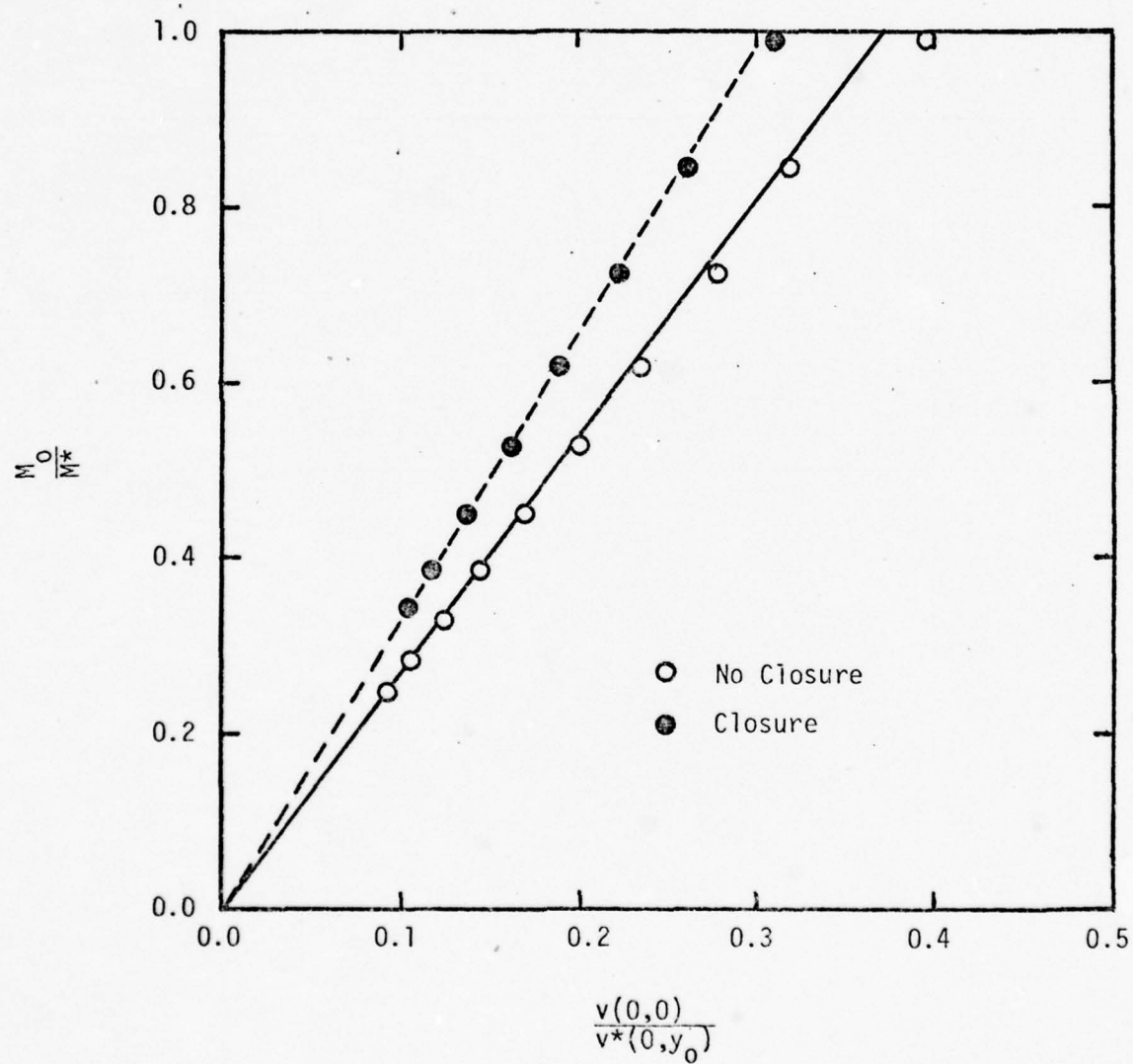
FIGURE 6-5

YIELD ZONES FOR THE NO CLOSURE CASE
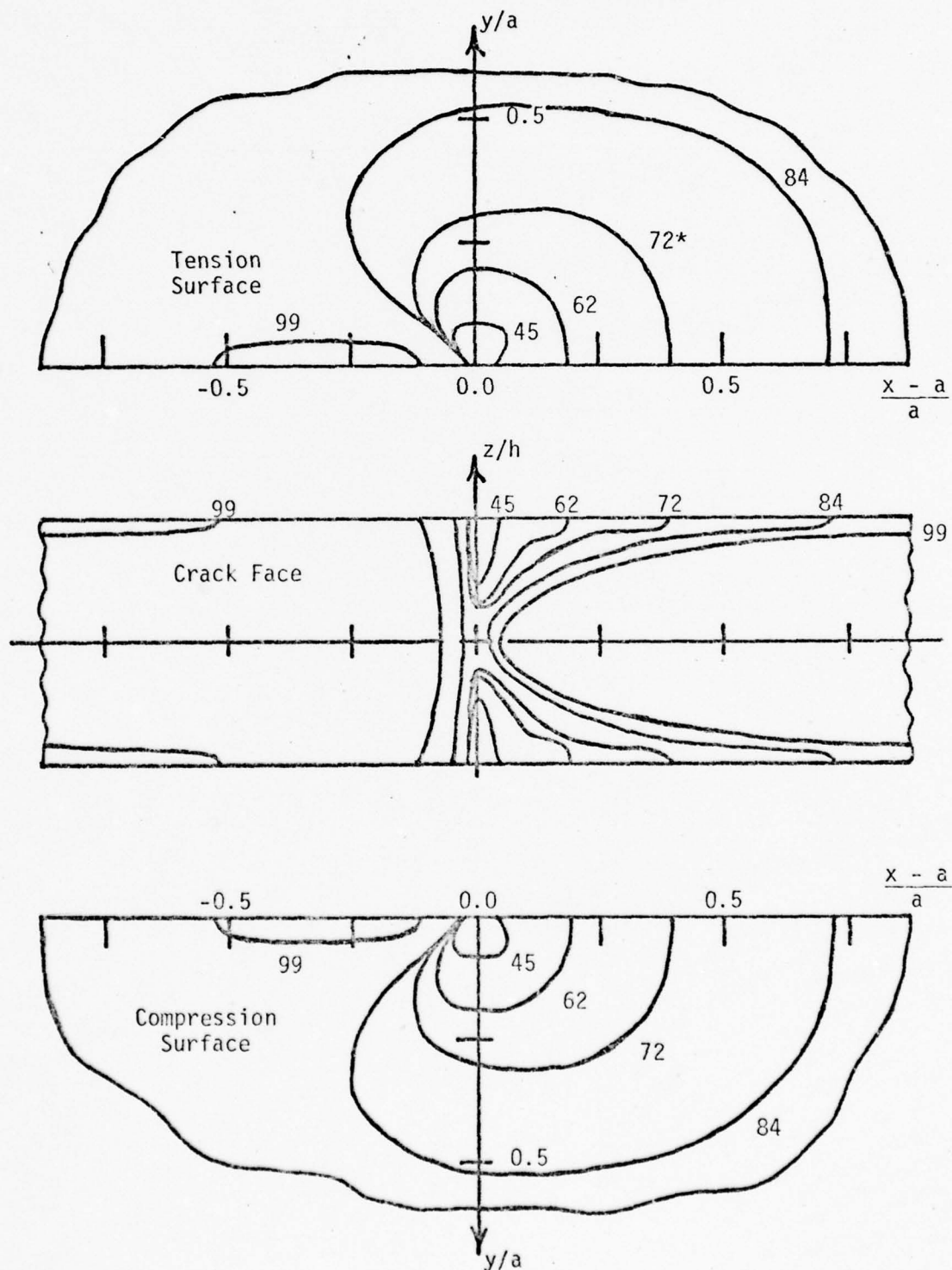
* Normalized Applied Load (σ_o/σ_L or M_o/M^*)
Expressed as a Percentage.

FIGURE 6-6

YIELD ZONES FOR THE CLOSURE CASE
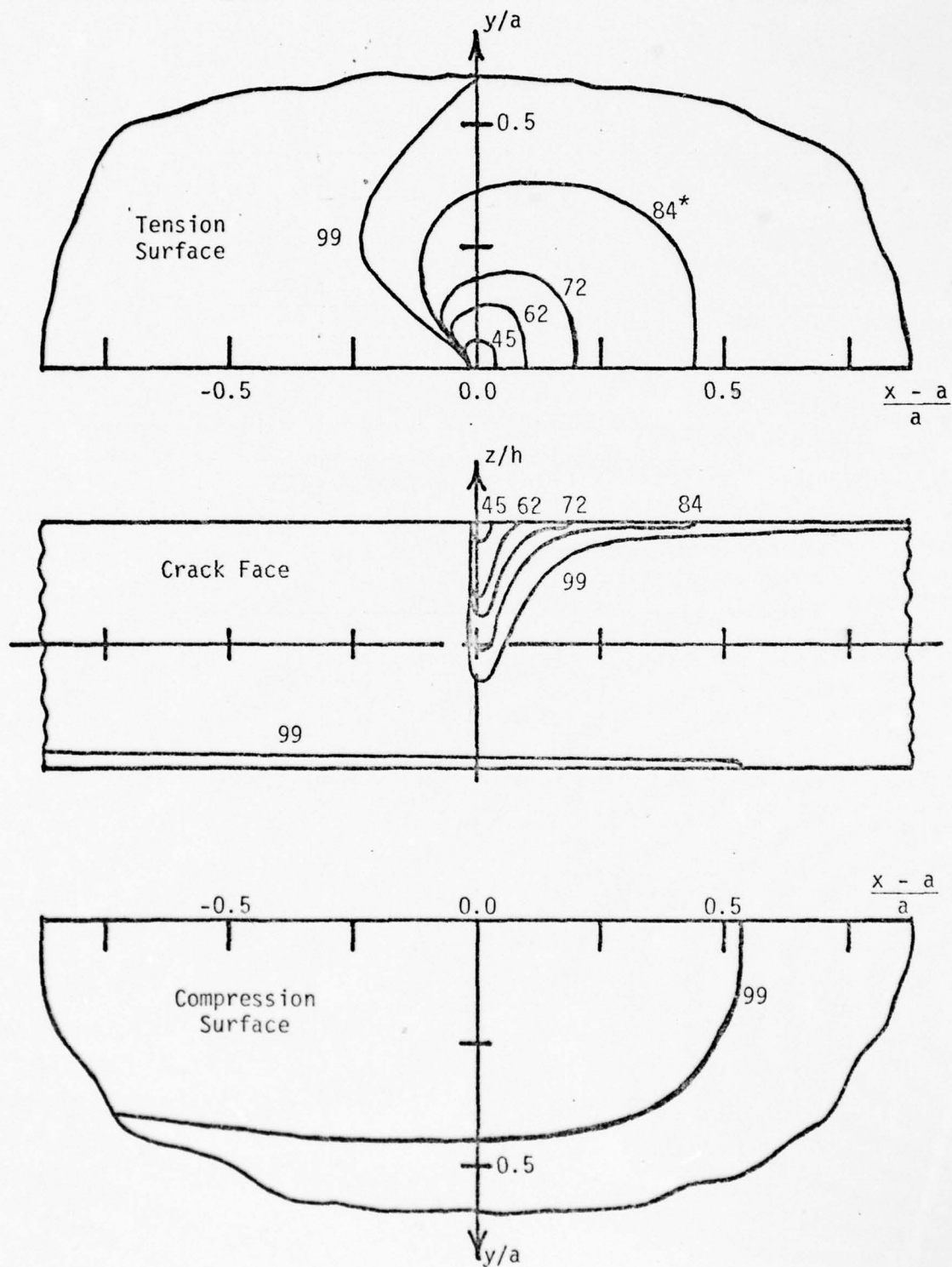
* Normalized Applied Load (σ_o/σ_L or M_o/M^*)
  Expressed as a Percentage.

FIGURE 6-7

CRACK TIP BLUNTING DUE TO

ELASTO-PLASTIC FLOW
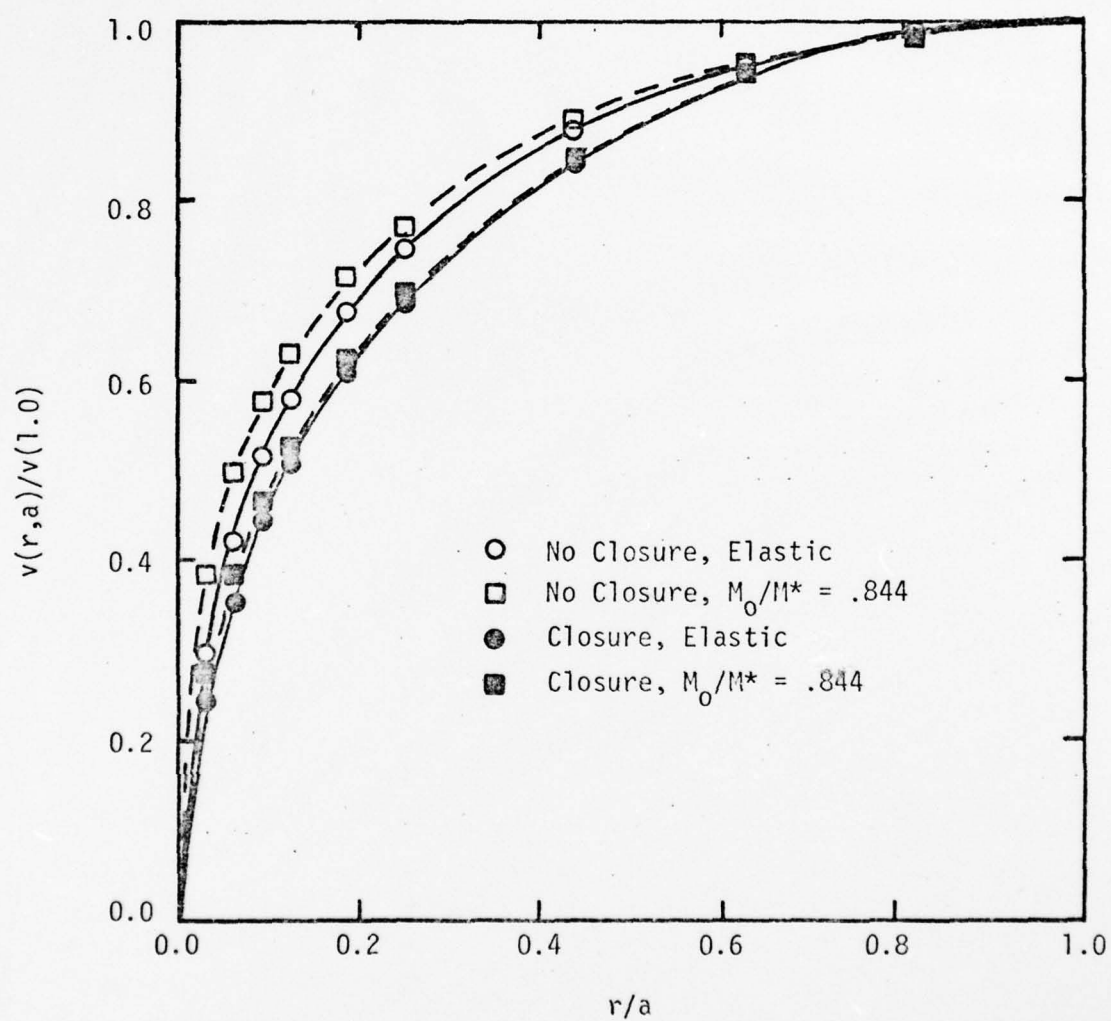
FIGURE 6-8

ELASTO-PLASTIC STRESS DISTRIBUTIONS

(σ_x/σ_0)

σ_x/σ_0 vs z/h at r/a = 3/16 and σ_0/σ_L = .988

——— No Closure

– – – Closure

$\theta = 0°$
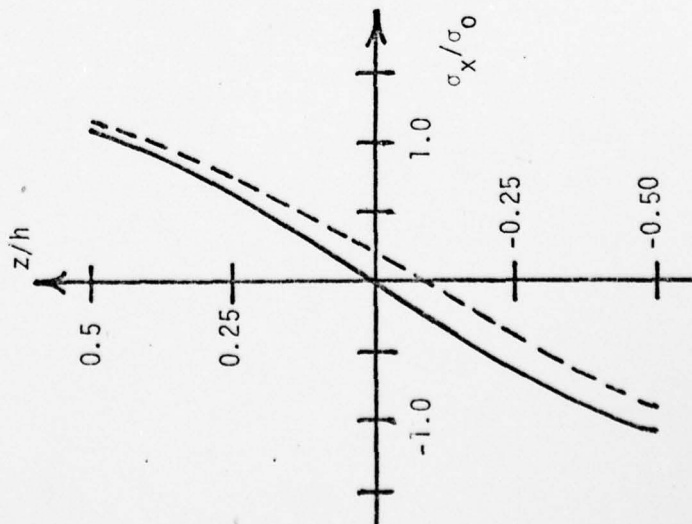
$\theta = 90°$
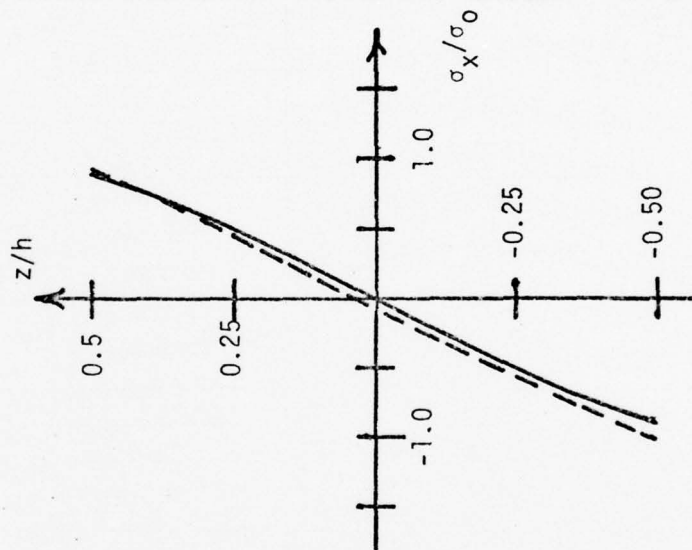
$\theta = 180°$
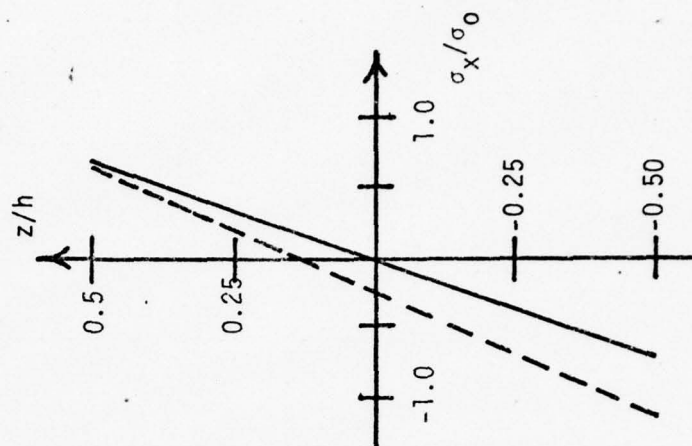
FIGURE 6-9

ELASTO-PLASTIC STRESS DISTRIBUTIONS

(σ_y/σ_0)

σ_y/σ_0 vs z/h at r/a = 3/16 and σ_0/σ_L = .988
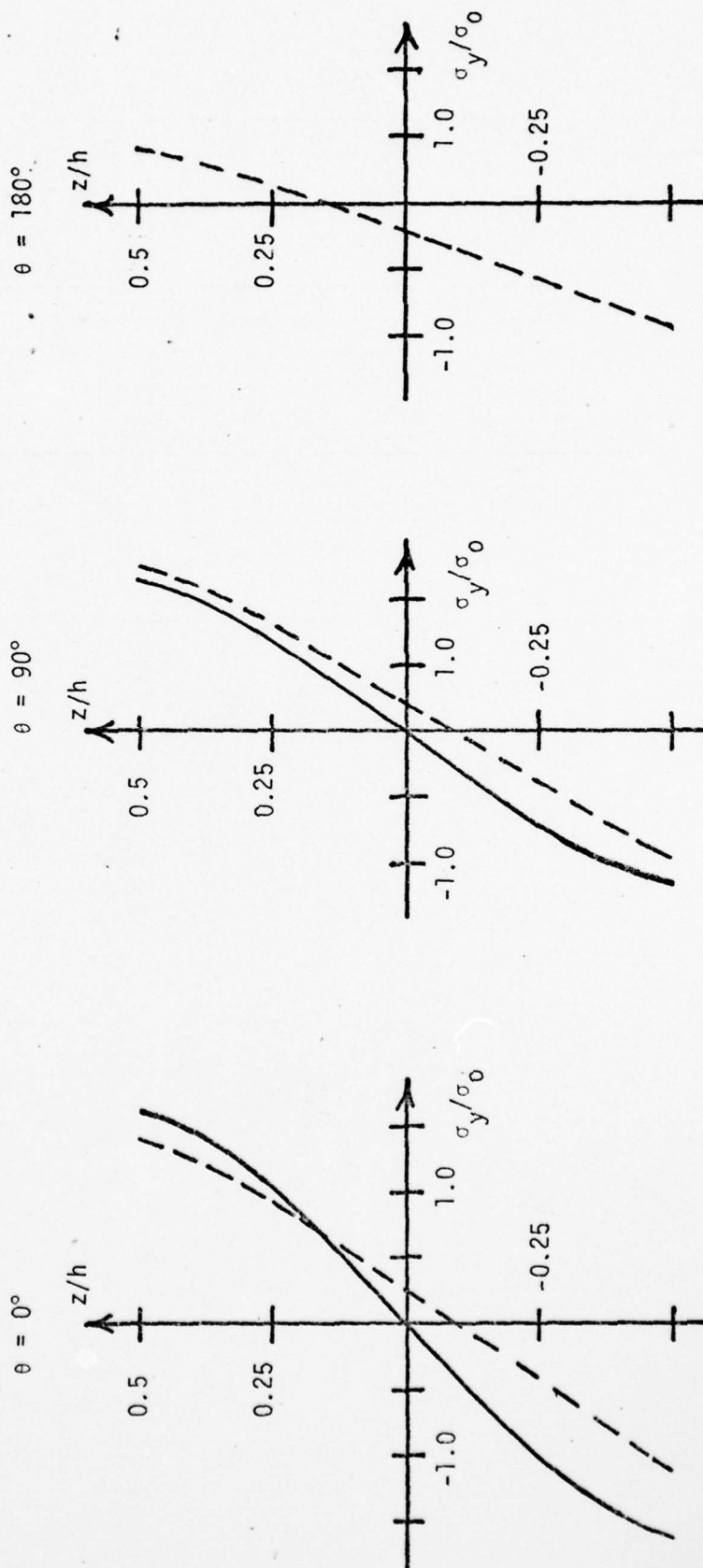
—— No Closure

--- Closure

FIGURE 6-10

ELASTO-PLASTIC STRESS DISTRIBUTION

$$(\tau_{xy}/\sigma_o)$$

τ_{xy}/σ_o vs z/h at r/a = 3/16, θ = 90° and σ_o/σ_L = .988

——— No Closure

‒ ‒ ‒ Closure
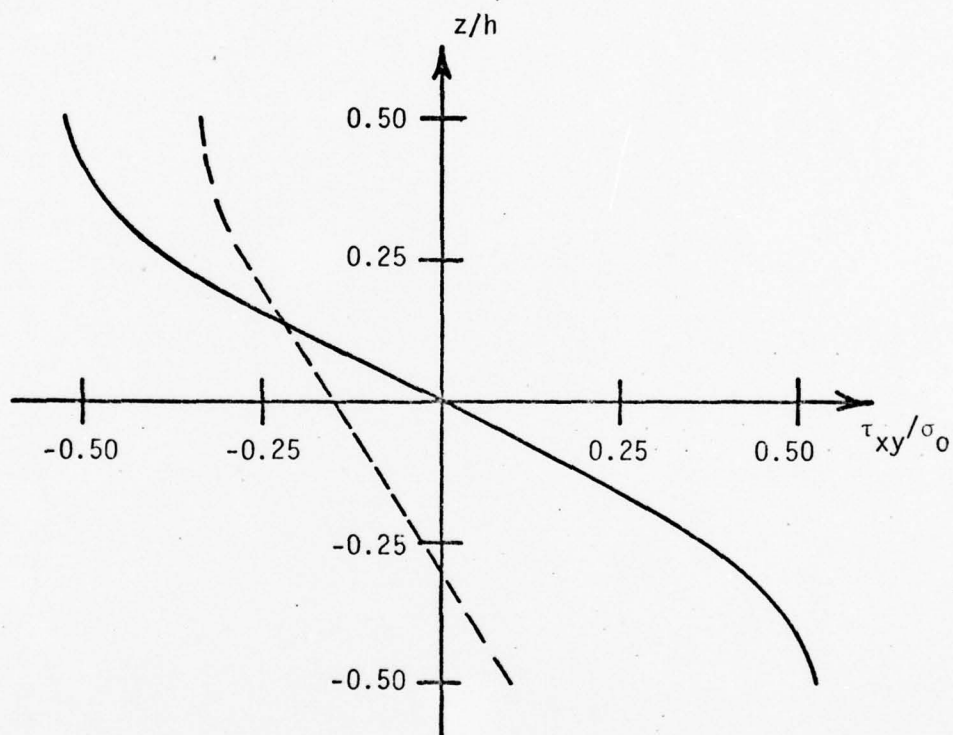
FIGURE 6-11

DISPLACEMENT BASED ELASTO-PLASTIC

BENDING STRESS INTENSITY FACTORS

$(Q/Q_{Elastic})$

$$Q = \lim_{r \to 0} \frac{Ev}{\sqrt{r}}$$

○ No Closure

● Closure

σ_o/σ_L (or M_o/M^*)
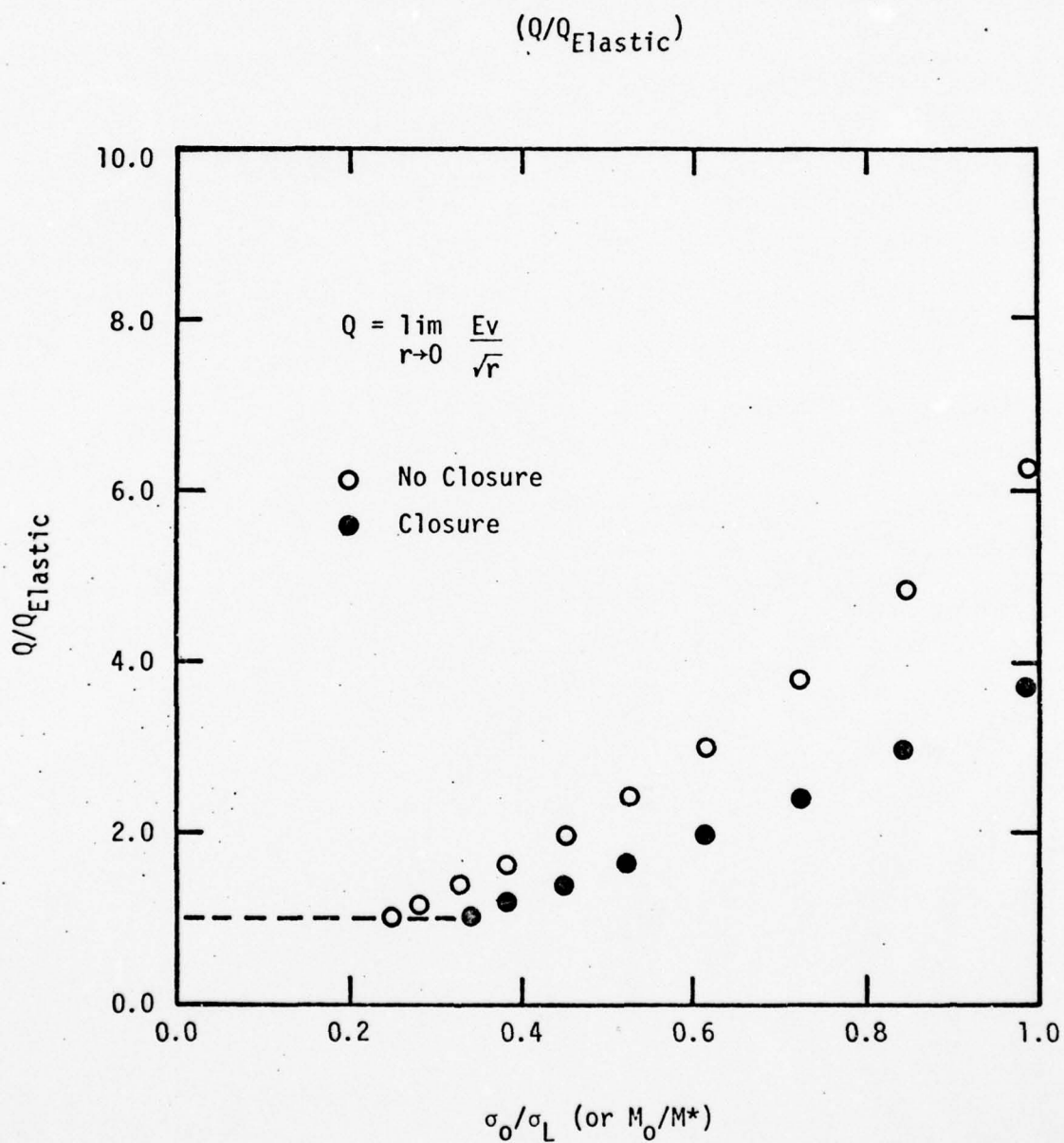
FIGURE 6-12

DISPLACEMENT BASED ELASTO-PLASTIC

BENDING STRESS INTENSITY FACTORS

$(Q/\sigma_0 \sqrt{\pi a})$

$$Q = \lim_{r \to 0} \frac{Ev}{\sqrt{r}}$$

○ No Closure

● Closure
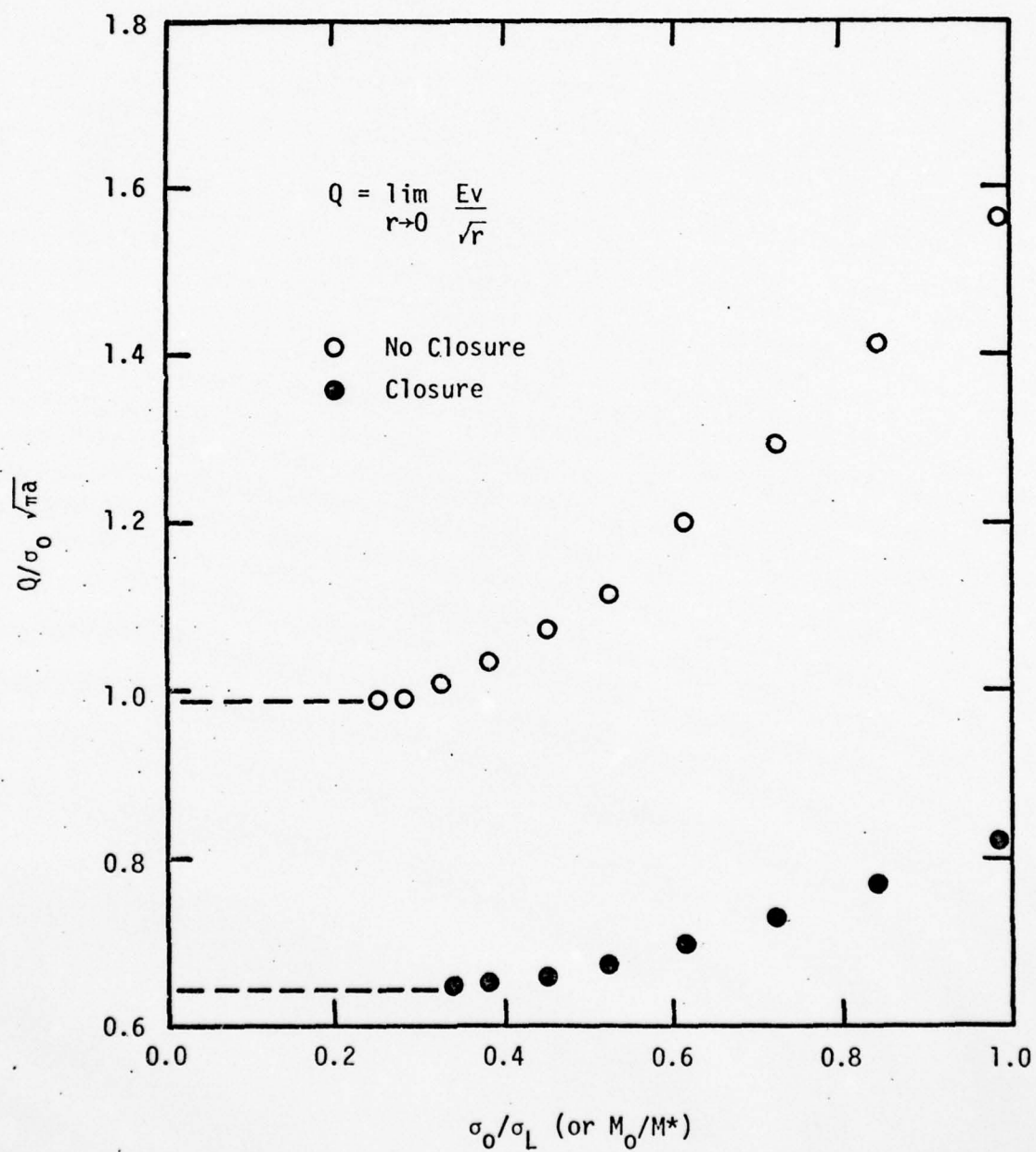
FIGURE 6-13

STRESS BASED ELASTO-PLASTIC BENDING

STRESS INTENSITY FACTORS ($K*/K*_{Elastic}$)

1.2

1.1

1.0

0.9

$K*/K*_{Elastic}$

0.8

0.7

0.6

0.0   0.2   0.4   0.6   0.8   1.0

○ No Closure

● Closure

$$K* = \lim_{r \to 0} \sigma_y \sqrt{2\pi r}$$

σ_0/σ_L (or $M_0/M*$)
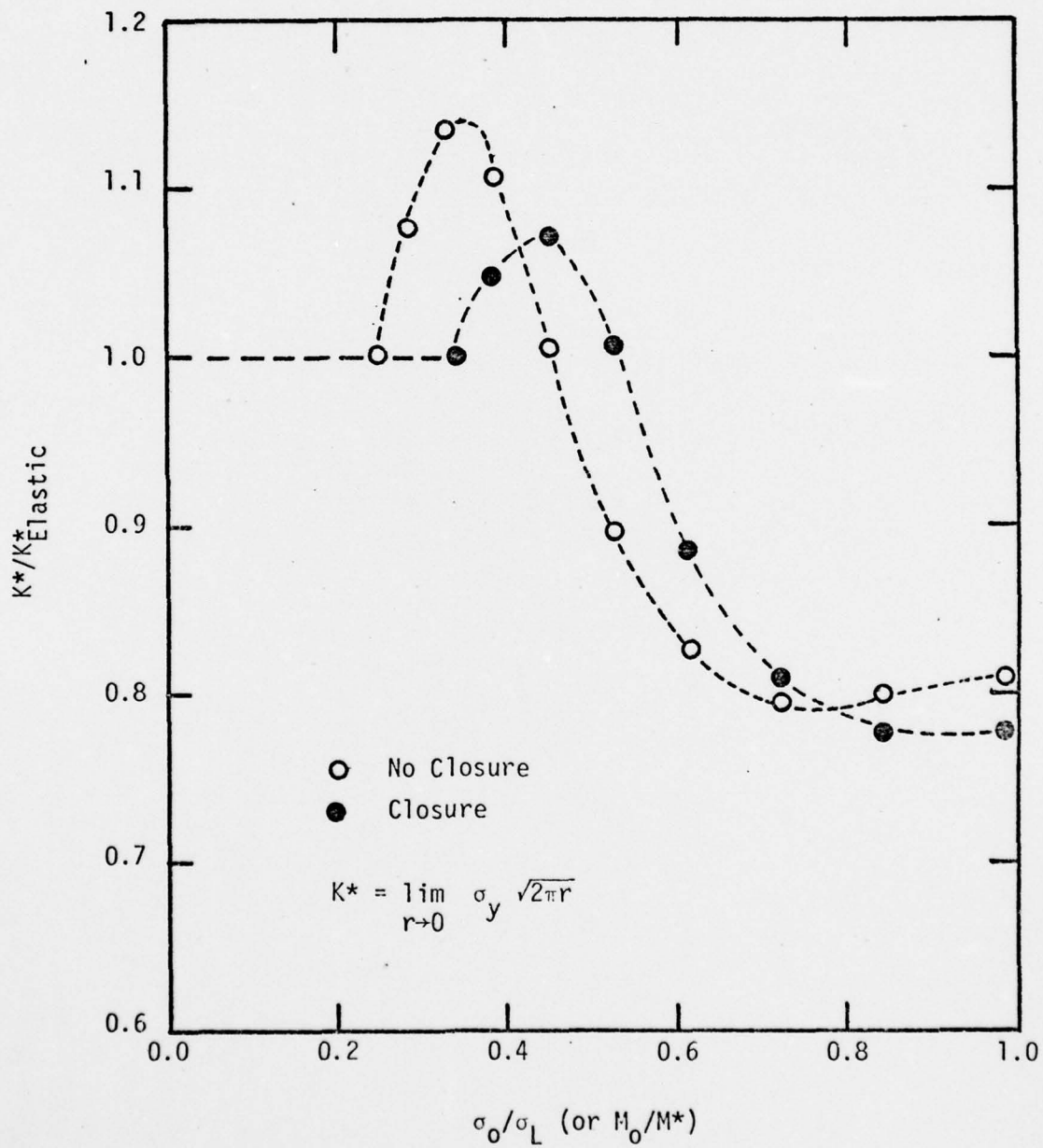
FIGURE 6-14

STRESS BASED ELASTO-PLASTIC

BENDING STRESS INTENSITY

FACTORS ($K*/\sigma_0 \sqrt{\pi a}$)
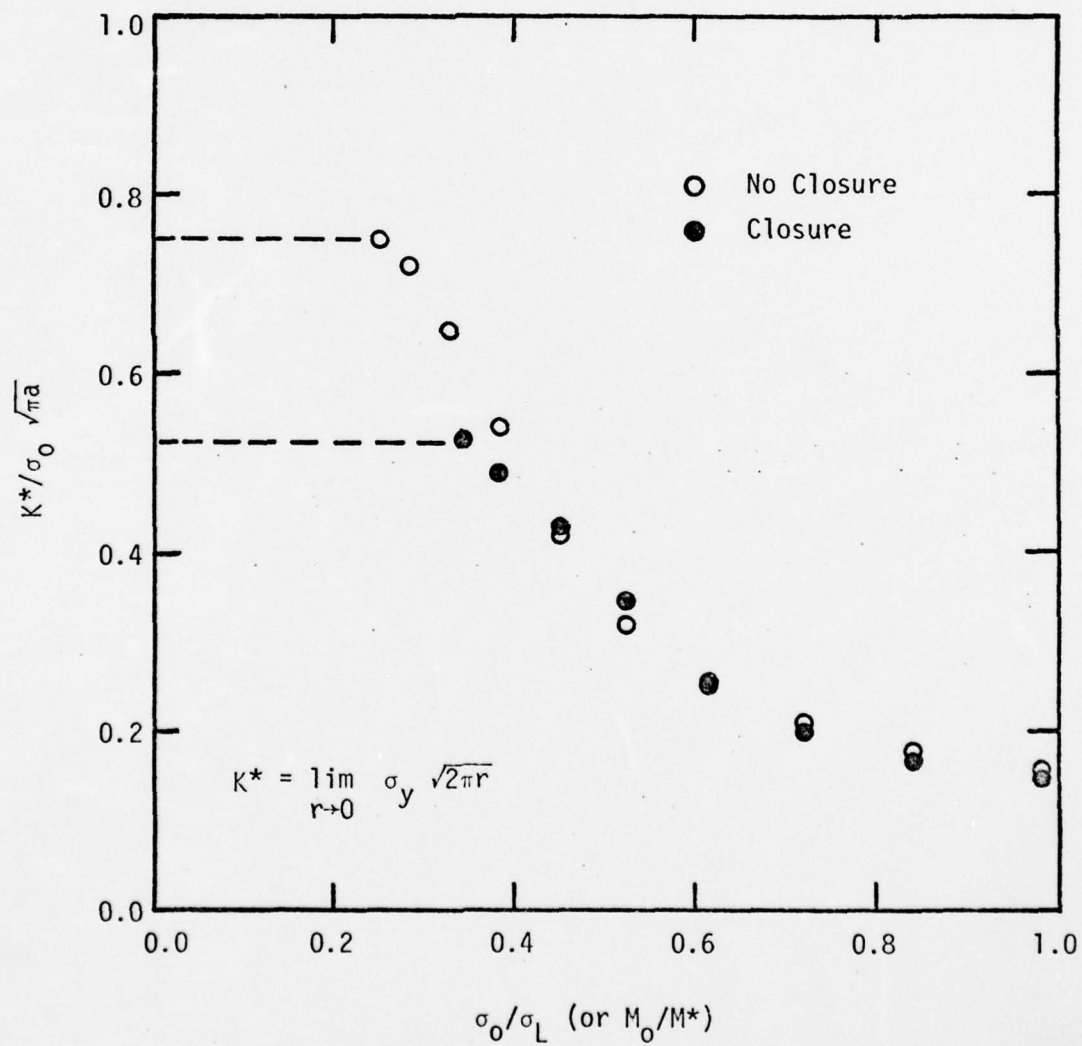
FIGURE 6-15

SHEAR EFFECTS: τ_{xz} AS A PERCENTAGE OF τ_0

(TENSION SURFACE)

78
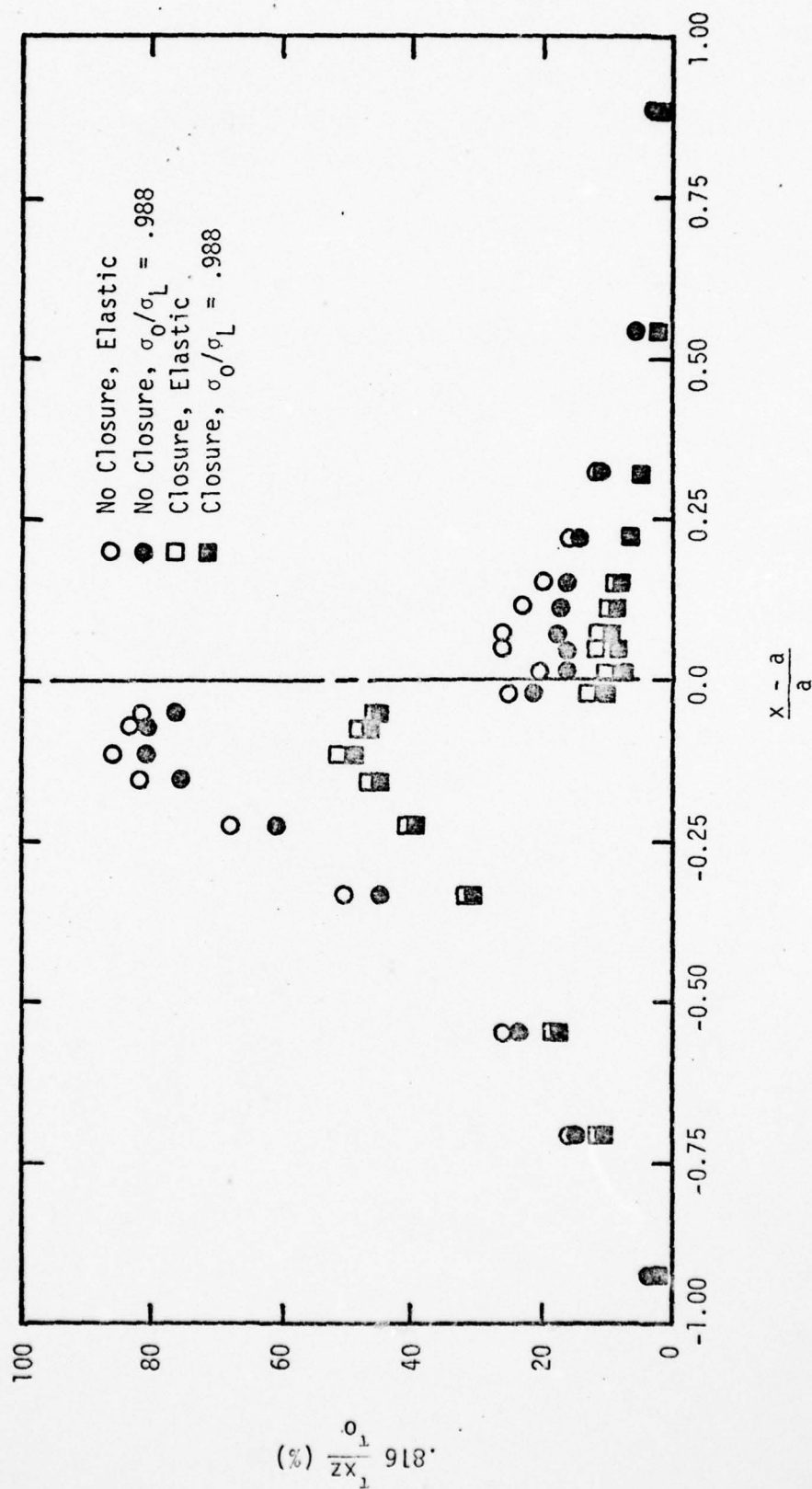
FIGURE 6-16

THROUGH THICKNESS SHEAR DISTRIBUTIONS

$$(\tau_{xz}/\sigma_0)$$

τ_{xz}/σ_0 vs z/h for r/a = 3/16, σ_0/σ_L = .988
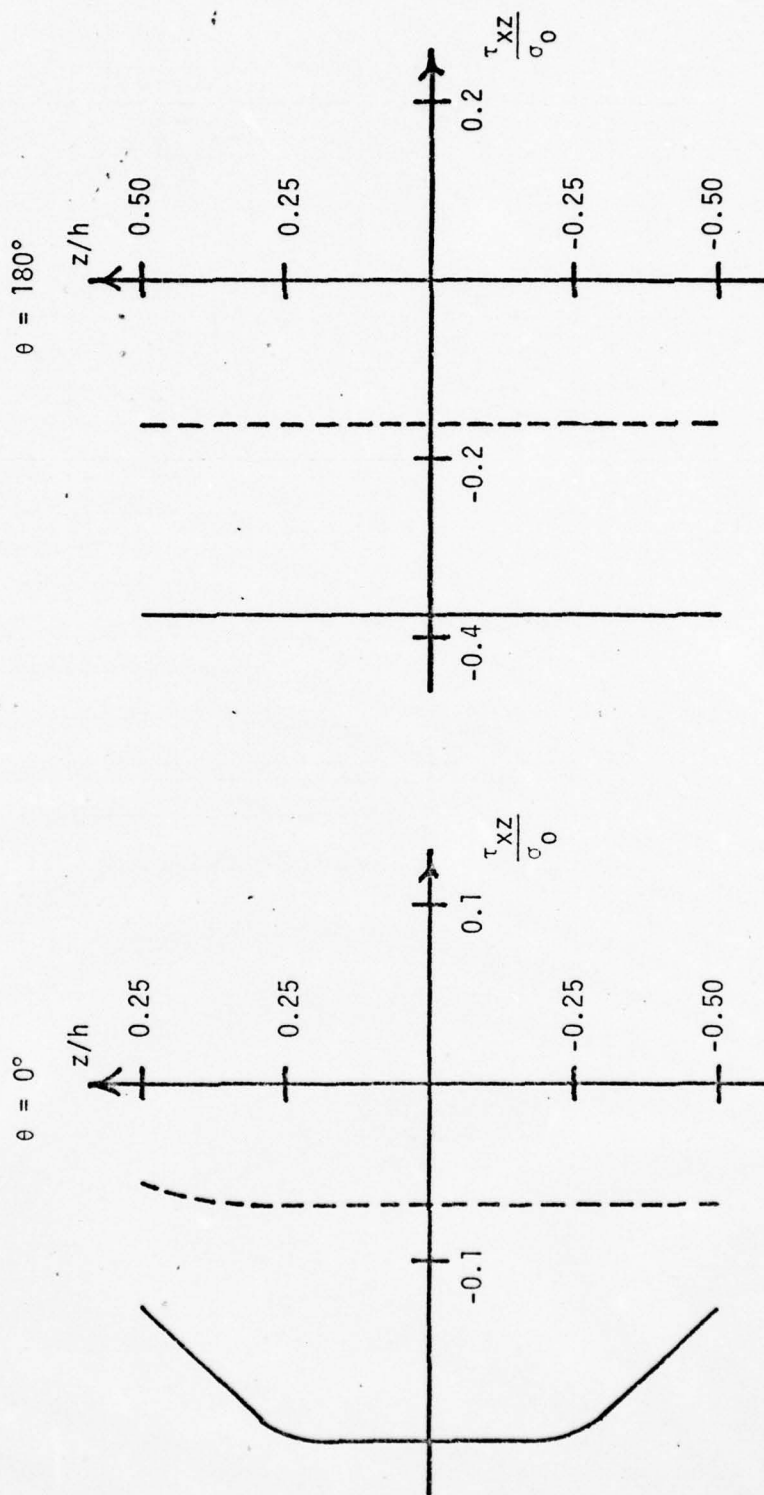
FIGURE 6-17

YIELD ZONE FOR THE UNIAXIAL NO
CLOSURE CASE
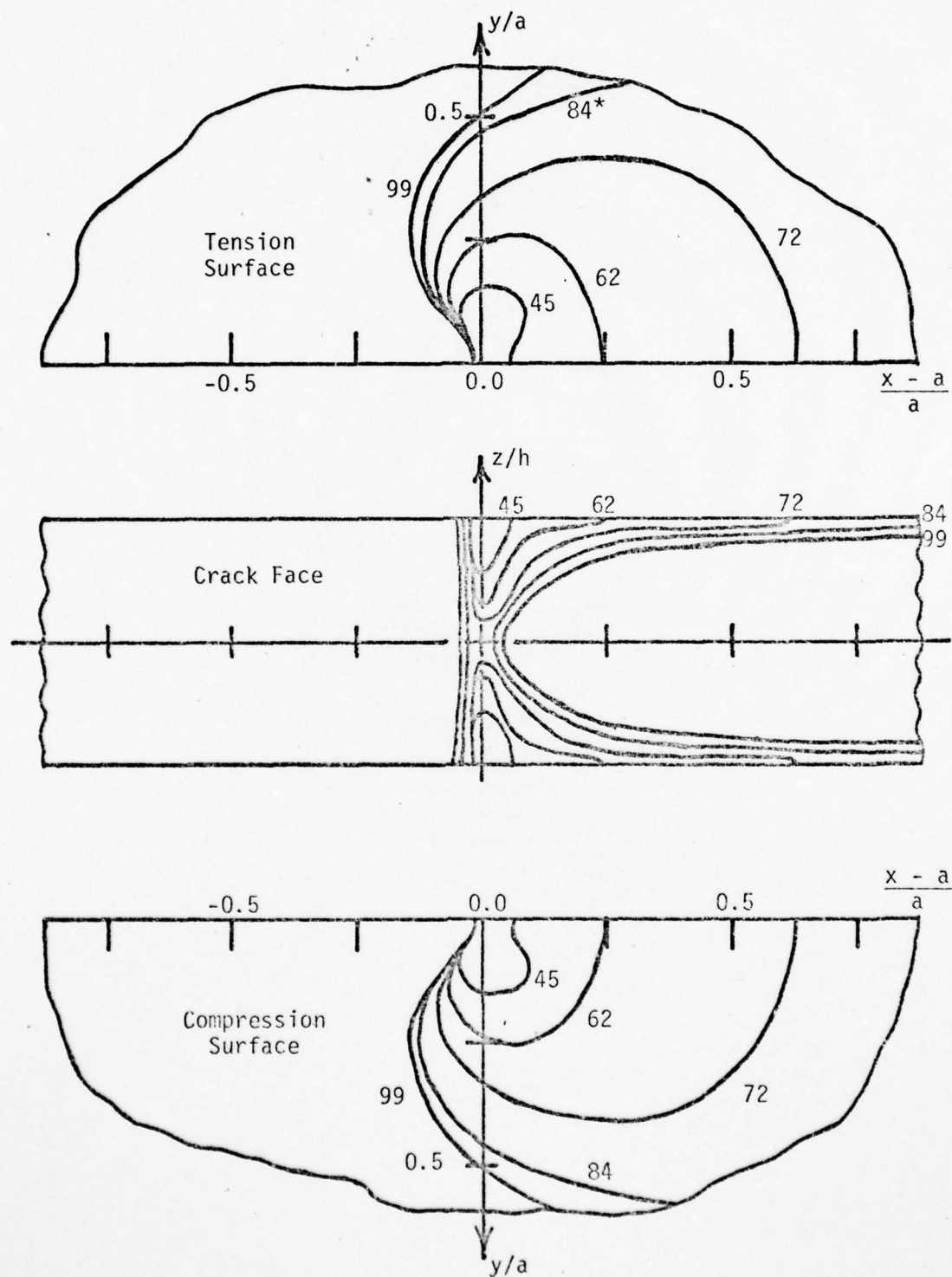
* Normalized Applied Load (σ_0/σ_L or M_0/M^*)
Expressed as a Percentage.

FIGURE 6-18

YIELD ZONES FOR THE UNIAXIAL
CLOSURE CASE
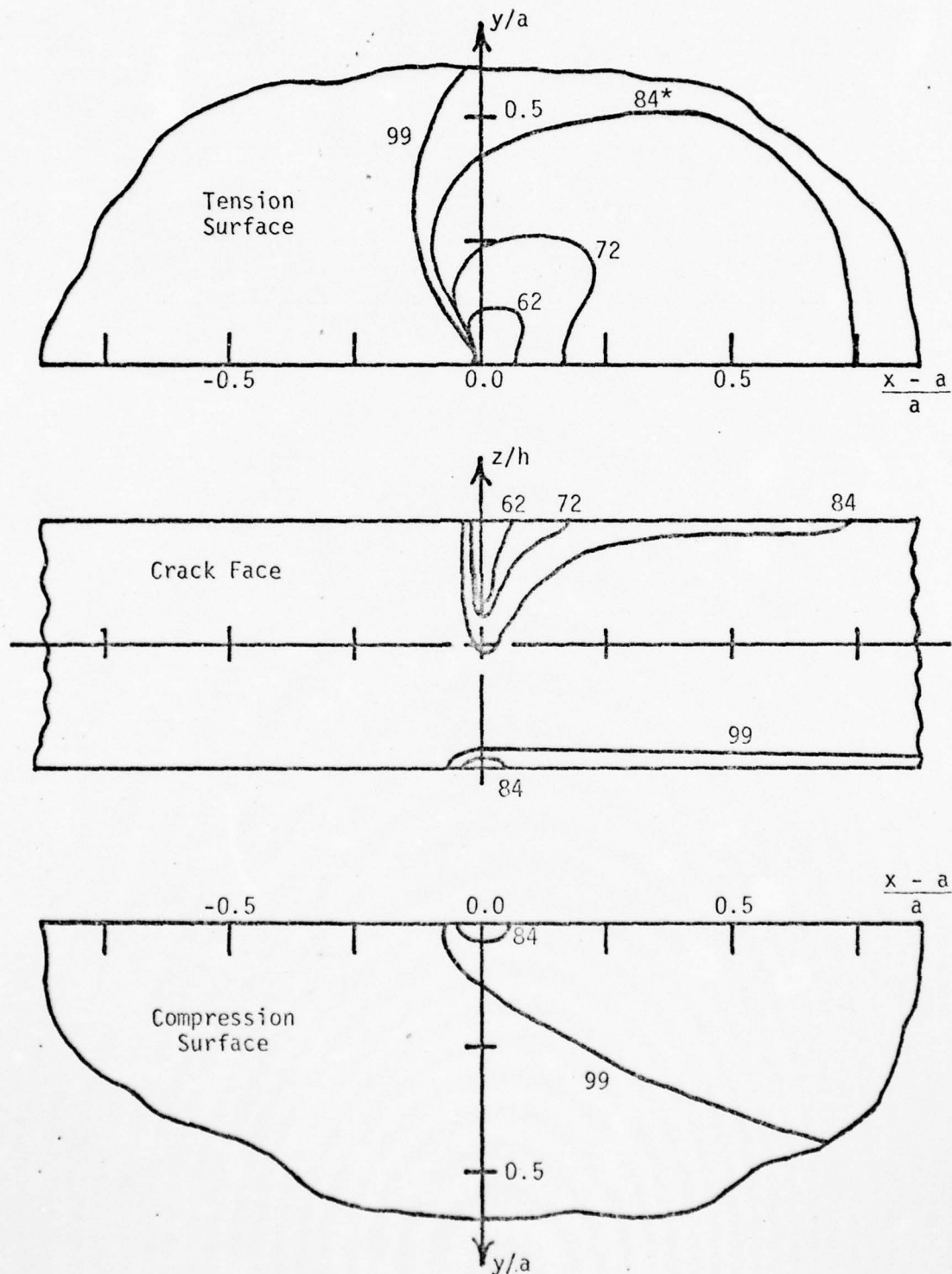
* Normalized Applied Load (σ_0/σ_L or M_0/M^*)
Expressed as a Percentage.

CHAPTER VII

DISCUSSION OF RESULTS

The results presented in the previous two chapters focused on various aspects of the bending problem. In this chapter these results are discussed in more detail and, where possible, are compared to previously published results. The discussion will generally follow the same order of presentation as the results, beginning with the elastic data.

7.1 Discussion of Elastic Results

The focus of the elastic discussion is on the comparison of the results with the expected behavior. That is, the capability of Mindlin theory to satisfy all three boundary conditions at any point should provide results that are close to the actual physical behavior. Comparisons are made with Jones' [11] Kirchhoff analyses of the no closure and closure cases and with Hartranft and Sih's [5] results for the no closure case.

7.1a Simple Beam Analogy

The initial issue to be resolved is a determination of the expected behavior when the closure constraint is imposed. The closure constraint results in the application of a line force along the compression surface of the crack flank. The line force is of sufficient magnitude to move the compression surface

from the displacement v obtained in the no closure case to the zero displacement required by the closure constraint. Some insight into the behavior resulting from closure is available from a simple, analogous situation.

Consider a simple beam with a compressive end force applied at the bottom surface (see Figure 7-1). Application of a force P at point B is statically equivalent to applying a force P and a clockwise moment M = Ph/2 at point O as shown in Figure 7-2. The effects of this force and moment are as follows.

From simple beam theory, which is the one dimensional analog of Kirchhoff plate theory, the displacement of point A, Δ, due to the equivalent force and moment loads comprises two parts. The force P produces an axial displacement Δ_L given by

$$\Delta_L = - \frac{PL}{AE} = - \frac{PL}{bhE} \tag{7-1}$$

An additional axial displacement of A, but in the opposite direction, is produced by the moment M and is given by

$$\Delta_R = + \frac{\theta h}{2} \tag{7-2}$$

where θ is the rotation about O due to the applied moment. From simple beam theory the rotation is

$$\theta = \frac{ML}{EI} \tag{7-3}$$

Substituting for M and noting that
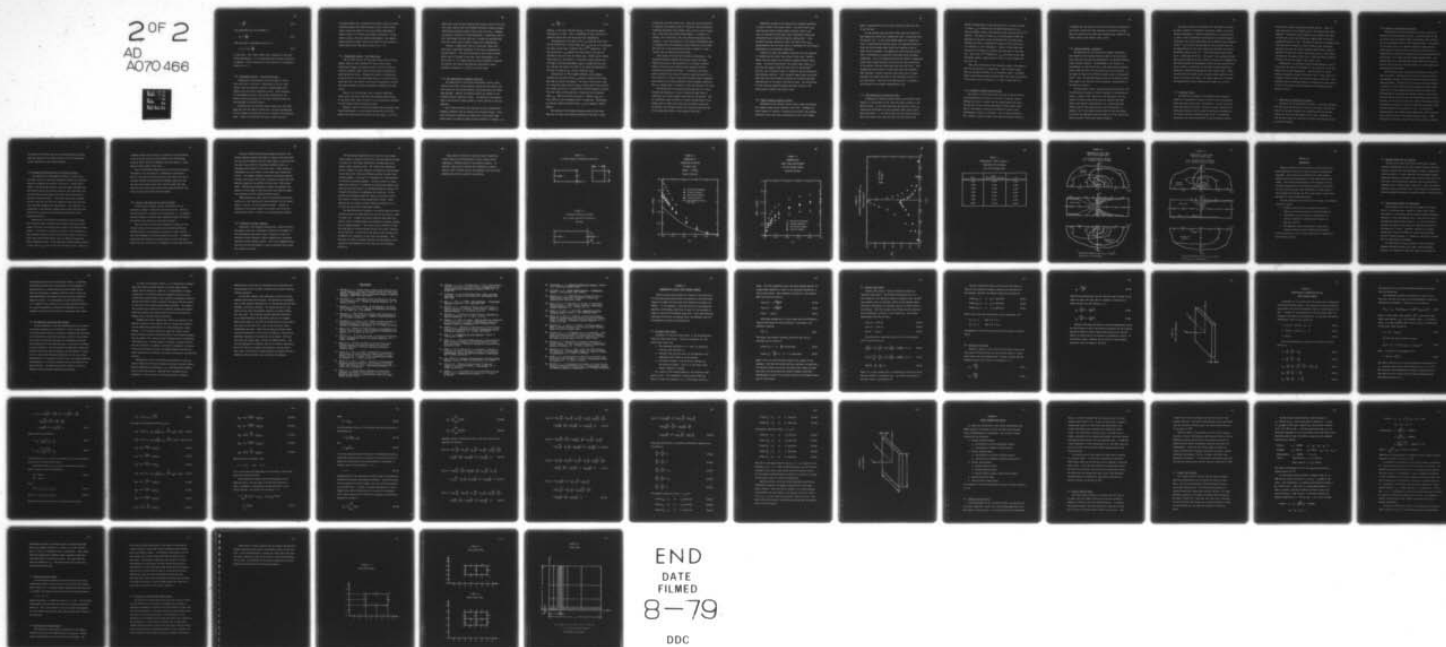
$$I = \frac{bh^3}{12} \qquad (7-4)$$

the displacement due to the moment is

$$\Delta_R = + \frac{3PL}{bhE} \qquad (7-5)$$

Thus, the total displacement of point A is

$$\Delta = \Delta_L + \Delta_R = \frac{2PL}{bhE} \qquad (7-6)$$

to the right. This result implies that a decrease in the crack flank displacement v is to be expected when the closure constraint is imposed. Further discussion of this conclusion is contained in Sections 7.1c, d.

7.1b Displacement Results - The No Closure Case

Comparisons of displacement results are made in the far field and local to the crack. Observation of the far field results shows the expected increases in displacements when compared with the results obtained by Jones. These increases in displacements are due to the greater flexibility of the Mindlin theory which allows for the shear deflections that are not contained in Kirchhoff theory.

An analysis of the localized effects along the crack flank shows that the same general trends occur, but that the magnitude of the increases are greater due to the strength of the localized shear. Figure 7-3 shows that for the no closure case the

transverse deflections w obtained using Mindlin theory are about one-third greater than those obtained by Jones with Kirchhoff theory, while the results for the crack flank displacements v shown in Figure 7-4 indicate even greater differences. On the tension surface, the crack opening displacements v are approximately two-thirds higher close to the crack tip and increase to almost double those reported by Jones at r/a = 1.0.

7.1c Displacement Results - The Closure Case

The far field results for the closure case follow the same general trends as those observed for the no closure case. Surprisingly though, the closure results in the far field are virtually identical (much less than one percent difference) to those obtained by Jones. Although this result is interesting, it may be that it is only fortuitous; thus, no conclusion can be drawn here until this result is verified or disproved by results from other problems in which the geometric parameters have been varied.

Analysis of the crack data leads to several additional observations, the first being that the transverse deflections w of the crack flank, shown in Figure 7-3, are practically identical to the Kirchhoff results produced by Jones.

Secondly, Figure 7-4 shows that Mindlin theory produces crack flank displacements v on the tension surface that are 13-15% greater than those reported by Jones for the range $0 \leq r/a \cong 0.5$.

Beyond this range the data converge and actually cross at r/a $\cong$ 0.8. This result implies that the Kirchhoff and Mindlin theories produce significantly different results close to the crack tip. Although the region of influence of these differences is apparently within a half crack length from the crack tip, it cannot be concluded that this will be the case for other cracked plate configurations.

Thirdly, a comparison of the no closure and closure data indicates a significant difference in the results obtained with the two theories. The results obtained by Jones using Kirchhoff theory show an increase in the crack flank displacements v of 20% in the r/a < 0.5 region when the closure condition is imposed. In contrast, the closure data obtained using Mindlin theory indicates a decrease in v of 30% in the same range.

7.1d The Significance of Boundary Conditions

The comparisons of the elastic displacement results clearly indicate that Mindlin theory produces results for the closure case that agree with the expected behavior (as determined by the simple beam analogy). However, the opposite effect was evident in the Kirchhoff results reported by Jones. The question to be answered then is why classical theory produces a result opposite to the one expected.

In an effort to answer this question, we have considered the boundary conditions that are imposed with Kirchhoff theory. Since only two boundary conditions are admissible in the fourth order plate theory, an effective shear boundary condition is imposed, i.e.,

$$Q_y - \frac{\partial M_{yx}}{\partial x} = 0 \qquad\qquad (7-7)$$

where Q_y is the shear resultant and M_{yx} is the twisting moment resultant on a y-face. Thus, a combination of shear and twist is specified rather than each being specified independently.

An examination of the shear stress τ_{xy} along the crack flank for the Kirchhoff [11] results shows that τ_{xy} goes up as it approaches the crack tip and that it exhibits the $(r)^{-1/2}$ singularity. For the closure case, τ_{xy} exhibits the same behavior, but does not increase as fast as in the no closure case. Another way of stating these results is that there is a relatively large, positive rate of change in the twisting moment, $\partial M_{yx}/\partial x$, approaching the crack tip, and that the effect of closure is to reduce the magnitude of the rate of change of M_{yx}, but not change the sign.

Consideration of the Kirchhoff effective shear boundary condition and the shear stress τ_{xy} behavior along the crack flank now leads to several conclusions. For the no closure case, there is a relatively large, positive $\partial M_{yx}/\partial x$ which requires the presence of a large, positive Q_y to satisfy the Kirchhoff boundary condition. This also implies the presence of a large, positive transverse shear τ_{yz}. When the closure constraint is imposed, $\partial M_{yx}/\partial x$ is still positive, but noticeably smaller in magnitude. Accordingly, Q_y (and the induced transverse shear τ_{yz}) also becomes a smaller quantity.

The presence of the induced transverse shear on the crack face acts to reduce the transverse deflection from what it would

be were the crack face stress free. When the closure constraint is imposed, the transverse shear is decreased, thus allowing the transverse deflection to be greater than it was in the no closure case. Since the crack opening displacement v is related to w through a first derivative, the crack opening displacement also increases. Thus, the decrease in crack opening displacement that is expected due to the compressive force induced by closure does not occur due to the substantially greater increase in v that results from the induced transverse shear.

These results are given the following interpretation. The observed differences between the expected results and those reported by Jones are due exclusively to a boundary condition effect arising from the effective shear boundary condition required by Kirchhoff plate theory. In contrast, the results based on Mindlin plate theory do show the expected results for v. This reduction in v occurs since Mindlin theory admits independent specification of the three physically natural boundary conditions. Thus, no induced shear is present to cause the opening of the crack.

The observations and conclusions presented thus far clearly indicate the importance of using a theoretical model that incorporates the correct boundary conditions for the problem. That is, the Mindlin model provides an accurate representation of the problem since it admits the three natural boundary conditions. In contrast, the Kirchhoff results are inherently deficient due to the approximate nature of the boundary conditions.

Additional evidence of the importance of boundary conditions is found in some of the stress results. The stress ratio σ_x/σ_y resulting from Mindlin theory remains positive ahead of the crack as expected from the plane stress extensional problem and the bending results reported by Knowles and Wang [3]. In the Kirchhoff analyses reported by Jones, the stress ratio σ_x/σ_y become negative near the crack tip as a consequence of the Kirchhoff approximation of the boundary conditions.

Another area where the boundary conditions are very important is in modelling the stress free surface of the crack. Mindlin theory correctly models this situation, whereas Kirchhoff theory cannot. As discussed previously, the inplane shear stress τ_{xy} is positive and singular along the crack flank in the Kirchhoff analyses, and a transverse shear is induced to satisfy the approximate boundary condition. Thus, Kirchhoff theory cannot accurately model the crack face boundary conditions nor provide an accurate representation of the stress distribution there. The implications of this inaccurate modelling become even more evident in the elasto-plastic problem (see Section 7.2a).

7.1e Pseudo Stresses Induced By Closure

Examination of the elastic closure results shows the presence of a nonzero normal stress along the crack flank. Although this result appears to indicate a violation of the stress free boundary condition on the crack face, consideration of the finite element

model's interpretation of the closure constraint shows that this
is not the case.

For the closure case, the crack flanks come into contact at
the compression surface and a compressive force is generated along
the contact line. In the finite element model this compressive
force is represented by discrete values, the Lagrange multipliers.
Since the finite element model admits only midplane values of
nodal forces and moments, the compressive force along the contact
line is interpreted as a statically equivalent force and moment
combination. Since the compressive force also induces a compressive
stress field, pseudo stresses arising from the static equivalent
of the contact force are calculated along the crack flank. Thus,
although the crack surface is stress free, the finite element
model generates stresses along the crack flank since it cannot
represent the compressive force at the compression surface in
any other manner. Note that this modelling quirk is present in
the Kirchhoff finite element representation also.

7.1f The Contribution of Transverse Shear

A fundamental difference between Mindlin and Kirchhoff plate
theories is the presence of the transverse shear stresses in the
Mindlin theory. It has been shown that the transverse shear τ_{xz}
contributes significantly to the octahedral shear stress along
the crack flank, i.e., as much as 86% in the no closure case and
58% in the closure case near the crack tip (see Figure 5-13).

Another representation of the transverse shear is shown in Figure 7-5 where τ_{xz} is normalized by the applied bending stress σ_o. With and without closure, the transverse shear exhibits the $(r)^{-1/2}$ behavior. The effect of closure is to significantly reduce the magnitude of the shear stress (by 50-63%) over the range shown. Although the shear is substantially reduced in the closure case, its influence is still substantial. Figure 7-5 also shows that the region of influence is primarily the area local to the crack tip. Due to the $(r)^{-1/2}$ behavior of τ_{xz}, the effect of the shear dissipates rapidly, roughly within a half of a crack length from the crack tip.

Thus, the contribution of the transverse shear to the behavior local to the crack tip is significant. Since Kirchhoff theory does not include the effects of the transverse shear, a Kirchhoff model of the problem cannot accurately model the stress distribution in the primary area of interest, i.e., local to the crack tip.

7.1g A Comment on Neutral Surface Shifts

One effect of crack closure that has been alluded to briefly in the presentation of results is the shift in neutral surface. Although the shift in neutral surface unquestionably does occur, the question of how to define the neutral surface remains open. That is, the neutral surface may be defined in terms of zero displacements, strains, or stresses. Each of these definitions will indicate a neutral surface shift when the closure constraint

is imposed, but the direction of the shift and the new location of the neutral surface will vary according to the definition used. Thus, no conclusions are drawn here concerning the strength of the closure effect on the neutral surface shift.

7.1h Fracture Mechanics Discussion

The importance of using the correct boundary conditions is also evident in the fracture mechanics analysis of the results. Jones used the crack opening displacements v to determine bending stress intensity factors. Corresponding to the increase in displacements for the closure case, Jones found that the bending stress intensity factor for the closure case also increases. As was shown in Figure 5-14 the Mindlin theory leads to the opposite result. Thus, the Kirchhoff approximation of the boundary conditions leads to an incorrect fracture mechanics interpretation of the effect of closure.

The experimental results reported by Smith and Smith [9, 10] also indicate an increase in stress intensity in the presence of closure. However, their results are not conclusive since the effects of closure could not be entirely isolated from other effects that operate simultaneously, e.g., three-dimensional effects such as crack extension and crack face warping. In contrast, the finite element analysis does isolate the effects of closure, but admittedly does not model all of the interacting effects present in the actual physical problem.

As shown in Figures 5-14 through 5-17, the effect of closure on stress intensity is internally consistent, whether it be crack opening displacement v, transverse deflection w, or bending stress σ_y that is used to determine the bending stress intensity factors. In addition, the stress based dimensionless bending stress intensity factor S^* (see Figure 5-16) obtained for the no closure case can be compared with the $\phi(1)$ value reported by Hartranft and Sih [5]. The Mindlin theory result ($S^* = .734$) and Reissner theory result ($\phi(1) = .700$) agree within 5%. This result is not unexpected since the two plate theories are very similar (as discussed in Appendix A). Note that although the displacement results are more accurate than stress results, no equations are available to make quantitative comparisons between displacement and stress based values. Hence, the definition of bending stress intensity factor remains an open issue in the sense that there is no obvious means for rectifying the computational results obtained (with respect to σ_y and v).

7.1i Thickness Effects

The effects of thickness on the bending stress intensity factor was illustrated in Figures 5-17 and 5-18 for displacement based and stress based values, respectively. For the no closure case, both figures indicate an increase in stress intensity with increasing thickness, and the shape of the curve corresponds to the results reported by Hartranft and Sih [5]. As mentioned previously, the stress based values S^* may be compared directly

with the $\phi(1)$ values obtained by Hartranft and Sih. Table 7-1
shows the results of this comparison for the range of h/2a values
analyzed. The Mindlin results compare very favorably with those
of Hartranft and Sih with differences ranging from 2-14% and an
average difference of 7.6%. The effect of closure is to substantially
lower the rate of increase of stress intensity with increasing
thickness such that the stress intensity remains fairly constant
over most of the range of h/2a values shown; that is, after sharp
increases for the range $0.0125 \leq h/2a < 0.075$ the stress intensity
rises only 8% for the range of $.075 \leq h/2a \leq 0.5$.

Additionally, it was found during the determination of the S^*
values that the value of S^* obtained is very sensitive to the data
points used for the extrapolation. The sensitivity is strong
enough to completely reverse the trend of the S^* versus h/2a curve
if points slightly further away from the crack tip are used. This
indicates that an additional measure of judgment and caution should
be used in the stress based determination of the bending stress
intensity factor.

7.2 Discussion of Elasto-Plastic Results

Discussion of the elasto-plastic results is primarily concerned
with the growth and shape of the plastic yield zones, both for the
biaxial and uniaxial problems, and comparisons with the results
reported by Jones [11] and Swedlow, et al. [12]. Attention is
also directed toward the variations in stress intensity that occur
as yielding proceeds.

7.2a Growth of the Plastic Yield Zones

The growth of the plastic enclave is the most interesting feature of the elasto-plastic results. The yield zones for the no closure case are symmetric about the midplane, and an elastic core is preserved for most of the loading sequence. The presence of the elastic core is an important feature in modelling the actual physical situation, and, as pointed out by Jones, is an improvement over the results reported by Brinson and Gonzalez [31] and Brinson, et al. [32] using the Dugdale bending model. The Dugdale model is a rigid/perfectly plastic model that allows no elastic core at the crack tip and results in a cusp shaped yield zone through the thickness.

For the closure case, significant differences in the yield zones are noted. Yielding occurs first on the tension surface and propagates through the thickness from the tension surface as loading proceeds. Imposition of the closure constraint induces a compressive stress field along the compression surface of the crack flank via the compressive forces along the contact line. The magnitude of the compressive forces increases in proportion with the applied load until they are sufficiently large to cause yielding. At this point yield occurs almost simultaneously along the compression surface of the crack flank and propagates rapidly into the material with increases in load. For the results presented here, the yielding on the compression surface does not occur until very late in the loading sequence ($\sigma_o/\sigma_L = .988$). The greater constraint present in the closure case also inhibits

the growth of the yield zones on the tension surface such that they are roughly half as large as those in the no closure case at the same point in the loading sequence.

7.2b Boundary Condition Effects on the Plastic Enclave

The importance of the boundary conditions is again very noticeable when the yield zones produced by Mindlin and Kirchhoff theory are compared (see Figures 7-6 and 7-7). Using Mindlin theory, with and without closure, the yield zones propagate into the material and do not generate along the crack face until late in the loading sequence when yield of the entire surface(s) of the plate is(are) imminent. In contrast, the results reported by Jones show that the yield zones generate along the crack face first and then propagate into the material. This behavior is a consequence of the dominant singular shear stress along the crack flank that is induced by the Kirchhoff approximation of the boundary conditions.

Comparison of the Mindlin and Kirchhoff results also shows that the yield zones (for both the no closure and closure cases) ahead of the crack tip grow much more slowly in the Mindlin theory results. This result is explained in terms of the differences in the Kirchhoff and Mindlin stress distributions ahead of the crack. Recall that the Kirchhoff stress ratio is negative and does not have a magnitude of one. On the other hand, Mindlin theory produces a stress ratio σ_x/σ_y that is positive and close to one. Since the

octahedral shear stress varies as the square of the differences
in the principal stresses, the Kirchhoff stress distribution
produces larger values of octahedral shear and, hence, a larger
plastic enclave ahead of the crack.

Thus, the Kirchhoff theory plastic yield zones are severely
distorted in size and shape as a consequence of two factors.
That is, the yield zones grow along the crack face first due to
the shear induced by the approximate boundary conditions, and
the yield zones ahead of the crack are much larger than they
should be due to the nature of the stress distribution near the
crack tip that results from Kirchhoff theory.

7.2c Plastic Yield Zones for the Uniaxial Problem

For the uniaxial problem, several significant, but not
unexpected, changes in the yield zones are observed. Since the
uniaxial problem is inherently less constrained, i.e., no applied
transverse moment, the yield zones propagate through the material
more quickly than they did in the biaxial problem.

The initiation of yield on the compression surface for the
uniaxial closure case also provides an interesting difference.
Yielding begins on the compression surface at a lower applied
load, and propagates very quickly ahead of the crack. In contrast
with the biaxial problem, no yielding occurs on the crack face,
except very near the crack tip, throughout the load range considered.

The most interesting difference between the uniaxial and biaxial problems concerns the change in shape of the yield zones. For the biaxial problem, the yield zones appear to lean back over the crack face, while for the uniaxial problem, there is a noticeable shift forward in the yield zones. These results, as anticipated, are very similar to the plane stress extensional results. For example, Swedlow, Williams and Yang [12] reported uniaxial plane stress results for a centrally cracked plate with material properties very similar to those used in the present study. Although some differences in detail are apparent, the general size and shape of the yield zones they reported compare very favorably with the uniaxial bending results.

These observations imply that the extensional plane stress results are a fair predictor of surface behavior for the elasto-plastic, uniaxial, no closure bending problem. However, no predictions can be made through the thickness due to the non-linear behavior that is present in the elasto-plastic problem.

7.2d Variations in Stress Intensity

Variations in the apparent bending stress intensity factors with applied load were illustrated in Figures 6-11 through 6-14. The displacement based values shown in Figures 6-11 and 6-12 indicate a steady increase in stress intensity with increasing load both with and without closure. This is not unexpected since the crack opening displacements v used to calculate these values also increase with load.

The interesting comparison here is that the stress based values, shown in Figures 6-13 and 6-14, indicate different trends. In Figure 6-13, the stress intensities are normalized by the elastic stress intensity value. The results here indicate an initial increase in stress intensity followed by a sharp decrease in the values until the curve flattens out near the end of the loading sequence. This result is indicative of a redistribution of stresses as yielding proceeds. The Gauss points in a given region are initially in a condition of proportional loading until they reach the yield point. As yielding reaches the region, the stresses redistribute to accommodate the plasticity. As the yielded zone increases beyond the region, a transition occurs that leads to a phase of quasi-proportional loading. These observations are similar to those reported by Swedlow, et al., [12] for the plane stress extensional problem.

The redistribution of stresses is not evident when the stress intensity values are normalized by the current load value as shown in Figure 6-14. Instead, the stress intensity drops below the elastic value as yielding begins and continues to decrease throughout the loading sequence. This trend is also consistent in that the curve depicts a moving current value of the stress intensity at the crack tip. As the size of the plastic zone increases the strength of the singularity at the crack tip decreases. Thus, the curve is simply a graphical depiction of the decrease in the strength of the singularity at the crack tip with increasing plasticity.

These results illustrate a variety of ways of depicting stress intensity for elasto-plastic results, each of which highlights a different aspect of the material behavior. In addition, these results indicate that references to elasto-plastic stress intensity factors are ambiguous since the values obtained vary with the method of presentation.

FIGURE 7-1

A SIMPLE BEAM WITH COMPRESSIVE END LOAD
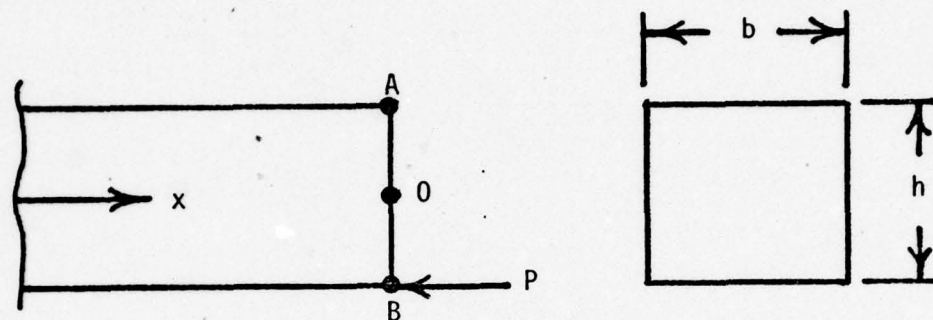
FIGURE 7-2

STATICALLY EQUIVALENT LOADING

FOR A SIMPLE BEAM WITH COMPRESSIVE

END LOAD

$M = Ph/2$
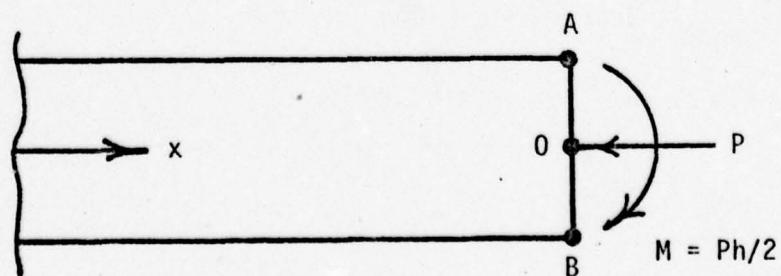
FIGURE 7-3

COMPARISON OF

TRANSVERSE DEFLECTION

OF CRACK FLANK

$$w[2D(1 + \nu)/a^2 M_0]$$

(ELASTIC RESULTS)
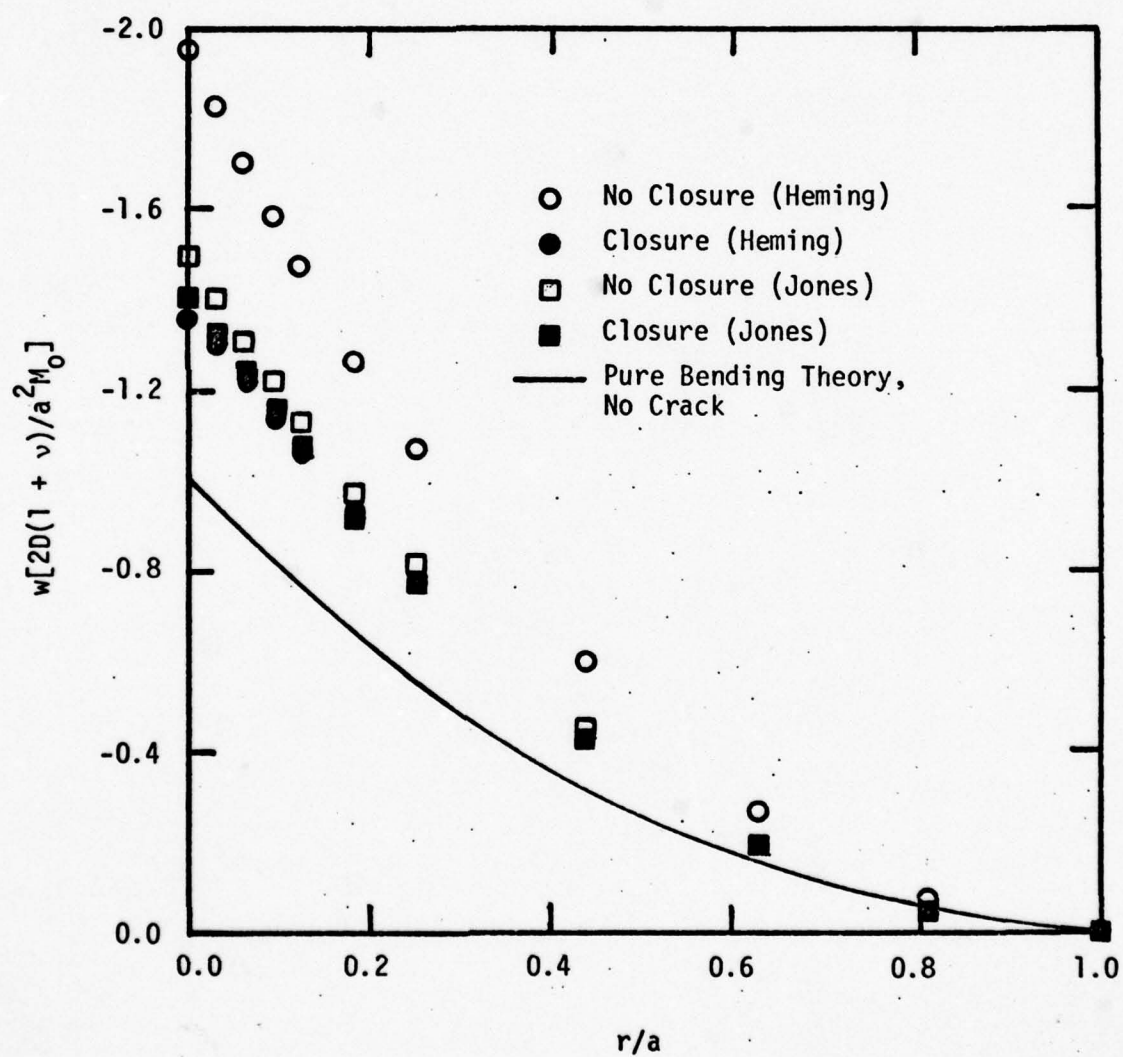
FIGURE 7-4

COMPARISON OF

CRACK FLANK DISPLACEMENTS

v ON THE TENSION SURFACE

(ELASTIC RESULTS)
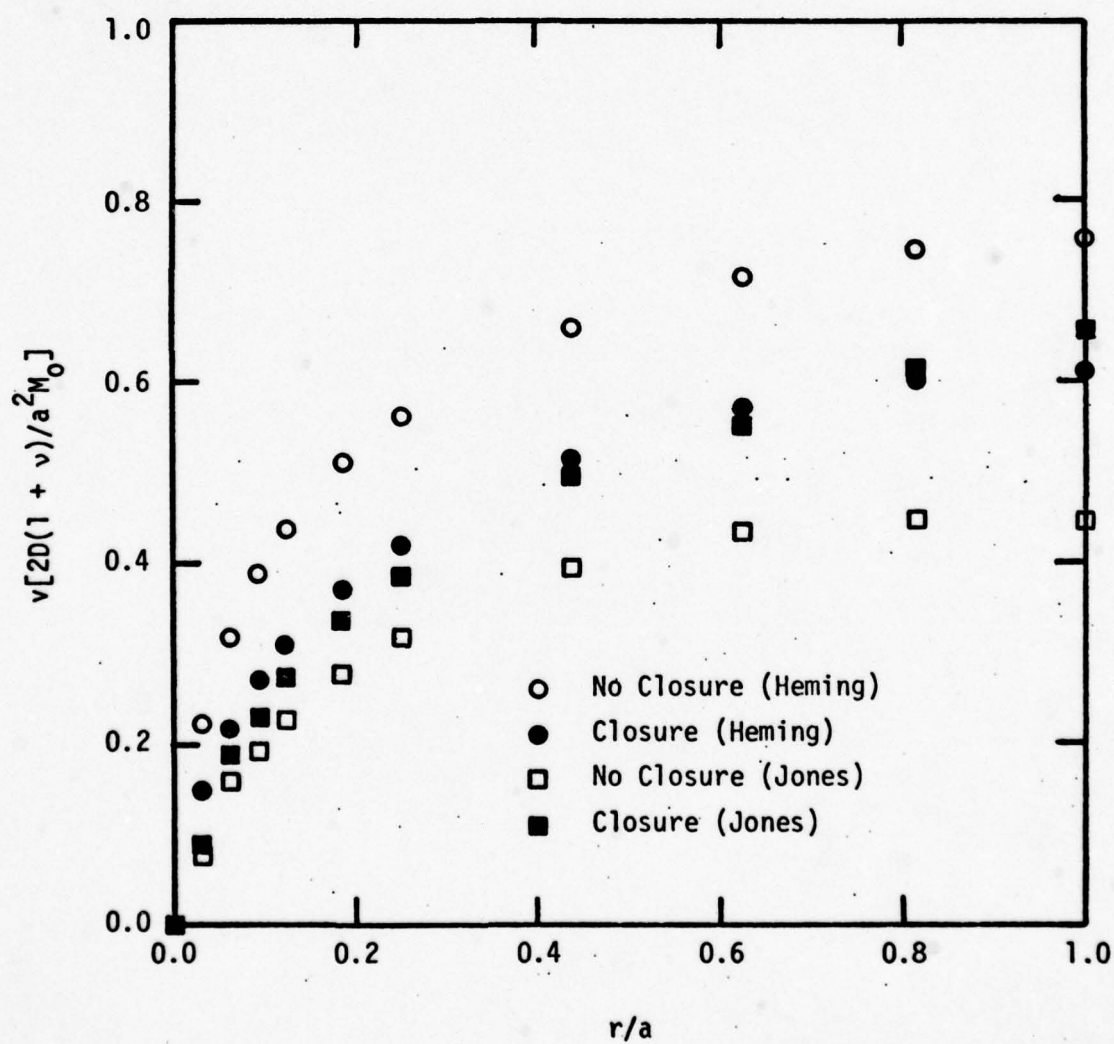
FIGURE 7-5

INFLUENCE OF TRANSVERSE SHEAR τ_{xz}

(ELASTIC RESULTS)
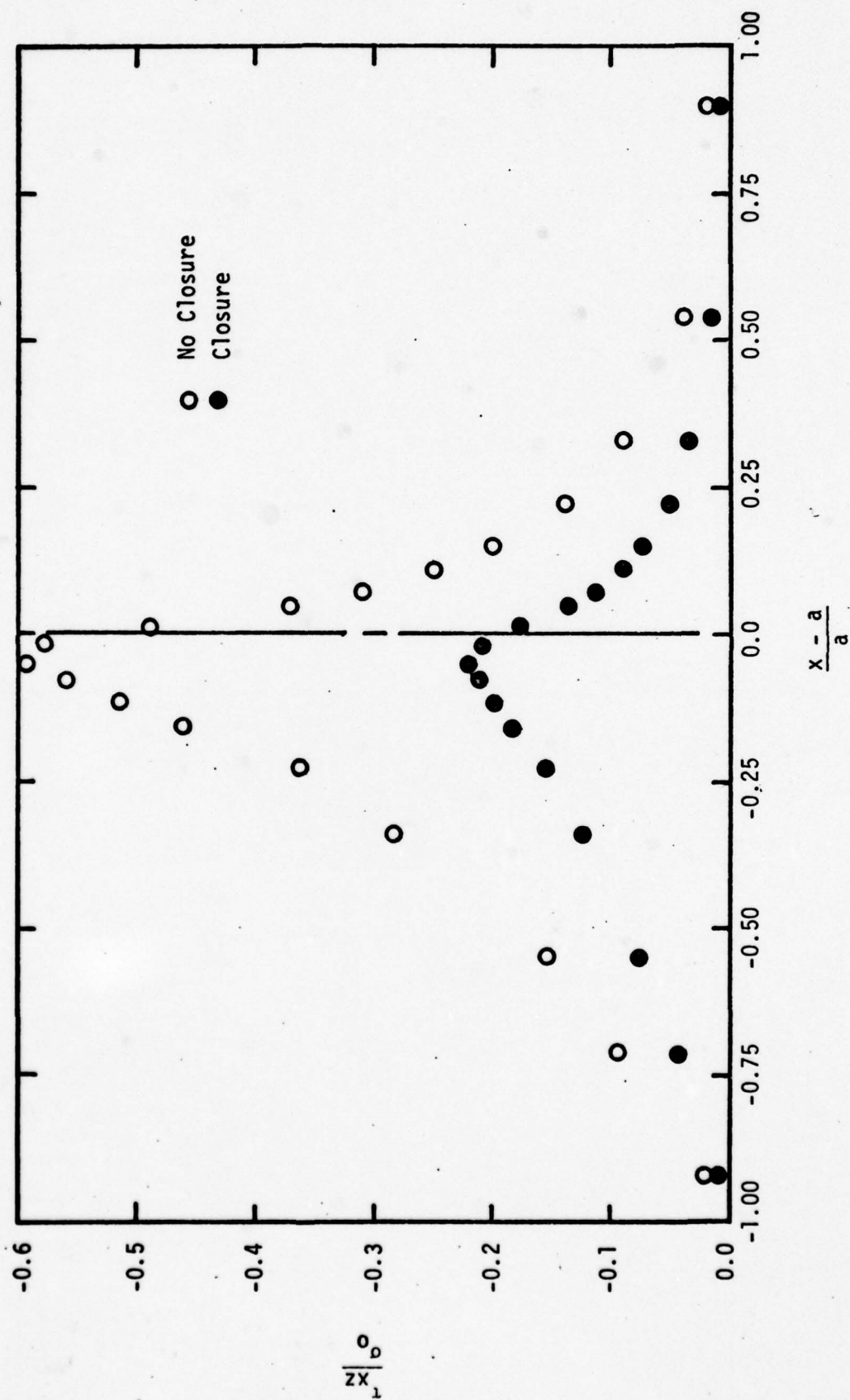
TABLE 7-1

COMPARISON OF STRESS INTENSITY

VARIATIONS WITH THICKNESS

FOR THE NO CLOSURE CASE

h/2a	$\phi(1)$ (Hartfranft and Sih)	S^*
.0125	0.489	0.422
.0250	0.570	0.536
.0750	0.628	0.624
.1250	0.660	0.674
.2500	0.700	0.734
.3750	0.720	0.802
.5000	0.739	0.844

FIGURE 7-6

COMPARISON OF YIELD ZONES
FOR THE NO CLOSURE CASE

—— Mindlin Results (Heming)
- - - Kirchhoff Results (Jones)
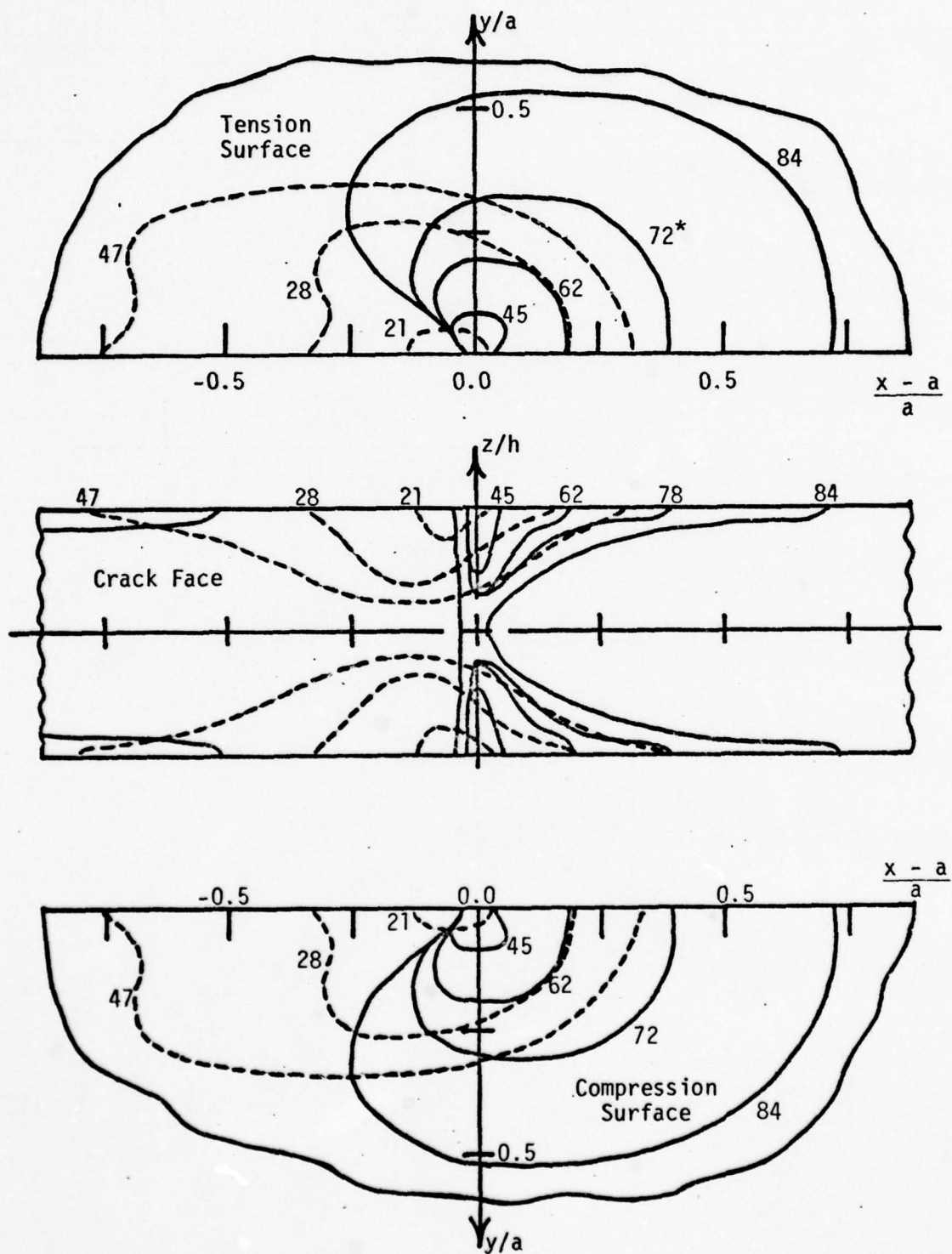
* Normalized Applied Load (σ_0/σ_L or M_0/M^*)
Expressed as a Percentage.

FIGURE 7-7

COMPARISON OF YIELD ZONES
FOR THE CLOSURE CASE

——— Mindlin Results (Heming)
- - - - Kirchhoff Results (Jones)
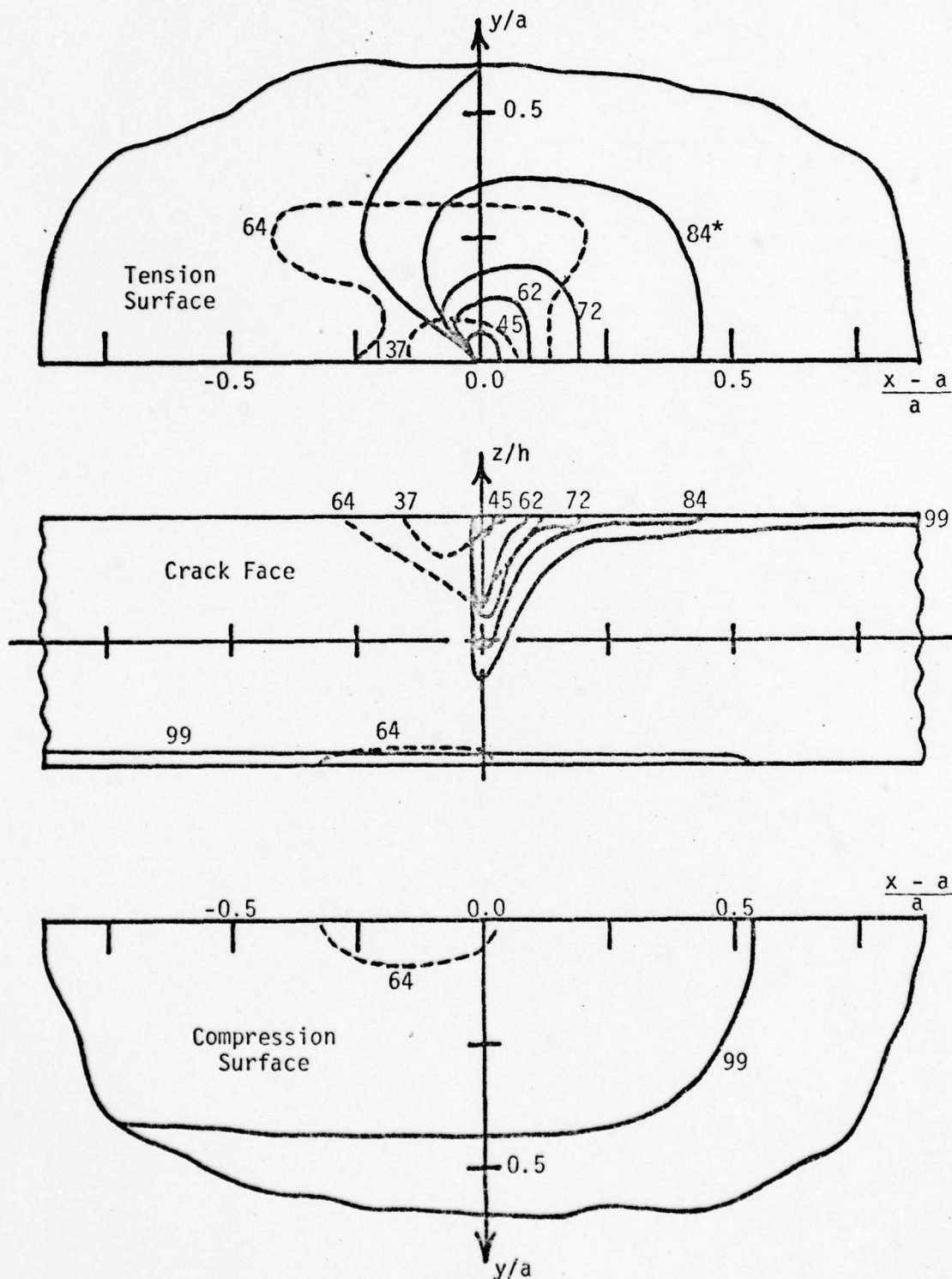
* Normalized Applied Load (σ_o/σ_L or M_o/M^*)
Expressed as a Percentage.

CHAPTER VIII

CONCLUSIONS

Numerical solutions to the problem of uniform bending of a plate containing a centrally located, through crack have been presented. The solutions were obtained from finite element analyses based on the assumptions of sixth order Mindlin plate theory. The distinguishing features of the analyses are that accurate representation of the boundary conditions was possible via the sixth order model, that the effects of crack closure were isolated and analyzed, and that elasto-plastic results were obtained for a work hardening material.

From the presentation and discussion of results, the following conclusions emerge:

1. Boundary conditions must be modelled correctly to obtain an accurate assessment of localized behavior.

2. The effects of crack closure are significant and must be considered in problems where closure is a physical reality.

3. The important issues regarding the cracked plate bending problem have been identified and analyzed.

A brief discussion of each of these conclusions is presented in the remaining sections.

8.1 Boundary Conditions are Important

The use of the sixth order Mindlin plate theory allowed
accurate representation of the three natural boundary conditions
and led to results that were consistent with what is known about
crack tip behavior. It was shown that the approximate boundary
conditions inherent to Kirchhoff theory lead to results (for both
the elastic and elasto-plastic problems) that are substantially
different and in certain respects inaccurate. Thus, the boundary
conditions play a significant role in the solution to the problem
and must be modelled correctly to obtain credible, accurate results.

8.2 Crack Closure Effects are Significant

The analyses of the crack closure phenomenon have shown
that it is much more than a second (or higher) order effect.
For example, in the elastic problem closure produced substantial
reductions in the displacements local to the crack and also in
the apparent bending stress intensity. In the elasto-plastic
problem, the plastic yield zones were completely different in
the presence of closure. Therefore, analyses of a bending
problem must include the effects of closure when the actual
physical situation demands it. Otherwise, the results obtained
will be inaccurate and misleading.

The implication of this conclusion is that the present
handbook solutions available for linear fracture mechanics
analyses are inadequate in that they contain no solutions for

the bending problem that include closure effects. In addition,
the bending solutions that are presented in the handbooks are
based primarily on results obtained using Kirchhoff theory.
Since the importance of boundary conditions and of closure has
been demonstrated, the handbook solutions available should be
used with caution. As a consequence of these observations,
it is imperative that results for the closure problem (relative
to a specific geometry) be obtained and tabulated for use by
designers and analysts in the field as dictated by their needs.

8.3 The Important Issues Have Been Covered

The main objective of the work presented here was to provide
an accurate assessment of the effects of closure in the context
of a plate bending problem, and thereby to complete the discussion
of the significant issues that have been raised in prior studies.
These issues include the importance of the boundary conditions,
the significance of the transverse shear, the effect of thickness
on stress intensity, the similarities and differences between the
uniaxial and biaxial bending problems, and the effects of closure
on the in plane and transverse deflections, on the local stress
distributions, on the neutral surface shifts, on fracture mechanics
interpretations, on crack tip blunting, and on the growth of the
plastic enclave. The objective has been achieved in that the
important issues have been identified and analyzed.

In light of the present results, it is interesting to consider what contributions further analyses of closure might provide, whether they be analytical, numerical, or experimental in nature. Analytically, if one could obtain an eigenvalue solution to the cracked plate problem based on the equations and boundary conditions derived from Mindlin theory, pertinent information that was lacking at the time of this analysis would become available. For example, the solution would provide explicit relations between the displacements and stresses, and would provide an ability to evaluate the bending stress intensity factor explicitly.

Although the results reported here contain the essence of the behavior induced by crack closure, they are necessarily limited by the two-dimensional approximation of a three-dimensional contact problem. It is certainly possible to model the contact surface more accurately by using a three-dimensional finite element approach. Such an analysis will require careful consideration of the modelling difficulties (e.g., how many nodes, or elements, through the thickness are sufficient to produce a significant improvement in accuracy, relative to the present results) as balanced against the time and effort involved and, ultimately, the actual requirements for additional accuracy.

Experimental efforts to date have been deficient in that the closure effects have not been completely isolated from other effects that are operating simultaneously, e.g., three-dimensional effects such as crack face warping. Assuming that a procedure can be developed to isolate closure, the difficulty comes in making a

determination of what type of information may be extracted from the experiment and of how that information may be used to portray closure accurately.

In this work, however, the significant issues in the plate bending problem have been analyzed. The question to be answered next is what physical characteristics of the problem have not been examined, but deserve attention. One unresolved issue is the effect of the crack flank warping induced by the shear effects near the crack. This issue may provide additional motivation for a three-dimensional finite element analysis, for example. Other issues emerge if the focus of attention moves to the region very close to the crack tip. Local to the crack tip, large deformations may occur: Would such an analysis provide a more accurate representation of the crack tip behavior, and would the additional complexity of the analysis be warranted? The crack front does not always remain straight (as modelled here): How can this phenomenon be modelled, and are its effects significant? We are not able yet to answer such questions, but the present work, done in the context of plate bending, has brought the basic problem to the point where these issues may be addressed.

BIBLIOGRAPHY

1. Williams, M. L., "Surface Stress Singularities Resulting from Various Boundary Conditions in Angular Corners of Plates Under Bending," Proceedings, First U.S. National Congress of Applied Mechanics, (June 1951), pp 325-329.

2. Williams, M. L., "The Bending Stress Distribution at the Base of a Stationary Crack," Journal of Applied Mechanics, Vol. 28 (1961), pp 78-82.

3. Knowles, J. K. and N. M. Wang, "On the Bending of an Elastic Plate Containing a Crack," Journal of Mathematics and Physics, Vol. 39 (1960), No. 5, pp 223-236.

4. Reissner, E., "The Effect of Transverse Shear Deformation on the Bending of Elastic Plates," Journal of Applied Mechanics, Vol. 12 (1945), pp A69-A77.

5. Hartranft, R. J. and G. C. Sih, "Effect of Plate Thickness on the Bending Stress Distribution Around Through Cracks," Journal of Mathematics and Physics, Vol. 47 (1968), pp 276-291.

6. Wang, N. M., "Effects of Plate Thickness on the Bending of an Elastic Plate Containing a Crack," Journal of Mathematics and Physics, Vol. 47 (1968), pp 371-390.

7. Folias, E. S., "A Finite Line Crack in a Pressurized Spherical Shell," International Journal of Fracture Mechanics, Vol. 1 (1965), pp 20-46.

8. Wynn, R. H., "Fracture of Centrally Cracked Plates Under Combined Bending and Extension Loading," Ph.D. Thesis, Virginia Polytechnic Institute, Engineering Mechanics (February 1969).

9. Smith, D. G. and C. W. Smith, "A Photoelastic Evaluation of the Influence of Closure and Other Effects Upon the Local Bending Stresses in Cracked Plates," International Journal of Fracture, Vol. 6 (1970), pp 305-318.

10. Smith, D. G. and C. W. Smith, "Influence of Precatastrophic Extension and Other Effects on Local Stresses in Cracked Plates Under Bending Fields," Experimental Mechanics, Vol. 11 (1971), No. 9, pp 394-401.

11. Jones, D. P., "Elasto-Plastic Bending of Cracked Plates, Including the Effects of Crack Closure," Ph.D. Thesis, Mechanical Engineering, Carnegie-Mellon University, Report SM-83A (October 1972).

12. Swedlow, J. L., M. L. Williams and W. H. Yang, "Elasto-Plastic Stresses and Strains in Cracked Plates," _Proceedings of the First International Conference on Fracture_ (1965), Vol. 1, pp 259-282.

13. Timoshenko, S. and S. Woinowsky-Krieger, _Theory of Plates and Shells_, Second Edition, McGraw-Hill Book Company, New York, 1968.

14. Dym, C. L. and I. H. Shames, _Solid Mechanics: A Variational Approach_, McGraw-Hill, Inc., New York, 1973.

15. Mindlin, R. D., "Influence of Rotary Inertia and Shear on Flexural Motions of Isotropic, Elastic Plates," _Journal of Applied Mechanics_, Vol. 18 (1951), pp 31-38.

16. Reissner, E., "On Bending of Elastic Plates," _Quarterly of Applied Mathematics_, Vol. 5 (1947), pp 55-68.

17. Pawsey, S. F. and R. W. Clough, "Improved Numerical Integration of Thick Shell Finite Element," _International Journal for Numerical Methods in Engineering_, Vol. 3 (1971), p 575.

18. Swedlow, J. L., "Character of the Equations of Elasto-Plastic Flow in Three Independent Variables," _International Journal of Nonlinear Mechanics_, Vol. 3 (1968), pp 325-336.

19. Fung, Y. C., _Foundations of Solid Mechanics_, Chapter 6, Prentice-Hall (1965).

20. Jones, D. P., "A Discrete Element Analysis of Elasto-Plastic Beam and Plate Structures by Energy Minimization," Report SM-61, Department of Mechanical Engineering, Carnegie-Mellon University (1971).

21. Ahmad, S., B. M. Irons and O. C. Zienkiewicz, "Analysis of Thick and Thin Shell Structures by Curved Finite Elements," _International Journal for Numerical Methods in Engineering_, Vol. 2 (1970), pp 419-451.

22. Cook, Robert D., _Concepts and Applications of Finite Element Analysis_, Chapters 5 and 9, Wiley and Sons, Inc. (1974).

23. Irons, B. M., "Engineering Applications of Numerical Integration in Stiffness Methods," _AIAA Journal_, Vol. 4 (1966), pp 2035-2037.

24. Swedlow, J. L., "A Procedure for Solving Problems of Elasto-Plastic Flow," _Computers and Structures_, Vol. 3 (1973), pp 879-898.

25. Scarborough, J. B., Numerical Mathematical Analysis, Chapter VIII, Oxford Book Company (1964).

26. Gallagher, R. H., Finite Element Analysis: Fundamentals, Chapter 7, Prentice-Hall, Inc. (1975).

27. Heming, F. S., Jr., "Modified Gauss Elimination Solver," Report SM78-9, Department of Mechanical Engineering, Carnegie-Mellon University (1978).

28. Chan, S. K., I. S. Tuba and W. K. Wilson, "On the Finite Element Method in Linear Fracture Mechanics, Engineering Fracture Mechanics, Vol. 2 (1970), pp 1-17.

29. Rooke, D. P. and D. J. Cartwright, Compendium of Stress Intensity Factors, Chapter 1, HMSO, England (1976).

30. Wilson, W. K. and D. G. Thompson, "On the Finite Element Method for Calculating Stress Intensity Factors for Cracked Plates in Bending," Engineering Fracture Mechanics, Vol. 3 (1971), pp 97-102.

31. Gonzalez, H., Jr. and H. F. Brinson, "The Bending Dugdale Model," Virginia Polytechnic Institute and State University Report VPI-E-70-14 (August 1970).

32. Brinson, H. F., J. H. Underwood and A. R. Rosenfield, "Yield Zones in Polymeric and Metallic Plates Under Pure Bending Containing a Through Crack," Virginia Polytechnic Institute and State University Report VPI-E-72-7 (April 1972).

33. Barsoum, R. S., "Application of Quadratic Isoparametric Finite Elements in Linear Fracture Mechanics," International Journal of Fracture, Vol. 10 (1974), pp 603-604.

34. Henshell, R. D. and K. G. Shaw, "Crack Tip Finite Elements Are Unnecessary," International Journal for Numerical Methods in Engineering, Vol. 9 (1975), pp 495-507.

35. Bloom, J. M., "An Evaluation of a New Crack Tip Element--The Distorted 8-Node Isoparametric Element," International Journal of Fracture, Vol. 11 (1975), pp 705-707.

36. Barsoum, R. S., "A Degenerate Solid Element for Linear Fracture Analysis of Bending and General Shells," International Journal for Numerical Methods in Engineering, Vol. 10 (1976), pp 551-564.

APPENDIX A

COMPARISON OF ELASTIC PLATE BENDING THEORIES

There are three plate theories of interest in the discussion
of the plate bending problem under consideration; the fourth order
theory of Kirchhoff and the sixth order theories of Reissner and
Mindlin. In this appendix, a brief discussion of the assumptions,
equations, and boundary conditions for each will be presented in
order to clarify the differences among them. Since the differences
discussed involve only the bending terms, the membrane terms will
be neglected to simplify the presentation.

A-1 Kirchhoff Plate Theory

Kirchhoff, or classical plate theory, is the two-dimensional
analog of simple beam theory. The basic assumptions for this
fourth order theory are:

1. The transverse deflection, w, is small in comparison
    with the plate thickness, h.

2. Straight lines that are normal to the midplane in the
    undeformed state remain so during bending.

3. The normal stresses in the direction transverse to
    the plate are ignored. That is, a thin plate, plane
    stress situation is assumed.

As a result of the second assumption, the transverse shear
strain is zero. This assumption is unsatisfactory when the
effects of shear are important, e.g., in the region local to a

crack. With the assumptions given, the plate bending behavior can be described completely in terms of the transverse deflection, w, and its derivatives. With reference to Figure A-1, the displacement field can be written as

$$u(x,y,z) = - z \frac{\partial w(x,y)}{\partial x} \tag{A-1a}$$

$$v(x,y,z) = - z \frac{\partial w(x,y)}{\partial y} \tag{A-1b}$$

$$w(x,y) = w(x,y) \tag{A-1c}$$

With these assumptions, it can be shown that the differential equation describing the elastic behavior of the plate is the biharmonic equation

$$\nabla^4 w = 0 \tag{A-2}$$

The natural and kinematic boundary conditions that must be satisfied can be written as

Either $M_n = 0$ or $\frac{\partial w}{\partial n}$ is prescribed $\tag{A-3a}$

Either $Q_n + \frac{\partial M_{nt}}{\partial t} = 0$ or w is prescribed $\tag{A-3b}$

where n and t are the directions normal to and tangent to the boundary. Note that the second condition represents an equivalent, or effective, shear force since the fourth order theory can model only two of the three physically natural boundary conditions. See References 13 and 14 for further discussion of Kirchhoff theory and its implications.

A-2 Mindlin Plate Theory

Mindlin plate theory is the two dimensional analog of Timoshenko beam theory. The Kirchhoff assumptions are still valid except for one important change to assumption two; straight line elements that are originally normal to the midplane remain straight on deformation (no warping), but do not remain normal to the midplane. With this change, shear effects are now accounted for by independent variables in the formulation. The assumed displacement field has the form:

$$u(x,y,z) = +z\phi(x,y) \tag{A-4a}$$

$$v(x,y,z) = -z\psi(x,y) \tag{A-4b}$$

$$w(x,y) = w(x,y) \tag{A-4c}$$

The differential equations derived from this displacement field can be shown to be:

$$D\left[\frac{\partial^2\phi}{\partial x^2} + \frac{1-\nu}{2}\frac{\partial^2\phi}{\partial y^2} + \frac{1-\nu}{2}\frac{\partial^2\psi}{\partial x\partial y}\right] + kGh\left[\frac{\partial w}{\partial x} + \phi\right] = 0 \tag{A-5a}$$

$$D\left[\frac{1-\nu}{2}\frac{\partial^2\psi}{\partial x^2} + \frac{\partial^2\psi}{\partial y^2} + \frac{1-\nu}{2}\frac{\partial^2\phi}{\partial x\partial y}\right] + kGh\left[\frac{\partial w}{\partial y} - \psi\right] = 0 \tag{A-5b}$$

$$kGh\left[\nabla^2 w + \frac{\partial\phi}{\partial x} - \frac{\partial\psi}{\partial y}\right] = 0 \tag{A-5c}$$

where k is a shear factor that is introduced to correct for the no warping statement in assumption two. For further discussion of the shear factor, see Reference 14.

The most significant feature of the sixth order theory is that all three physical boundary conditions are accounted for. The boundary conditions for Mindlin theory may be stated as:

Either $M_n = 0$ or β_n is specified   (A-6a)

Either $M_{nt} = 0$ or β_t is specified   (A-6b)

Either $Q_n = 0$ or   w is specified   (A-6c)

where n and t have the same meaning as given previously, and

$\beta_n = \beta_t = \phi$ when n or t is x

$\beta_n = \beta_t = \psi$ when n or t is y

See References 14 and 15 for more detailed discussions of Mindlin theory.

A-3 Reissner Plate Theory

Reissner's theory is very similar to the Mindlin theory with the primary difference being that the Reissner theory is stress-based rather than displacement-based. Reissner assumed that the bending stresses vary linearly with thickness, i.e.,

$$\sigma_x = \frac{12 M_x z}{h^3}$$ (A-7a)

$$\sigma_y = \frac{12 M_y z}{h^3}$$ (A-7b)

$$\tau_{xy} = \frac{12M_{xy}z}{h^3} \tag{A-7c}$$

Equilibrium considerations and the condition that the faces of the plate are shear free then lead to a parabolic distribution of shear stresses over the thickness, i.e.,

$$\tau_{xz} = \frac{3V_x}{2h} \left[1 - \left(\frac{z}{h/2}\right)^2\right] \tag{A-8a}$$

$$\tau_{yz} = \frac{3V_y}{2h} \left[1 - \left(\frac{z}{h/2}\right)^2\right] \tag{A-8b}$$

Reissner then used the theorem of minimum complementary energy for the stresses to obtain the governing equations and the Lagrange multiplier method to obtain approximate stress-strain relations. Details of these results are contained in References 4 and 16. As with Mindlin theory, Reissner theory allows for three boundary conditions along the edges of the plate.

FIGURE A-1

PLATE SIGN CONVENTION
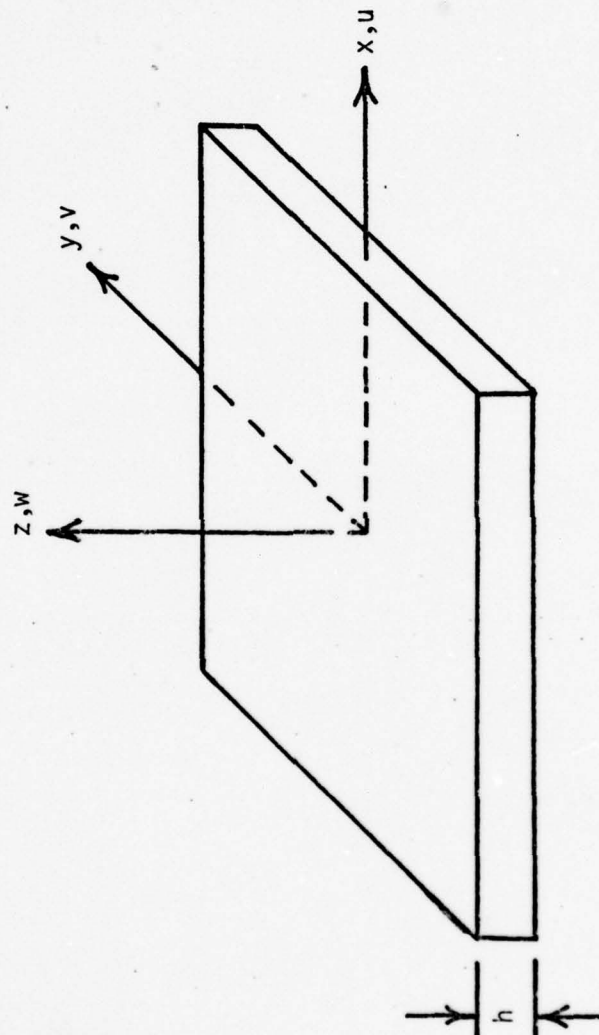
APPENDIX B

ELASTO-PLASTIC FORMULATION FOR THE
PLATE BENDING PROBLEM

Presented here is an outline of the elasto-plastic formulation of the plate bending problem. The formulation is based on Mindlin plate theory [15] and the incremental theory of elasto-plastic flow [18]. Inherent in the development are the thin plate, small displacement, and plane stress assumptions. In rate form the assumed displacement field is (see Figure B-1):

$$\dot{u} = \dot{u}_s(x,y) + z\dot{\phi}(x,y) = \dot{u}_s + z\dot{\phi} \tag{B-1a}$$

$$\dot{v} = \dot{v}_s(x,y) - z\dot{\psi}(x,y) = \dot{v}_s - z\dot{\psi} \tag{B-1b}$$

$$\dot{w} = \dot{w}(x,y) \tag{B-1c}$$

The strain-displacement relations in rate form can now be written as:

$$\dot{\epsilon}_x = \frac{\partial \dot{u}}{\partial x} = \frac{\partial \dot{u}_s}{\partial x} + z\,\frac{\partial \dot{\phi}}{\partial x} \tag{B-2a}$$

$$\dot{\epsilon}_y = \frac{\partial \dot{v}}{\partial y} = \frac{\partial \dot{v}_s}{\partial y} - z\,\frac{\partial \dot{\psi}}{\partial y} \tag{B-2b}$$

$$\dot{\gamma}_{xy} = \frac{\partial \dot{u}}{\partial y} + \frac{\partial \dot{v}}{\partial x} = \left(\frac{\partial \dot{u}_s}{\partial y} + \frac{\partial \dot{v}_s}{\partial x}\right) + z\left(\frac{\partial \dot{\phi}}{\partial y} - \frac{\partial \dot{\psi}}{\partial x}\right) \tag{B-2c}$$

$$\dot{\gamma}_{xz} = \frac{\partial \dot{u}}{\partial z} + \frac{\partial \dot{w}}{\partial x} = \dot{\phi} + \frac{\partial \dot{w}}{\partial x} \tag{B-2d}$$

$$\dot{\gamma}_{yz} = \frac{\partial \dot{v}}{\partial z} + \frac{\partial \dot{w}}{\partial y} = -\dot{\psi} + \frac{\partial \dot{w}}{\partial y} \tag{B-2e}$$

The expression for $\dot{\varepsilon}_z$ will be determined presently from constitutive relationships.

The incremental stresses are related via a flow rule; in this case, the flow rule used is the form developed by Fung [19] from Drucker's hypothesis. The flow rule is written as:

$$2\mu\dot{\varepsilon}_{ij} = \dot{\sigma}_{ij} - [\frac{\nu}{1 + \nu}]\dot{\sigma}_{kk}\delta_{ij} + (\mu/\mu_0^{(p)})s_{ij}s_{k\ell}\dot{\sigma}_{k\ell}/3\tau_0^2 \qquad (B-3)$$

where μ is the elastic shear modulus, $\mu_0^{(p)}$ is the plastic octahedral shear modulus, δ_{ij} is the Kronecker delta, ν is Poisson's ratio, τ_0 is the octahedral shear stress, and s_{ij} is the deviator of the stress tensor defined by

$$s_{ij} = \sigma_{ij} - \delta_{ij}\sigma_{kk}/3 \qquad (B-4)$$

The flow rule may be inverted to give

$$\dot{\sigma}_{ij}/2\mu = \dot{\varepsilon}_{ij} + [\frac{\nu}{1 - 2\nu}\dot{\varepsilon}_{kk}\delta_{ij} - s_{ij}s_{k\ell}\dot{\varepsilon}_{k\ell}/\kappa] \qquad (B-5)$$

where κ is defined for convenience to be

$$\kappa = 3\tau_0^2 (1 + \mu_0^{(p)}/\mu) \qquad (B-6)$$

The inverse flow rule is now used to determine the expression for $\dot{\varepsilon}_z$. Assuming a plane stress distribution for $\dot{\sigma}_z$, i.e., $\dot{\sigma}_z = 0$, and using the strain-displacement relations of equations (B-2), the inverse flow rule yields (after suitable rearranging) the following expression for $\dot{\varepsilon}_z$:

$$\dot{\epsilon}_z = (A - Bs_x)[\frac{\partial \dot{u}_s}{\partial x} + z\frac{\partial \dot{\phi}}{\partial x}] + (A - Bs_y)[\frac{\partial \dot{v}_s}{\partial y} - z\frac{\partial \dot{\psi}}{\partial y}]$$

$$- Bs_{xy}[\frac{\partial \dot{u}_s}{\partial y} + \frac{\partial \dot{v}_s}{\partial x} + z(\frac{\partial \dot{\phi}}{\partial y} - \frac{\partial \dot{\psi}}{\partial x})]$$

$$- Bs_{xz}[\frac{\partial \dot{w}}{\partial x} + \dot{\phi}] - Bs_{yz}[\frac{\partial \dot{w}}{\partial y} - \dot{\psi}] \qquad (B-7)$$

where A and B are defined as

$$A = \frac{\nu\kappa}{(1 - 2\nu)s_z^2 - (1 - \nu)\kappa} \qquad (B-8)$$

$$B = \frac{(1 - 2\nu)s_z}{(1 - 2\nu)s_z^2 - (1 - \nu)\kappa} \qquad (B-9)$$

This expression for $\dot{\epsilon}_z$ is used to eliminate $\dot{\epsilon}_z$ from the incremental stress-strain relations which follow.

The inverse flow rule is now used to determine the elasto-plastic materials matrix [M] defined by

$$\{\dot{\sigma}\} = [M] \{\dot{\epsilon}\} \qquad (B-10)$$

$$5x1 \quad 5x5 \ 5x1$$

where

$$\lfloor \dot{\sigma} \rfloor = \lfloor \dot{\sigma}_x \ \dot{\sigma}_y \ \dot{\tau}_{xy} \ \dot{\tau}_{xz} \ \dot{\tau}_{yz} \rfloor \qquad (B-11)$$

and $\lfloor \dot{\epsilon} \rfloor = \lfloor \dot{\epsilon}_x \ \dot{\epsilon}_y \ \dot{\gamma}_{xy} \ \dot{\gamma}_{xz} \ \dot{\gamma}_{yz} \rfloor \qquad (B-12)$

Noting that the materials matrix is symmetric and defining

$$m_{ij} = \frac{\nu}{1 - 2\nu} \delta_{ij} - \frac{s_z s_{ij}}{\kappa} \qquad (B-13)$$

the terms of the materials matrix M_{ij} are:

$$M_{11} = 2\mu\left\{\frac{1}{1 - \nu} + \frac{\nu^2}{(1 - 2\nu)(1 - \nu)} - \frac{s_x^2}{\kappa} + m_{xx}(A - Bs_x)\right\} \qquad (B-14a)$$

$$M_{12} = 2\mu\left\{\frac{\nu}{1 - \nu} + \frac{\nu^2}{(1 - 2\nu)(1 - \nu)} - \frac{s_x s_y}{\kappa} + m_{xx}(A - Bs_y)\right\} \qquad (B-14b)$$

$$M_{13} = 2\mu\left\{- \frac{s_x s_{xy}}{\kappa} - m_{xx}Bs_{xy}\right\} \qquad (B-14c)$$

$$M_{14} = 2\mu\left\{- \frac{s_x s_{xz}}{\kappa} - m_{xx}Bs_{xz}\right\} \qquad (B-14d)$$

$$M_{15} = 2\mu\left\{- \frac{s_x s_{yz}}{\kappa} - m_{xx}Bs_{yz}\right\} \qquad (B-14e)$$

$$M_{22} = 2\mu\left\{\frac{1}{1 - \nu} + \frac{\nu^2}{(1 - 2\nu)(1 - \nu)} - \frac{s_y^2}{\kappa} + m_{yy}(A - Bs_y)\right\} \qquad (B-14f)$$

$$M_{23} = 2\mu\left\{- \frac{s_y s_{xy}}{\kappa} - m_{yy}Bs_{xy}\right\} \qquad (B-14g)$$

$$M_{24} = 2\mu\left\{- \frac{s_y s_{xz}}{\kappa} - m_{yy}Bs_{xz}\right\} \qquad (B-14h)$$

$$M_{25} = 2\mu\left\{- \frac{s_y s_{yz}}{\kappa} - m_{yy}Bs_{yz}\right\} \qquad (B-14i)$$

$$M_{33} = 2\mu\left\{\frac{1}{2} - \frac{s_{xy}^2}{\kappa} - m_{xy}Bs_{xy}\right\} \qquad (B-14j)$$

$$M_{34} = 2\mu\{-\frac{s_{xy}s_{xz}}{\kappa} - m_{xy}Bs_{xz}\} \qquad \text{(B-14k)}$$

$$M_{35} = 2\mu\{-\frac{s_{xy}s_{yz}}{\kappa} - m_{xy}Bs_{yz}\} \qquad \text{(B-14\ell)}$$

$$M_{44} = 2\mu\{\frac{1}{2} - \frac{s_{xz}^2}{\kappa} - m_{xz}Bs_{xz}\} \qquad \text{(B-14m)}$$

$$M_{45} = 2\mu\{-\frac{s_{xz}s_{yz}}{\kappa} - m_{xz}Bs_{yz}\} \qquad \text{(B-14n)}$$

$$M_{55} = 2\mu\{\frac{1}{2} - \frac{s_{yz}^2}{\kappa} - m_{yz}Bs_{yz}\} \qquad \text{(B-14o)}$$

Noting that for the elastic case,

$$A \rightarrow -\frac{\nu}{1 - \nu} \qquad \text{and} \qquad B \rightarrow 0$$

it is easily shown that [M] reduces to the elastic, plane stress form of the materials matrix.

Having defined the stress-strain relationships via the materials matrix, the next step is to form the functional π that is analogous to the potential energy functional in the elastic problem. One form of the functional π is

$$\pi = \int_{Vol} [\frac{\lambda}{2}(\dot{\epsilon}_{kk})^2 + \mu\dot{\epsilon}_{ij}\dot{\epsilon}_{ij} - \frac{\mu}{\kappa}(s_{ij}\dot{\epsilon}_{ij})^2] \, dVol$$

$$- \int_{s_\sigma} \dot{T}_i\dot{u}_i \, ds \qquad \text{(B-15)}$$

where

$$\dot{T}_i = \dot{\sigma}_{ij} n_j \tag{B-16}$$

are the traction rates, S_σ is the surface over which stresses are prescribed, and

$$\lambda = \frac{E\nu}{(1 + \nu)(1 - 2\nu)} \tag{B-17}$$

and

$$\mu = \frac{E}{2(1 + \nu)} \tag{B-18}$$

It has been shown by Jones [19] that of all displacement rates $\dot{u}_i$ satisfying the given boundary conditions, those that satisfy the equations of equilibrium are distinguished by a stationary, or extreme, value of the functional π, i.e.,

$$\delta\pi = 0 \tag{B-19}$$

Implementation of this stationary principle leads to the governing differential equations and boundary conditions. Since the details of this procedure are quite lengthy, only the resulting equations are presented here. In order to present the equations in a more compact form, certain definitions are now made for convenience. First, three expressions are defined to represent the integration through the thickness:

$$P_{ij} = \frac{1}{2} \int_{-h/2}^{h/2} M_{ij} dz \tag{B-20a}$$

$$Q_{ij} = \frac{1}{2} \int_{-h/2}^{h/2} M_{ij} z \, dz \tag{B-20b}$$

$$R_{ij} = \frac{1}{2} \int_{-h/2}^{h/2} M_{ij} z^2 \, dz \tag{B-20c}$$

Secondly, groups of expressions found in the final form of the equations are defined:

$$F_1(x,y) = 2P_{11} \frac{\partial \dot{u}_s}{\partial x} + 2Q_{11} \frac{\partial \dot{\phi}}{\partial x} + P_{12} \frac{\partial \dot{v}_s}{\partial y} - Q_{12} \frac{\partial \dot{\psi}}{\partial y} + P_{13}\left[\frac{\partial \dot{u}_s}{\partial y} + \frac{\partial \dot{v}_s}{\partial x}\right]$$

$$+ Q_{13}\left[\frac{\partial \dot{\phi}}{\partial y} - \frac{\partial \dot{\psi}}{\partial x}\right] + k_2 P_{14}\left[\frac{\partial \dot{w}}{\partial x} + \dot{\phi}\right] + k_2 P_{15}\left[\frac{\partial \dot{w}}{\partial y} - \dot{\psi}\right] \tag{B-21a}$$

$$F_2(x,y) = 2P_{33}\left[\frac{\partial \dot{u}_s}{\partial y} + \frac{\partial \dot{v}_s}{\partial x}\right] + 2Q_{33}\left[\frac{\partial \dot{\phi}}{\partial y} - \frac{\partial \dot{\psi}}{\partial x}\right] + P_{13} \frac{\partial \dot{u}_s}{\partial x} + Q_{13} \frac{\partial \dot{\phi}}{\partial x}$$

$$+ P_{23} \frac{\partial \dot{v}_s}{\partial y} - Q_{23} \frac{\partial \dot{\psi}}{\partial y} + k_2 P_{34}\left[\frac{\partial \dot{w}}{\partial x} + \dot{\phi}\right] + k_2 P_{35}\left[\frac{\partial \dot{w}}{\partial y} - \dot{\psi}\right] \tag{B-21b}$$

$$F_3(x,y) = 2P_{22} \frac{\partial \dot{v}_s}{\partial y} - 2Q_{22} \frac{\partial \dot{\psi}}{\partial y} + P_{12} \frac{\partial \dot{u}_s}{\partial x} + Q_{12} \frac{\partial \dot{\phi}}{\partial x} + P_{23}\left[\frac{\partial \dot{u}_s}{\partial y} + \frac{\partial \dot{v}_s}{\partial x}\right]$$

$$+ Q_{23}\left[\frac{\partial \dot{\phi}}{\partial y} - \frac{\partial \dot{\psi}}{\partial x}\right] + k_2 P_{24}\left[\frac{\partial \dot{w}}{\partial x} + \dot{\phi}\right] + k_2 P_{25}\left[\frac{\partial \dot{w}}{\partial y} - \dot{\psi}\right] \tag{B-21c}$$

$$F_4(x,y) = 2Q_{11} \frac{\partial \dot{u}_s}{\partial x} + 2R_{11} \frac{\partial \dot{\phi}}{\partial x} + Q_{12} \frac{\partial \dot{v}_s}{\partial y} - R_{12} \frac{\partial \dot{\psi}}{\partial y} + Q_{13}[\frac{\partial \dot{u}_s}{\partial y} + \frac{\partial \dot{v}_s}{\partial x}]$$

$$+ R_{13}[\frac{\partial \dot{\phi}}{\partial y} - \frac{\partial \dot{\psi}}{\partial x}] + k_3 Q_{14}[\frac{\partial \dot{w}}{\partial x} + \dot{\phi}] + k_3 Q_{15}[\frac{\partial \dot{w}}{\partial y} - \dot{\psi}] \qquad \text{(B-21d)}$$

$$F_5(x,y) = 2Q_{33}[\frac{\partial \dot{u}_s}{\partial y} + \frac{\partial \dot{v}_s}{\partial x}] + 2R_{33}[\frac{\partial \dot{\phi}}{\partial y} - \frac{\partial \dot{\psi}}{\partial x}] + Q_{13} \frac{\partial \dot{u}_s}{\partial x} + R_{13} \frac{\partial \dot{\phi}}{\partial x}$$

$$+ Q_{23} \frac{\partial \dot{v}_s}{\partial y} - R_{23} \frac{\partial \dot{\psi}}{\partial y} + k_3 Q_{34}[\frac{\partial \dot{w}}{\partial x} + \dot{\phi}] + k_3 Q_{35}[\frac{\partial \dot{w}}{\partial y} - \dot{\psi}] \quad \text{(B-21e)}$$

$$F_6(x,y) = 2R_{22} \frac{\partial \dot{\psi}}{\partial y} - 2Q_{22} \frac{\partial \dot{v}_s}{\partial y} - Q_{12} \frac{\partial \dot{u}_s}{\partial x} - R_{12} \frac{\partial \dot{\phi}}{\partial x} - Q_{23}[\frac{\partial \dot{u}_s}{\partial y} + \frac{\partial \dot{v}_s}{\partial x}]$$

$$- R_{23}[\frac{\partial \dot{\phi}}{\partial y} - \frac{\partial \dot{\psi}}{\partial x}] - k_3 Q_{24}[\frac{\partial \dot{w}}{\partial x} + \dot{\phi}] - k_3 Q_{25}[\frac{\partial \dot{w}}{\partial y} - \dot{\psi}] \qquad \text{(B-21f)}$$

$$F_7(x,y) = 2k_1 P_{44}[\frac{\partial \dot{w}}{\partial x} + \dot{\phi}] + k_2 P_{14} \frac{\partial \dot{u}_s}{\partial x} + k_3 Q_{14} \frac{\partial \dot{\phi}}{\partial x}$$

$$+ k_2 P_{24} \frac{\partial \dot{v}_s}{\partial y} - k_3 Q_{24} \frac{\partial \dot{\psi}}{\partial y} + k_2 P_{34}[\frac{\partial \dot{u}_s}{\partial y} + \frac{\partial \dot{v}_s}{\partial x}]$$

$$+ k_3 Q_{34}[\frac{\partial \dot{\phi}}{\partial y} - \frac{\partial \dot{\psi}}{\partial x}] + k_4 P_{45}[\frac{\partial \dot{w}}{\partial y} - \dot{\psi}] \qquad \text{(B-21g)}$$

$$F_8(x,y) = 2k_1P_{55}[\frac{\partial \dot{w}}{\partial y} - \dot{\psi}] + k_2P_{14}\frac{\partial \dot{u}_s}{\partial x} + k_3Q_{14}\frac{\partial \dot{\phi}}{\partial x}$$

$$+ k_2P_{35}[\frac{\partial \dot{u}_s}{\partial y} + \frac{\partial \dot{v}_s}{\partial x}] + k_3Q_{35}[\frac{\partial \dot{\phi}}{\partial y} - \frac{\partial \dot{\psi}}{\partial x}]$$

$$+ k_4P_{45}[\frac{\partial \dot{w}}{\partial x} + \dot{\phi}] + k_2P_{25}\frac{\partial \dot{v}_s}{\partial y} - k_3Q_{25}\frac{\partial \dot{\psi}}{\partial y} \qquad \text{(B-21h)}$$

With these definitions, the governing differential equations may be written as

$$\frac{\partial F_1}{\partial x} + \frac{\partial F_2}{\partial y} = 0 \qquad \text{(B-22a)}$$

$$\frac{\partial F_2}{\partial x} + \frac{\partial F_3}{\partial y} = 0 \qquad \text{(B-22b)}$$

$$\frac{\partial F_4}{\partial x} + \frac{\partial F_5}{\partial y} = -F_7 \qquad \text{(B-22c)}$$

$$\frac{\partial F_5}{\partial x} + \frac{\partial F_6}{\partial y} = -F_8 \qquad \text{(B-22d)}$$

$$\frac{\partial F_7}{\partial x} + \frac{\partial F_8}{\partial y} = 0 \qquad \text{(B-22e)}$$

The boundary conditions along $y = \pm y_0$ are:

Either $\dot{N}_{yx} = F_2$ or $\dot{u}_s$ specified   (B-23a)

Either $\dot{N}_y = F_3$ or $\dot{v}_s$ specified   (B-23b)

Either $\dot{M}_{yx} = F_5$ or $\dot{\phi}$ specified   (B-23c)

Either $\dot{M}_y = F_6$ or $\dot{\psi}$ specified   (B-23d)

Either $\dot{Q}_y = F_8$ or $\dot{w}$ specified   (B-23e)

The boundary conditions along $x = \pm x_0$ are:

Either $\dot{N}_x = F_1$ or $\dot{u}_s$ specified   (B-24a)

Either $\dot{N}_{xy} = F_2$ or $\dot{v}_s$ specified   (B-24b)

Either $\dot{M}_x = F_4$ or $\dot{\phi}$ specified   (B-24c)

Either $\dot{M}_{xy} = F_5$ or $\dot{\psi}$ specified   (B-24d)

Either $\dot{Q}_x = F_7$ or $\dot{w}$ specified   (B-24e)

Note that in the expressions for $F_i(x,y)$, $i = 1, 8$, there are four constants k_j, $j = 1, 4$. These constants represent the shear factors analogous to the single shear factor used in the elastic theory. For the analyses performed here the values of k_j were all set equal to the elastic value ($k = 5/6$) for convenience.

Equations (B-22), (B-23) and (B-24) completely describe the differential equations and boundary conditions for the elasto-plastic problem. Since the entire problem is an initial-boundary value problem, all that remains is to specify the initial values of u_s, v_s, ϕ, ψ and w which are generally taken to be zero. Note that in the elasto-plastic formulation the extensional and bending terms are fully coupled.

FIGURE B-1

PLATE GEOMETRY
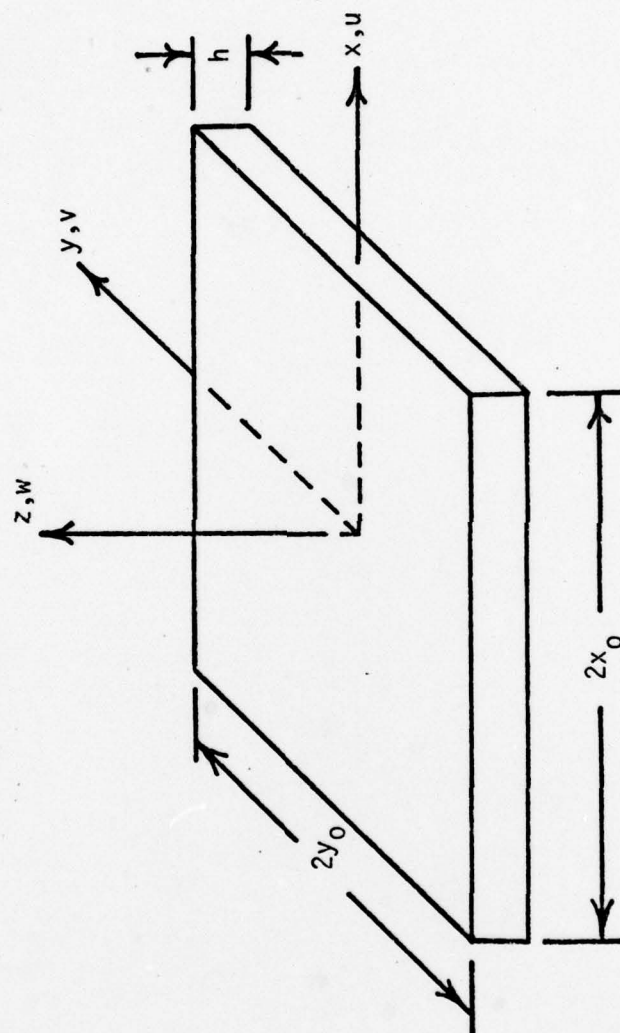
APPENDIX C

PLABEP PROGRAM VERIFICATION

To insure the correctness of the results obtained with the PLABEP program, a hierarchy of checks and test cases was made during the development of the program. This series of checks consisted of the following:

1. Element Formation Checks

    a. Verification of strain-displacement matrix

    b. Verification of element stiffness matrix

2. Elastic Program Checks

    a. Verification of structure stiffness matrix

    b. Verification of boundary conditions and solution

3. Elastic Test Problems

    a. Biaxial Tension Problem

    b. Uniform Bending Problem

    c. Unaxial Tension, Center-cracked Plate Problem

4. Closure Constraint Check

5. Elasto-Plastic Program Checks

The remainder of the discussion deals with each of these categories in turn.

C.1 Element Formation Checks

In the development of an individual element, two matrices are of primary importance, namely, the strain-displacement matrix and the element stiffness matrix. To validate the strain-displacement

matrix, a series of twenty-five test cases were run for a one element model (Figure C-1). In each of these cases, a specific displacement vector was input which when multiplied by the strain-displacement matrix produces the appropriate strain vector. All rigid body, constant strain, and linear strain vectors admissible by the assumed displacement field were checked and found to agree exactly with the expected values. In addition, a case comprising a linear combination of all the other cases was run and verified with the results again agreeing exactly with those predicted.

The verification of the element stiffness matrix proceeds in a similar manner. In this case, multiplying a specified displacement vector by the stiffness matrix produces a specified force vector. Using the same twenty-five displacement vectors for input as was used to verify the strain-displacement vector, and determining the appropriate nodal forces from theoretical considerations, the formation of the element stiffness was verified (correct to one part in 10^6).

C.2 Elastic Program Checks

Once the element formation is verified, the next step is to insure that the element stiffness matrices are assembled properly to form the structure stiffness matrix. To validate the assembly process, the same twenty-five cases were run but with two and four element models (Figures C-2 and C-3). Thus,

a nodal force vector was obtained for the entire two or four
element structure. The results obtained were correct and showed
that the structure stiffness matrix was being formed correctly
(to one part in 10^6).

The final phase of the validation of the elastic program
involved a check of the boundary conditions and solution routine.
Admissible boundary conditions for this program consisted of
applied uniform tension and bending loads and prescribed zero
displacements. Using the four element model of Figure C-3,
various combinations of boundary conditions were input, and the
resulting displacements, strains, stresses, and forces were
checked for correctness. In this manner, the boundary condition
and solution routines were verified (correct to one part in 10^6).

C.3 Elastic Test Problems

As a further check on the validity the elastic program,
three test problems were run for which the results are well
known. The first two modelled a plate with biaxial tension
and uniform bending loads. The third was the problem of a
center-cracked plate loaded under uniaxial tension. For these
problems a quarter of the plate was modelled with 66 elements
as shown in Figure C-4. Note that since this grid is the same
one to be used for the closure and no closure analyses, a check
is also provided for the input data pertinent to the grid
itself.

For the biaxial tension problem, tensile stresses of σ_x = 320 psi and σ_y = 80 psi were applied along the x = x_0 and y = y_0 edges of the plate, respectively, and material constants of E = 30 x 10^6 psi and ν = 0.25 were used (note that σ_y is of sufficient magnitude to cancel the effects of Poisson contraction). With these applied loads and material properties, the expected results are as follows:

Strains: $\quad\quad\quad\epsilon_x$ = .000010 $\quad\quad\epsilon_y = \gamma_{xy} = \gamma_{xz} = \gamma_{yz}$ = 0

Stresses: $\quad\quad\quad\sigma_x$ = 320 psi $\quad\quad\sigma_y$ = 80 psi $\quad\tau_{xy} = \tau_{xz} = \tau_{yz}$ = 0

Displacements: $\quad$ u = .000010x $\quad\quad$ v = w = 0

Forces: $\quad\quad\quad$ Total Force on x = x_0 is 5120 lb

$\quad\quad\quad\quad\quad\quad\quad$ Total Force on y = y_0 is 1320 lb

The results obtained match all of the expected quantities to within one part in 10^6.

For the uniform bending problem, a bending stress of σ_b = 3000 psi was applied along the x = x_0 and y = y_0 edges of the plate. This corresponds to an applied uniform bending moment of M_0 = 500 in-lb/in. Since this is a pure bending problem, no shear is present, and both Kirchhoff and Mindlin theory give the same results. These results, for the given loading and material properties of E = 10^7 psi and ν = 0.3, are as follows:

Strains: $\quad \epsilon_x = \epsilon_y = \dfrac{M_0 z}{D(1 + \nu)}$ = .000420z

$$\gamma_{xy} = \gamma_{xz} = \gamma_{yz} = 0$$

Stresses: $\sigma_x = \sigma_y = \dfrac{E}{1 - \nu^2} (\epsilon_x + \nu\epsilon_y) = 600z$

$$\tau_{xy} = \tau_{xz} = \tau_{yz} = 0$$

Displacements: $\phi = \dfrac{M_o x}{D(1 + \nu)} = .000420x$

$$\psi = \dfrac{M_o x}{D(1 + \nu)} = .000420y$$

$$w = \dfrac{M_o(x^2 + y^2)}{2D(1 + \nu)} = .000210(x^2 + y^2)$$

where $D = \dfrac{Eh^3}{12(1 - \nu^2)}$ is the plate rigidity.

Comparison of the theoretical and numerical results showed excellent agreement (correct to one part in 10^6).

To complete the validation of the elastic program, the problem of a center-cracked plate under uniaxial tension was analyzed. The problem was run twice; once using a 2 x 2 inplane Gauss quadrature, the other using a 3 x 3 quadrature. Thus, in addition to helping in the verification of the elastic program, the two cases were also used to determine if any increase in accuracy is obtained with the 3 x 3 quadrature. The results were obtained by applying a uniform tensile stress of $\sigma_y = 10,000$ along the $y = y_o$ edge with $E = 10^7$ psi and $\nu = 0.3$. A comparison of both far field and crack data indicated no significant differences between the 2 x 2 and 3 x 3 quadrature results (see Reference 17 for further discussion on the use of reduced integration).

In order to validate the results of the problem, the crack-tip stress intensity factor, K_1, was determined using the displacement

extrapolation method as outlined by Chan, Tuba and Wilson [28].
Use of this method resulted in K_1 values of 1.07 and 1.06 for
the 2 x 2 and 3 x 3 quadrature cases, respectively. These values
were then compared with handbook values compiled by Rooke and
Cartwright [29] to validate the results. The value obtained
from the handbook is K_1 = 1.08 which agrees quite closely with
the results obtained here.

C.4 Closure Constraint Checks

To insure that the closure constraint equations were being
implemented correctly, test cases were run using the four element
model (Figure C-3). A uniform bending moment was applied along the
y = 0 edge of the plate for each case and the constraint equation

$$v = v_s - z\psi = 0$$

applied along the y = 4 edge for values of z = $\pm$ h/2. The resulting
displacements indicated that the constraint was being implemented
correctly. Also, an inspection of the crack flank displacements
for the closure problem easily shows that the constraint condition
was being met.

C.5 Elasto-Plastic Program Checks

The addition of elasto-plastic capability to the program
completed the version of PLABEP used for the analysis. Several
checks were made here also to verify the final program. The

first cases involved replication of the elastic closure and no closure results to insure that program changes had not affected any of the elastic results. In addition, elasto-plastic runs of the closure and no closure cases were made for three and ten load steps. The purpose of these runs was twofold: to verify the correctness of quantities arising from the elasto-plastic calculations, to insure that the trends indicated by the program were reasonable, and to gain insight as to how many load steps would be necessary for the final analyses of the two cases. From these test cases, hand calculations were made where possible to validate the results, and the PLABEP program was found to be consistently accurate for the results examined.

C.6 A Comment on the Distorted 8-Node Element

The elastic no closure and closure cases were also run using the distorted form of the eight-node isoparametric element as developed independently by Barsoum [33] and Henshell and Shaw [34]. The distorted element is formed by moving the midside nodes around the crack tip to the quarter point. The consequence of this distortion is to automatically generate the square root singularity of the crack tip. Bloom [35] has reported that the distorted element produces excellent results for the stress intensity factor when the displacement extrapolation method is used. However, the stress intensity value based on stresses was found to be uniform.

Comparisons of results obtained from the regular and distorted elements indicated differences in displacement values of less than 6.5%. Since the differences in results was fairly small and since the stress results are known to be inferior, the distorted element was not used. See Reference 36 for further discussion on the use, accuracy and application of the distorted element.
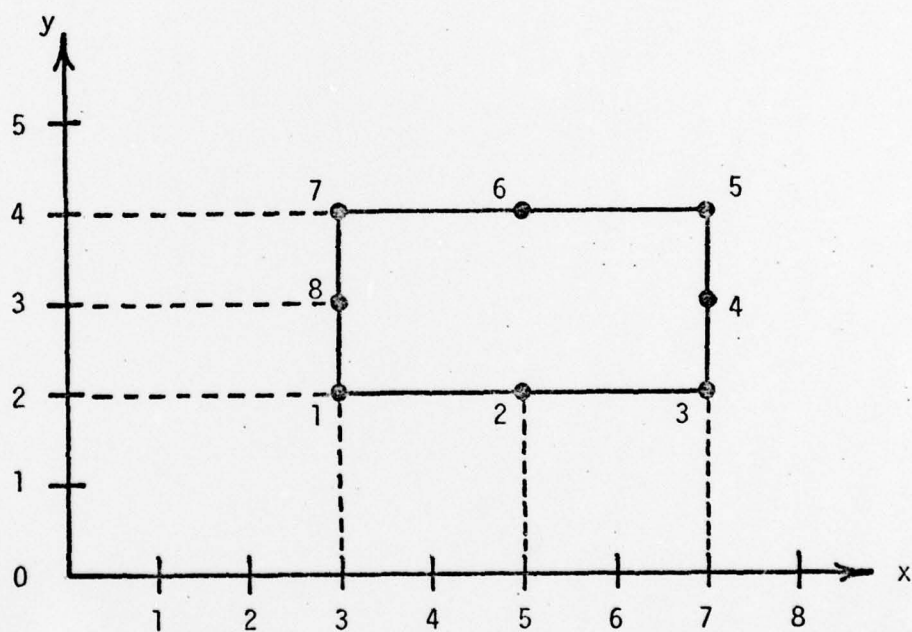
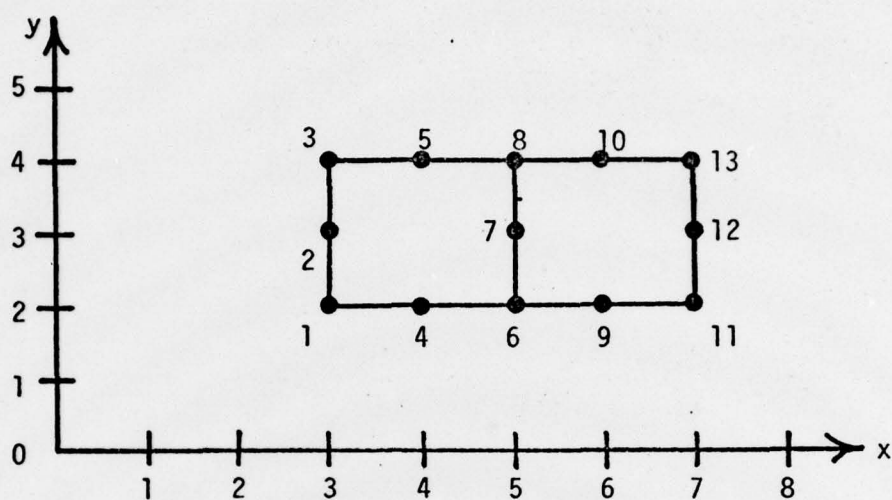FIGURE C-1

ONE ELEMENT MODEL

FIGURE C-2

TWO ELEMENT MODEL
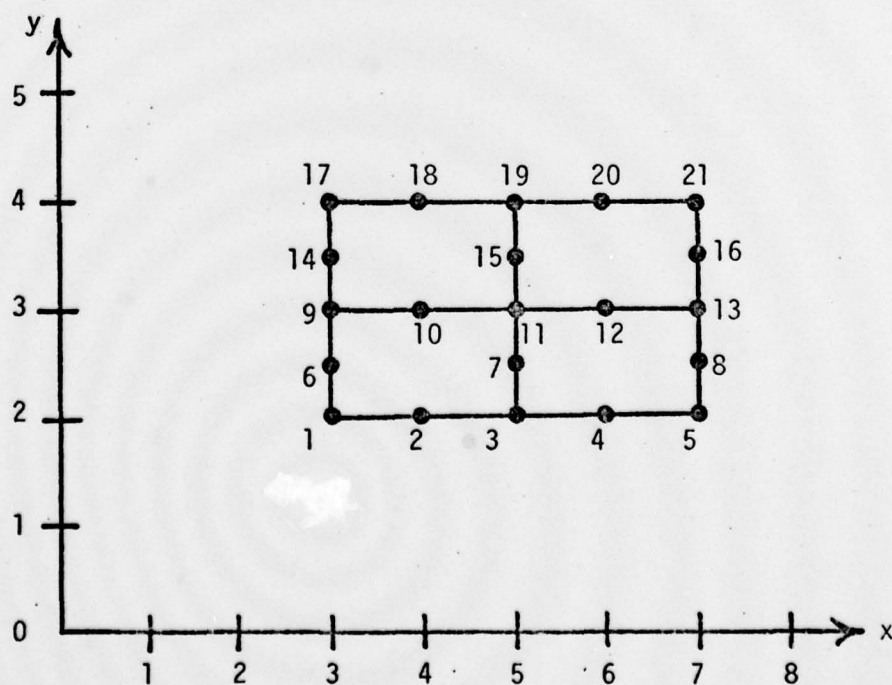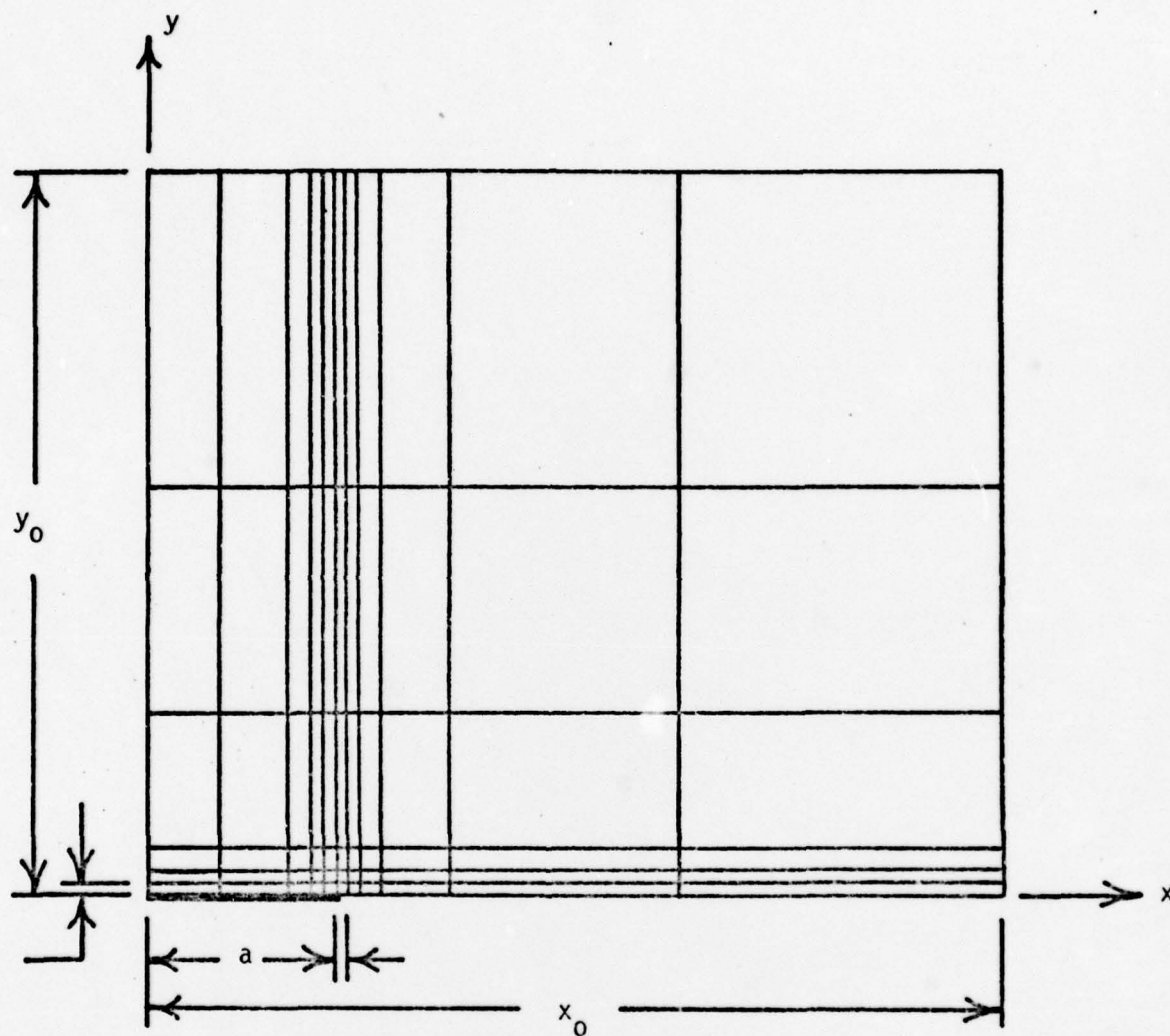

FIGURE C-3

FOUR ELEMENT MODEL

FIGURE C-4

PLATE MODEL

x_o = 9.25 in., y_o = 8.00 in., h = 1.00 in.,

a = 2 in. for the crack problem

66 Elements, 233 Nodes